Control of the Optical and Physical Characteristics of Conjugated Polyelectrolytes in the Solution and Solid Phase

by
Martin Edward Henry Heeley

Victoria
UNIVERSITY OF WELLINGTON
Te Whare Wānanga
o te Ūpoko o te Ika a Māui

A thesis
submitted to Victoria University of Wellington
in fulfilment of the
requirements for the degree of
Master of Science
in Chemistry

Victoria University of Wellington
2012

Abstract

Conjugated Polyelectrolytes (CPEs) are a branch of conducting polymers that combine the electronic and solution processability of conjugated polymers (CPs) with the ionic and self-assembling nature of polyelectrolytes. These systems have been shown to exhibit high sensitivity with changes in aggregation state and optical character dependant on the local environment. The ionic character of the CPEs can be used as scaffolds for post-synthetic alterations allowing for control of the optical and physical characteristics.

In this thesis, the control of the optical and physical characteristics of the conjugated polyelectrolytes (CPEs) sodium poly[2-(3-thienyl)ethoxyl-4-butylsulfonate] (PTEBS) and poly(9,9-bis[6-(N,N,N-trimethylammonium)hexyl]fluorine-co-alt-phenylene] (FPQ-X, where X denotes the various counter-ions of the polymers) is investigated though the addition of various extrinsic ions to dilute solutions and concentrated solutions used for film casting, with the main focus being in the solution phase behavior. The CPE characteristics were studied primarily through UV/Vis absorption and fluorescence spectroscopy coupled with dynamic light scattering and surface tension techniques.

Controlling the solution phase characteristics of the CPE was investigated through a study of through of solvent composition effects, monovalent and divalent ion addition, organic salt addition, and surfactant additions to dilute aqueous solutions of the CPEs. Solvent composition effects were shown to result in fluorescence enhancement with changes in the polarity of the solvent, while the addition of monovalent and divalent ions was shown to induce fluorescence quenching through ionic strength, ion condensation, and cross-linking of CPE molecules dependant on the concentration and valency of the metal ion.

Organic salt additions of a range of concentrations were shown to result in both concentration and alkyl chain length dependant fluorescence intensity enhancements with little changes in the particle size of aggregates in solution. The lack of change

in particle size suggested that the effects were localized to the aggregate surface with the size of the organic salt inducing a steric prying effect on the CPE aggregate. A proposed model of this was created to this effect.

Large changes in the optical and physical characteristics of the CPEs were found with addition of surfactants to the CPE solutions. Fluorescence quenching and enhancements, particle size increases and decreases, and absorption hypsochromic shifts have been noted, with surfactant structure and concentration dependence. The resulting effects are shown to be hydrophobically, electrostatically, and self-assembly driven. Concentration control of the CPE aggregate size and optical characteristics is completed with surfactant micelles being noted at pre-CMC concentrations within the solutions. A model of interactions at the various concentration levels of surfactant has been developed explaining these results. Transferring this system to the solid state has been shown to exhibit both bathochromic and hypsochromic shifts in absorption and have two optically active phases. The dual phase absorption and emission was attributed to a CPE-surfactant complex where the CPE backbone and surfactant self assemblies result in lamellar type structures within the cast films.

The optical overlap of the emission and absorption of the CPEs used was also shown to be favorable for FRET based transfer from FPQ-X to PTEBS. Films created by the layer-by-layer technique showed FRET based signal of PTEBS via excitation of FPQ-Br showing effective FRET based energy transfer between the two species. The absorption signatures of the films with multiple layer-by-layer processes showed that the films do not result in unique layers but rather interdigitated mixtures within the film.

Proof of concept P3HT with DOD addition OFET devices were then created in the attempt to alter the electrode potentials using mobile ions. The devices were found to be less efficient than that of the controls due to the disruption of self assembled structures within the devices hampering electron movement.

Acknowledgments

Throughout the months that have been lost in writing this thesis, the acknowledgments were the last thing on my mind and the last thing I was going to write, and I kidded myself that this would be easy. But here I am, writing the last thing of my thesis, and its not as easy as I hoped. Who do I thank? Will they get annoyed if I name them specifically? What if I forget someone? So, to all of you who either don't want to be named and have been, or I've forgotten to name and should have, I'm sorry.

First of all, I really need to thank my lab mates especially Joe (douche) and Cole (grandpa clomas) who have been with me right from the start and founding of the ResJHo group, but also Kai, Alex, Omar, Galen, and Cam. You guys have made the long days of study and lab work just that little bit more interesting (and in some cases highly distracting) with the jokes, odd conversations, and help with ideas of how to interpret results. There is also the small matter of putting up with the literally thousands of samples and sample vials that have been scattered around the lab in a not so orderly (some may even say messy) fashion, which you lot dealt with rather well.

The honours year crew also deserve one rather large thank you. So to Thomas, Eldon, Joe, Cole, and Bryan, Thanks for the friendship and help throughout the last few years. Those endless nights sitting in AM 206 studying for exams and tests or doing assignments until stupid hours of the morning, I honestly couldn't have done it without you lot. Same goes for the late night write up room crew, Brad, Bryan, and Cole, the late nights were a little more bearable with company.

I would also like to thank the lab techs Jackie, Jamie-anne, Sherkira, and Teresa for allowing me to steal a wide range of stuff from lab equipment through to biscuits when I needed it and also for the chats in that little office whenever I fancied wandering in. You lot are great.

I was also helped greatly in the final devices stages of my masters by Dr. Natalie Plank and her PhD student Hannah. You both taught me so much in so little time right from the basics of how to use the instruments to fabricate the devices, through to how to analyze them and what the data actually means. That was a truly great help.

I would also like to thank Aish, even while you've been away, our phone calls everyday and encouragement to just keep going and get it done have been great. You have no idea. Thanks. A similar thanks needs to go to my mother whose constant supply of nice comfort foods has keep the busy nights that little bit sweeter.

The two people that have the my utmost respect and thanks however are my supervisor Justin Hodgkiss and my father. You both have stuck with me all through this work keeping me on track with work, giving me ideas of how to test things, ideas of whats going on with the results and most importantly, editing this thesis. We both know that editing this has been no easy task with some of my attempts at writing chapters being truly horrible. Yet you both "battled through" (to quote Justin) and didn't give up on me to a point that, you're probably going to edit this too. Thank you both so much.

Table of Contents

List of Figures

List of Schemes

List of Tables

Glossary

CMC	Critical Micelle Concentation
CP	Conjugated Polymer
CPE	Conjugated Polyelectrolyte
DEC	Decylamine
DLS	Dynamic Light Scattering
DMSO	Dimethylsulfoxide
DOD	Trimethyldodecylammonium bromide
EtOH	Ethanol
FPQ	poly(9,9-bis[6-(N,N,N-trimethylammonium)hexyl]-fluorine-co-alt-phenylene]
FRET	Forster Resonance Energy Transfer
HOMO	Highest Occupied Molecular Orbital
LUMO	Lowest Unoccupied Molecular Orbital
M	mol L^{-1}
MeCN	Acetonitrile
MeOH	Methanol
Me_2CO	Acetone
OFET	Organic Field Effect Transistor
PE	Polyelectrolyte
PEDOT:PSS	Poly(3,4-ethylenedioxythiophene) poly(styrenesulfonate)
PLED	Polymer Light Emitting Diode
PPV	Poly(p-phenylene vinylene)
PTEBS	Sodium poly[2-(3-thienyl)ethoxyl-4-butlysilfonate]
P3HT	poly(3-hexylthiophene)
SANS	Small Angle Neutron Scattering
SAXS	Small Angle X-Ray Scattering
SDS	Sodium dodecylsulfate
SMS	Sodium methylsulfate
SPS	Sodium propylsulfate
ssDNA	Single Strain Deoxyribonucleic Acid
TCSPC	Time Correlated Single Photon Counting
TEA	Tetraethylammonium bromide

THF	Tetrahydrofuran
TMA	Tetramethylammonium bromide
TPA	Tetrapropylammonium bromide
UV/Vis	Ultra-Violet/Visible
VUW	Victoria University Wellington

Chapter 1

Introduction

1.1 Conjugated Polymers and Polyelectrolytes

Conjugated polymers (CPs) are organic polymer materials composed of a π conjugated sp^2 hybridized hydrophobic backbone with side chains composed of hydrophobic aliphatic chains for increased solubility in polar solvents.[1] These materials are solution processable and combine the optical and electronic properties of semiconductors with the mechanical and processing abilities of plastics.[2] The semiconducting nature of these materials results in CPs being used as emissive or absorbent layers for devices such as polymer light emitting diodes (PLEDs)[3] or organic solar cells.[4] A distinct advantage CPs have over their inorganic counterparts is, when used in a device, thin CP films adopt their plastic nature allowing for flexibility without effecting charge transport properties.[5]

Traditionally CPs are highly soluble in organic solvents such as chloroform, and are cast into films for device fabrication from these solvents. However, the toxic nature of these solvents provides the drive for the polymers to be altered through structural modification to become soluble in safer, polar solvents such as ethanol or water.[6] Whilst CPs some polar soluble CPs have been produced based on esters and amines,[7] water soluble systems remain highly desirable.

Conjugated polyelectrolytes (CPEs) are hydrophilic derivatives of CPs that are soluble in more environmentally friendly polar solvents such as water or alcohols. The hydrophilic nature of CPEs is derived from the side chains which have ionisable groups attached to the ends of the aliphatic chains to allow for increased solubility in polar solvents. This modification results in CPEs combining the

electronic characteristics of CPs, and the polar solubility of non-conjugated ionic polyelectrolytes (PEs).[8] Figure 1.1 shows the structure of a common CP poly(3-hexylthiophene) (P3HT), its CPE derivative sodium poly[2-(3-thienyl)ethoxyl-4-butlysulfonate] (PTEBS), and a non-conjugated PE polyacrylic acid (PAA).

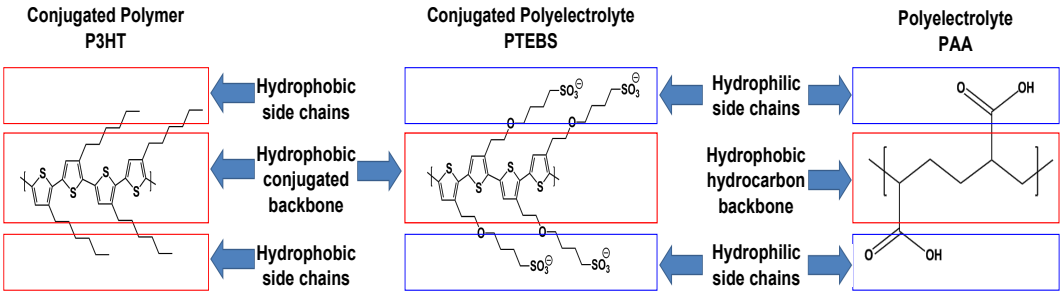

Figure 1.1 Comparison between conjugated polymers, conjugated polyelectrolytes, and non-conjugated polyelectrolytes. Left shows a conjugated polymer (P3HT), middle shows a conjugated polyelectrolyte (PTEBS), and right shows a non-conjugated polyelectrolyte (PAA).

CPEs are amphiphilic in nature with the ionic side chains imparting hydrophilic character, while the π-conjugated backbone results in hydrophobic character.[6] Ionic salts of CPEs can be both cationic (such as the quaternary ammonium group) or anionic (such as the sulfate group). This allows for selection of the charge required.[9] Further alterations of the aliphatic side chain (such as the oxygen substitution at the 3 position of the side chain in PTEBS above) also allows for increased solubility of the CPE in highly polar solvents such as water.

The introduction of ionic side chains to the conjugated polymer structure also has secondary effects along with the changes in solubility of the CPE (described above). The first is the ionic character of the chains provides scaffolds for potential post synthetic tuning of the structure of the CPE through direct interaction of the side chain.[10] The second effect is due to the induced amphiphilic character of the CPEs. Due to the hydrophobic/hydrophilic nature of the CPE, competition between the two forces results in an increased affinity for self-assembly and subsequent aggregation of the molecules within the solution.[2]

In both CP and CPE systems, the optical character comes from the π-conjugated units of the backbone, with different backbone units resulting in different optical characteristics.[11] However, the side chains also impart significant effects to the optical and physical characteristics of CPs and CPEs. Using the highly studied CP polythiophene as a reference, Figure 1.2 shows the absorbance spectra of a range of thiophene based polymers.[12] As can be seen, the side chains size and structure (free chain or cyclic) have large effects on the peak absorption wavelength, with a general trend of larger more sterically hindered side chains resulting in a hypsochromic (blue) shifted absorbance.

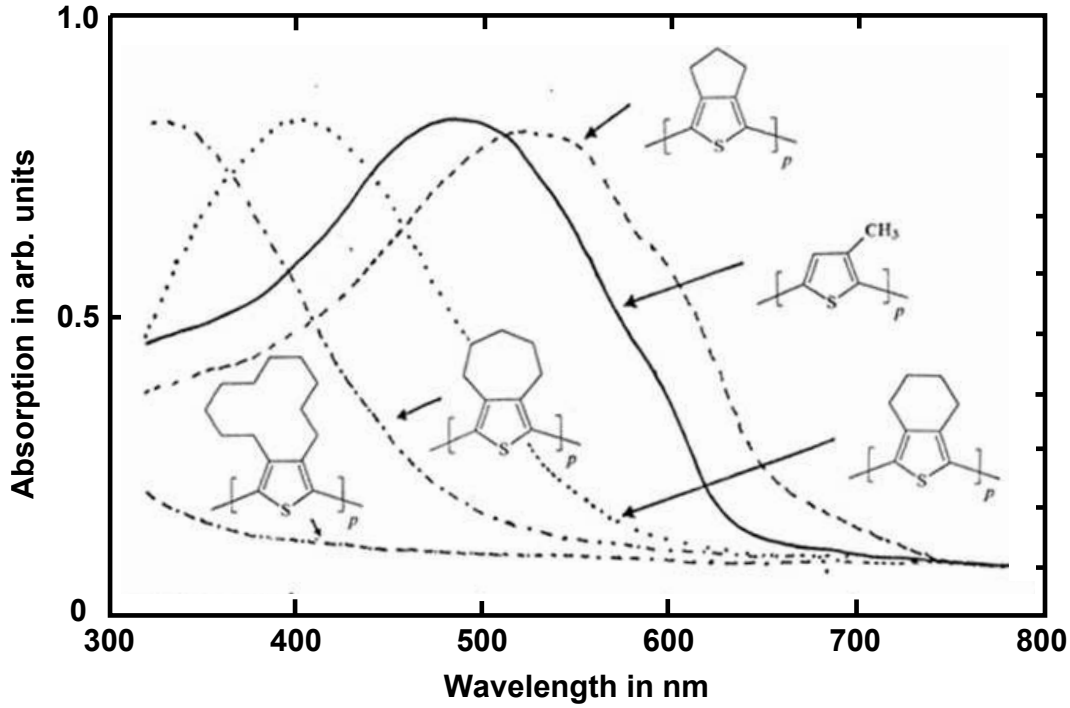

Figure 1.2 Absorbance spectra of polythiophene with various side chains showing how side chains effect optical characteristics of CPs. Figure adapted from Chan *et al.*[12]

This figure also shows how optical spectroscopy can be used as a probe into specific aggregation states within solutions and films of CP and CPEs. The above mentioned trend shows how the larger more sterically hindered side chains result in a peak absorbance towards higher energy while the smaller side chains are found more towards lower energy. The larger side chains cause both inter- and intra-molecular steric hindrance between monomer units resulting in a greatly reduced affinity for aggregation. The shorter chains such as the methyl side chain (second to the right) have significantly reduced steric hindrance in comparison to the larger side chains allowing for a greatly increased self-assembly effects resulting in aggregation of these systems. This shows that aggregation is shown to induce bathochromic (red) shifts in optical spectra while loss of aggregation is seen as hypsochromic (blue) shifts in the optical spectra of solutions and films of CPs and CPEs.[12]

The side chain effect on the optical nature of the CPs also enhances the desire for post-synthetic alterations to the scaffolds of side chains due to the significant changes in optical characteristics of the thiophene based polymers. With each of the above thiophene derivatives, an entirely new synthesis was required. Each of the syntheses are both time consuming and require expensive catalysts such as palladium.[13] The addition of ionic characteristics to CPEs allows for post-synthetic alterations through addition of extrinsic ions such as surfactants[14] and metal salts[15] to alter the self-assembly of these materials leading to interesting structures.

1.2 Molecular Self-Assembly and Induced of CPs and CPEs

Nature has perfected the role of self-assembly in molecules allowing for many strong and useful designs of supramolecular structures made through this system such as the DNA double helix in the human body,[16] and chlorophyll in plants for light harvesting.[17] Controlling and mimicking these self-assembly effects in other systems has a large potential in future applications with the field of "DNA nanotechnology" being formed for this purposes.[18]

The following sections will briefly introduce the types of self-assembly seen in CPs, PEs, and CPEs with reference to examples of how changing the environment of the polymer, or addition of additives to solutions, can alter to the self-assembly of the polymers being studied.

1.2.1 Self-Assembly of CPs and CPEs in the Solutions and Films

The natural structure of CPs and CPEs result in a strong affinity for self-assembly in the solution and solid phase. The π-conjugated backbone of the CPs results in strong inter- and intramolecular interactions through the highest occupied molecular orbital (HOMO) and lowest unoccupied molecular orbital (LUMO) of nearby monomers. This results in a strong stacking effect through the backbone of CPs and CPEs which can limit their solubility.[1,19]

In the case of some CPs, the natural van der Waals interactions of the hydrocarbon side chains induces a second "horizontal" stacking through the side chains of the CPs. This combined with the backbone stacking results in a strong 3-dimensional self-assembly of CPs within aggregates. This effect is very strong in highly regio-regular polymers resulting in highly ordered and π-stacked systems.[20] This effect is shown in Figure 1.3 with P3HT as a reference. The image also shows the resulting polymer separation distances with two different self-assembly regimes. The strong π-interactions of the backbone resulting in a strong network of CPs with an approximate 0.38 nm separation of the thiophene units, while a 1.6 nm separation of the backbones of CPs van der Waals coupled though the side chains.[1]

The introduction of ionic side chains to CPEs results in a greatly reduced potential for side chain interactions due to ionic repulsion of ionic groups making "horizontal"

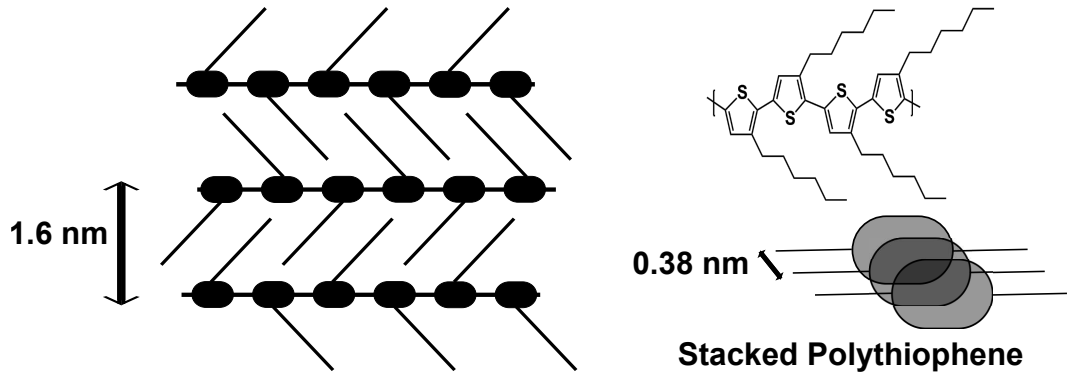

Figure 1.3 Example of P3HT self-assembly. Shown are the calculated spacings between horizontal and vertical stacking of regioregular P3HT. Figure reproduced from McCullough *et al.*[1]

aggregation limited. The change in solubility of CPEs in comparison to that of CPs and their amphiphilic nature makes CPE self-assembly quite complex. As CPEs are generally soluble in aqueous (or strongly polar media), the self-assembly of the hydrophobic π-conjugated backbone becomes much more pronounced in order to reduce the unfavorable solvent interactions. This results in the optical and physical characteristics of CPEs in solution being strongly environment dependant.[2]

CPE aggregates are known to be somewhat micellular in their structure.[21] The π-conjugated backbone makes up the core of the aggregate while the hydrophilic side chains point outwards into the polar solvent medium. This results in the CPE aggregates being considered as a large spherical ball in solution with a dense polymer backbone core and charged outer layer.[22] The ionic charge of the spheres and tightly bound hydrophobic core result in the aggregates becoming susceptible to alterations through changes in the CPE environment. As the system is highly amphiphilic, changes in the environment can come through a variety of different means such as polarity of the solvent,[23] or the pH of solutions.[24] The following section details literature examples of these effects with reference to both CPs and CPEs and how they were used to control self assembled structures within the resulting solutions and films.

1.2.2 Concentration Induced Assembly of CPs and CPEs

The concentration of components within a system is known to have a large effect on the characteristics of CPs and CPEs in the solution and solid phase. Figure 1.4 shows the optical signature of the CP poly[2-methoxy-5-(2-ethyl-hexyloxy)-1,4-phenylene-vinylene] (MEH-PPV) at a range of concentrations in tetrahydrofuran (THF) in the solution and solid phase.[25]

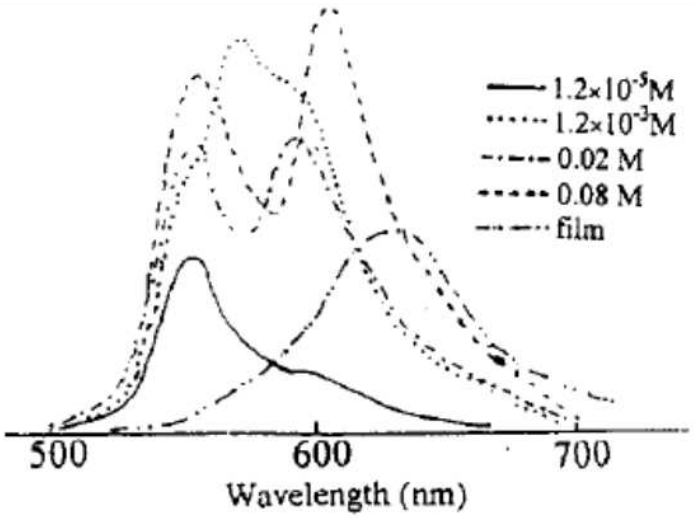

Figure 1.4 Example of concentration effects of CPs. Shown are the emission spectra of MEHPPV at a range of concentrations. Figure taken from M.Zheng et al.[25]

As can be seen from this figure the increased concentration has a large effect on the emission spectra of the solutions with the increased concentration resulting in a greatly increased 590 nm emission band similar to that of the solid state, and red-shifted peak maxima. This peak is known to be that of low energy trapped aggregate states within the solution.[26] This results in the conclusion that the polymer solution is becoming increasingly aggregated with increased polymer concentration.[25] The inter- and intrachain exciton recombination events (excimers) due to the increased locality of polymer chains within the solution is a common effect within CPE aggregate states.[27,28] This results in aggregation causing changes in the optical signature of CP solutions and films, and another optical tool for identifying aggregation events. Excimers are not always seen in emission spectra however, as these processes are low energy and can be very weakly emissive.

Increased concentration effects are also seen in non-conjugated polyelectrolyte (PE) systems. Taking the case of a simple PE in solution; at low PE concentration, the PE counter-ions are dispersed in solution resulting in the inter-molecular interactions of the PEs being low due to the repulsive electrostatic forces of the side chains. This results in a PE chain in solution as a long chain with the side chain counter ions dispersed in the polar media. However, with increased concentration of the PE, the electrostatic forces become larger resulting in the counter ions of the PE becoming bound to the side chains causing a stiffening of the polymer chain and a reduction in the electrostatic repulsion between PE molecules (electrostatic screening effect). This results in an increased potential for inter-molecular interactions due to the loss of repulsive forces.[29,30]

This allows a level of control of the optical and physical characteristics of CPs and PEs through changes in polymer concentration. CPs and CPEs/PEs are shown to interact differently due to polylectrolyte based systems ionic side chains and subsequent amphiphilic nature giving rise to counter-ion condensation effects. The amphiphilic nature also increases potential effects due to solvent composition, as a single solvent is unlikely to have favorable interactions with both the backbone and the side chains of the CPE. Solvent effects on the optical and physical characteristics of CPEs are discussed in the following section.

1.2.3 Solvent Induced Assemblies of CPs and CPEs

Solvent effects on the optical and physical characteristics of CPs and CPEs is a common means of controlling self-assembly in the solution phase due to the simplicity and reliability of the technique. Solvent effect techniques involve either dissolving the CP or CPE in a range of solvents ranging from highly soluble ("good" solvent) through to poorly soluble ("bad" solvent), or via titrating a bad solvent for a component of the polymer into a solution of the CP or CPE dissolved in a good solvent, (or vice versa) and monitoring the change in optical and/or physical characteristics.

An example of the effect of solvent effects though changing the solvent from a good to bad solvent is reported by Yang *et al.* and is shown in Figure 1.5.[23] This plot shows the absorption (left) and fluorescence (right) of the CPE in water, methanol, DMSO, and solid films. Focusing on the absorption characteristics, there are observable shifts (440–480 nm) in the absorption peak maxima with changes in the polarity of solvent and through to the solid state. This showed that the π-conjugated backbone changes conformation in the different (or lack of) solvents with increasing levels of inter- and intramolecular π-interactions with changes in solubility of the backbone units.

An interesting use of these solvent induced self-assembly effects has been reported by Shen et al.[31] The authors report titrating an organic solvent (THF) into a water dissolved solution of a CPE/CP copolymer. This yielded both increases and decreases in fluorescence intensity and maxima peak wavelengths depending on the concentration of THF in the distilled water:THF solvent mixture (see Figure 1.6). The copolymer was composed of a dual monomer system in which the repeating unit was composed of an ionic side chain monomer component (hydrophilic CPE), and a non-ionic side chain monomer component (hydrophobic CP), connected by a triple bond (see inset of Figure 1.6 for molecular structure). The characteristics of the solutions are monitored as the composition of water:THF changes from 0-100%.

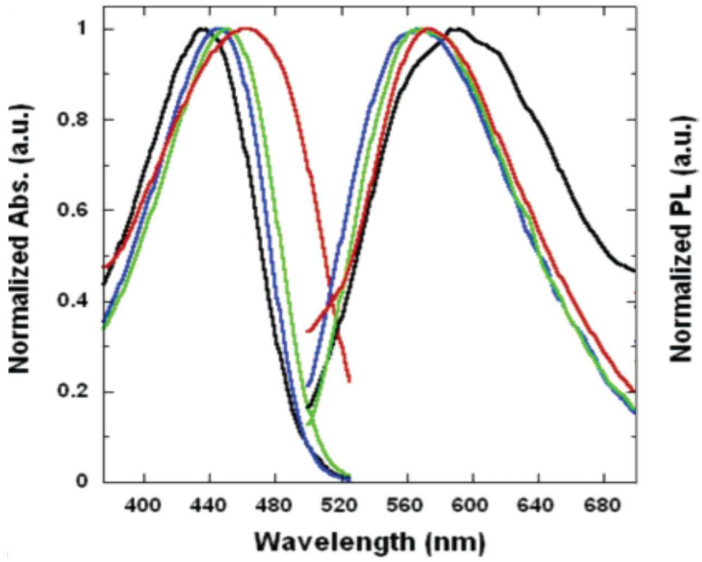

Figure 1.5 Example of solvent effects on the optical characteristics of PTBT-Br in CPE in water (black), methanol (blue), and DMSO (green) in the solution phase and in a thin solid film (red). Figure adapted from Yang et al.[23]

Figure 1.6 shows the emission intensity and wavelength of the copolymer analyzed by Shen *et al.*[31] at the different solvent compositions. In pure water, the polymers hydrophobic side chains and backbone are aligned while the hydrophilic side chains point towards the aqueous environment (lamellar/micelle like structure). Initial additions of THF resulted in favorable solvation of the hydrophobic backbone and side chains, which resulted in a reduction of intra-molecular fluorescence quenching within the aggregate system. This caused a large blue shift with associated increased fluorescence intensity.

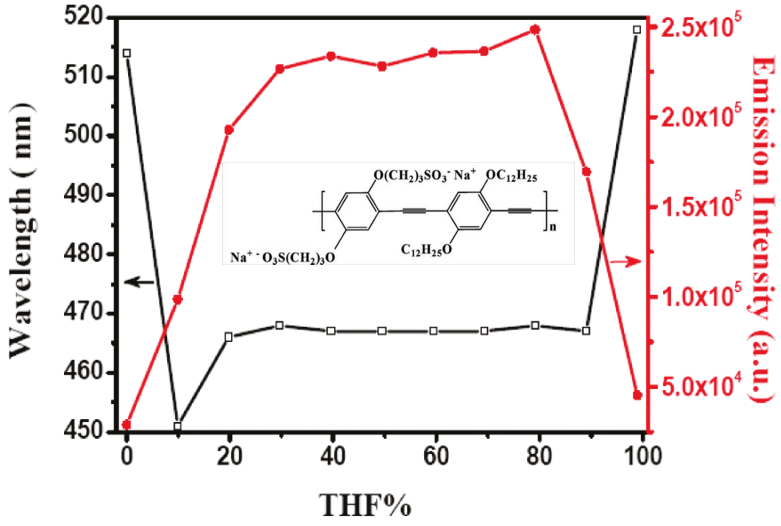

Figure 1.6 Example of the effect of solvent composition on the optical character of $PPESO_3OR$ (inset). Figure adapted from Shen et al.[31]

With the increased THF concentration, more favorable solvation of the hydrophobic backbone and side chains resulted in a reduction in the hydrophobic effect felt by the

backbone, but subsequently increased the amount of unfavorable interactions of the ionic hydrophilic side chains. This resulted the copolymer being in its most favorable state where the backbone and hydrophobic side chain self-assembly was while the side chains are still solvated by the water content of the solvent system. This resulted in little change in the levels of inter- and intra-molecular fluorescence quenching. Further increases (post 80% composition) in THF concentration within this system resulted in increased favorable interactions for the backbone and hydrophobic side chains, however, much larger unfavorable interactions of the hydrophilic groups resulting in alignment of the ionic species within the aggregates. This caused the formation of an inverse micelle structure with reformed inter-molecular aggregation, and associated fluorescence quenching. 100% THF composition resulted in further assembly of these structures with tightening of aggregates and further aggregation of the system with associated red shifted peak maxima.

This effect is not limited to copolymers with authors having shown that the addition of favorable or unfavorable solvents to CP or CPEs in solution has large effects on the optical characteristics of the systems.[23,32] A common associated effect with unfavorable solvent addition is where a large quenching of the main fluorescence band is observed with the associated growth of a low energy, weakly emissive, broad peak. As stated above, this effect is attributed to excimer like states within CP or CPE aggregates.[33]

1.2.4 Salt Induced Assemblies of PEs and CPEs

PEs and CPEs are composed of ionic side chains allowing for favorable electrostatic interactions with both counter-ions and other extrinsic ions. As previously stated, the increased concentration of PE in the system is shown to result in the electrostatic forces beginning to dominate the system allowing for counter-ion condensation onto the PE backbone. This effect is not limited to PE concentration however. Addition of charged salts is common throughout literature with the observed changes in the optical and physical characteristic being both salt type, and salt concentration dependant with low concentration CPE or PE.[29,34]

Kaur *et al.* has shown the effects of monovalent salt addition to solutions of CPEs over a wide range of concentrations. The low concentration salt addition has been shown to have little effect due to the hydrophobic effects dominating the system resulting in the electrostatic attraction to the PE being slight. However, with increased concentration of salt to the "electroylte" levels (approximately 100 mM), dramatic quenching of the fluorescence intensity (approximately 50%), red shifted

absorbance, and five fold increase in the radius of aggregates in solution is observed due to coopertive condensation of ions onto the PE causing charge neutralisation and precipitation.[34]

Authors have attributed this effect to the electrostatic attraction of salt ions to the CPE causing screening of the ionic side chains electrostatic repulsion. With the loss of repulsion, the inter- and intra-molecular interactions further associate through the backbone π-orbitals causing the larger aggregates, fluorescence quenching, and in some cases, precipitation of the PE/CPE.[34,35] Computational simulations of these effects with monovalent ions have confirmed the electrostatic screening effects seen with monovalent ion additions.[36]

Similar quenching effects are also noted for divalent metal ions, however additional effects are also observed. The divalent nature of the ion in these cases allowed for the coupling and screening of two PE or CPE chains with a single ion. This resulted in a much tighter and compact aggregate system with an increased fluorescence quenching effect due to divalent ion additions.[37,38] Physically larger aggregates induced by multivalent ion cross-linking or bridging PE/CPE chains leading to similar effects have also been reported.[39]

The increased quenching effect with divalent metal ions has resulted in CPEs being applied for sensing type applications. Kim *et al.* have clearly shown dramatic changes in the fluorescence intensity of a poly(para-phenyleneethynylene) (PPE) based CPE with complexation to divalent metal ions. Large quenches in fluorescence intensity were observed when complexed to mercury(II) ions, which resulted in the proposal of a mercy based sensor based on this premise.[40]

1.2.5 Surfactant Induced Self-Assembly of PEs and CPEs

Surfactant Self-Assembly

Surfactants are molecules that have either an ionic or non-ionic hydrophilic head group with hydrophobic alkyl tails. This makes the molecules inherently amphiphilic resulting in self-assembly in highly polar or highly non-polar solvent systems. Traditionally, when dissolved in the low concentration regime and in a highly polar solvent such as water, the surfactant molecules are located at the air-water interface with the hydrophilic head groups immersed into the water and tails aligned in the air[41] (see Figure 1.7 (A)).

Increasing the concentration of surfactant in the solution results in a steady build-up at the surface with further self-assembly and alignment of the surfactant molecules with a portion being located in the bulk. Continued increases in concentration results in a larger quantity in the bulk with favorable van der Waals interactions of tails of neighboring molecules coupling in order to reduce unfavorable interactions. This process continues until a critical point where the van der Waals assembly of the molecules becomes more favorable than assembly at the surface. This concentration is known as the critical micelle concentration (CMC) of the surfactant, with the specific concentration, shape, and size, being unique to each surfactant and solvent used.[42]

At the CMC the surfactants self-assemble into spherical micelles within the bulk, however other shapes such as ellipsoids and lamellar structures can be formed under certain circumstances.[43] The micelles are composed of multiple surfactant molecules with the head groups pointing towards the aqueous environment and the tails coupling within the core[41] (see Figure 1.7 (B) for an example of this effect).

This is not limited to highly polar solvents however. Due to the amphiphilic nature of the surfactants, inverse micelles are also capable of forming in non-polar environments. These assemblies are where the tails are solubilized by the solvent system, while the ionic head groups are not. This results in the head groups being located in the core of the micelle while the tails are pointing into the non-polar environment. These systems are not commonly solvent induced however due to the electrostatic repulsion of the head group and are often the result of trapped polar solvents in non-polar environments or metal ions.[44] Figure 1.7 (C) shows a basic example of these structures.

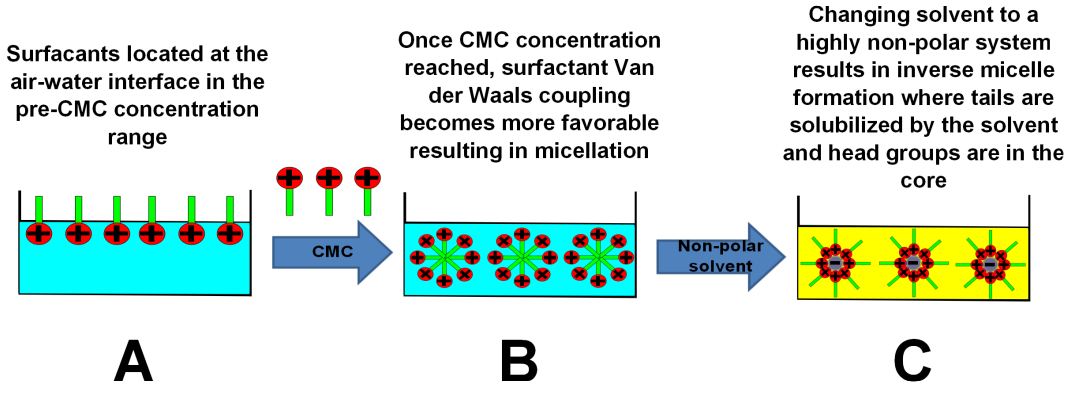

Figure 1.7 Example of surfactant self-assembly. Low concentration surfactant addition results in assembly at the air–water interface (A). Post-CMC concentrations result in micelles in aqueous environments (B) and charge stabilized inverse micelles in highly non-polar environments (C).

This shows that the surfactants have a natural self-assembly based on concentration and solvent environment, giving rise to similar interactions to those seen with CPs

and CPEs. The charged nature of the surfactant also allows for complementary electrostatic interactions with CPEs. The following details the literature examples of PE and CPE with surfactant interactions.

Surfactant Induced Self-Assembly of PEs and CPEs

The similarities in the self-assembly, and the complementary charges between PEs and surfactants head group, shows potential for large scale changes in the structure of the solution phase and solid phase characteristics of CPEs with strong concentration dependant effects. Surfactants have been used to aid in the configuration and solubility of polyelectrolytes for some time with publications regarding surfactant and polyelectrolyte complexes dating back to the 1940-50's.[45] Advancements in this field are still being seen, with both experimental and computational studies being completed on these systems.

The changes in optical and/or physical characteristic of any system that is induced by ionic charges is collectively known as "ionic induced assembly".[46] The process involves the utilization of the strong electrostatic forces between two complementary ionic charges and the cooperative binding mechanism *i.e.* a single unit binding results in many more units binding resulting in the final structure.[47]

In the case of surfactants, it is not only the electrostatic components that cause self-assembly. Anotnetti *et al.* published a review on the surfactant–ionic species interactions resulting in supramolecular structures. In this publication, many different types of structures and building blocks are discussed with the potential driving forces for these structures ranging from van der Waals interactions, to hydrogen bonding (H-bonding), through to ionic and covalent interactions. This shows that there are a large number of potential interactions that need to be accounted for when working with ionic self-assembly. Table 1.1 reproduces the table of ionic self-assembly interactions shown by Antonetti *et al.*[46]

Studies of polyelectrolyte–surfactant complexes have shown them to form interesting 3-dimensional networks with various concentrations of surfactant and polyelectrolyte. Many interesting structures can be formed with the type and size being attributed to the structure of the PE in terms of number of repeating units,[48] flexibility of the PE chain,[49] charge density of the backbone,[50] surfactant used[51] and the relative concentration (pre-or post-micellular) and type of surfactant added (charge and alkyl chain length).[52]

Table 1.1 Methods of self-assembly in ionic self-assembled systems

Type of interaction	Strength (kJ mol^{-1})	Range	Character
van der Waals	51	short	non-selective, non-directional
H-Bonding	5-65	short	selective, directional
coordination binding	50-200	short	directional
"fit interaction"	10-100	short	very selective
"amphiphilic"	5-50	short	non-selective
ionic	50-250	long	non-selective
covalent	350	short	irreversible

Distinct phases have been shown to occur when surfactants are added to PEs over a range of surfactant concentrations. In the low concentration regime, addition of a complementary charged surfactant is known to directly interact with the ionic side chains of the PE. Winnik *et al.* have completed experiments proving the direct surfactant–PE side chain interactions using an amine based PE with slow surfactant addition. Within this study. sodium dodedcylsulfate (SDS) was added to the amine based PE with pH and molecular weight measurements taken with each addition. With increased SDS concentration, the interaction of the surfactant to the CPE resulted in an equilibrium being formed with the protonated amine and the bound surfactant resulting in an increased pH and relative molecular weight[53] showing that the surfactant directly interacts with the side chains of the PE. Similar initial binding interactions of surfactant to PE are reported by Messzaros *et al.* with pH measurements and binding isotherms confirming this proposal.[54]

Continued addition of complementary charged surfactant to PE systems to the point of charge neutralization, results in an increase in aggregate size of the PE-surfactant complexes which is often coupled with small levels of precipitation (clouding) of the solution.[55,56] Small angle X-ray (SAX) or neutron (SANS) scattering have shown these aggregate states to be composed of a mixture of ordered and disordered structures with dense and light polymer phases.[57] The relative level of order and phase density increases with surfactant concentration. Studies into these structures have shown the solutions to contain lamellar phases throughout the aggregates where the surfactant tails van der Waals interact with each other forming an ordered surfactant rich (low polymer) phase, while the PE backbones align forming the polymer dense phase.[58,59]

Magny *et al.* have attributed this ordering and aggregation to the formation of mixed hydrophobic clusters between PE side chains and bound surfactant molecules causing a cross-linking of neighboring polymer chains. Further increases in aggregation past the charge neutralization point is then attributed to enhanced cross-linking effects

where unbound surfactant molecules interacting with bound molecules cause mixed micelle clusters near the PE side chains.[60] This causes small levels of surfactant self-assembly within the PE–surfactant networks. Cooperative association of surfactant then causes rapid association of further surfactant molecules resulting in further surfactant self-assembly and large PE–surfactant aggregation.[53]

Further addition of surfactant results in the formation of surfactant only micelles bound to PE chains at concentrations relating to,[60] or below that of the CMC.[61] Within this state, there is a transformation in the backbone structure where the polyelectrolyte begins to wrap around the micelle causing a reduction of the previously formed aggregate and the formation of the ball-and-chain type structure. These structures have been observed both experimentally,[62] and through Monte Carlo computational calculations[50,63,64]

In summary, this shows that the natural self-assembly of the surfactant can induce changes in the PEs conformation in solution. The complementary electrostatic forces result in favorable interactions of the surfactant head and PE side chains. Cross-linking of PEs chains with subsequent further self-assembly is then induced in order to reduce hydrophobic effects felt by both the surfactant hydrophobic tails and the PE hydrophobic backbone. The result is an aggregated form of a PE–surfactant complex. Further surfactant self-assembly is then seen with formation of micelles at concentrations below that of the CMC.

1.3 Transition of Solution Phase to the Solid Phase

Over recent years, great interest has been placed in the organic photovoltaic device production with specific interest in water soluble conjugated polymers due to the potential for application in the biosensor applications and environmentally friendly synthesis. As stated above, CPs and CPEs are solution processable resulting in the films being initially made via a solution–solid phase casting process. This process is known to have changes in the optical and physical characteristics with the loss of solvent composition, however, controlling this process is possible.

The long range ordering of CPs is commonly seen in the solid state where the initial deposition of the CP to the substrate results in a highly disordered aggregation of the polymer over the surface. This resulting UV/Vis absorption absorption spectrum of the film will commonly be broad and lack vibronic detail due to the disordered

nature of the film. Taking one of the most commonly used CPs, (P3HT) as an example, the transition of the polymer from the solution to the solid phase is shown to have large red shifts in the optical spectrum with a loss of vibronic features throughout the spectrum due to the above mentioned effects.[65]

Annealing processes such as thermal annealing or solvent vapor annealing of the film allows for a slight melting of the P3HT allows for a slight thermal melt of the film (providing the temperature is above the glass transition temperature, T_g, of the film) with subsequent energy provided for diffusion controlled self-assembly of the polymer chains within the film. This results in the favorable π-interactions of the backbone and side chains to reform with associated phase separation of the polymer and other components within the film.[66] Fluorescence quenching due to reformation of the backbone π-interactions, and the absorption spectra regaining the vibronic structure is observed as a consequence of these annealing processes.[67] An example of the vibronic reformation and red shifted absorption is shown in Figure 1.8.

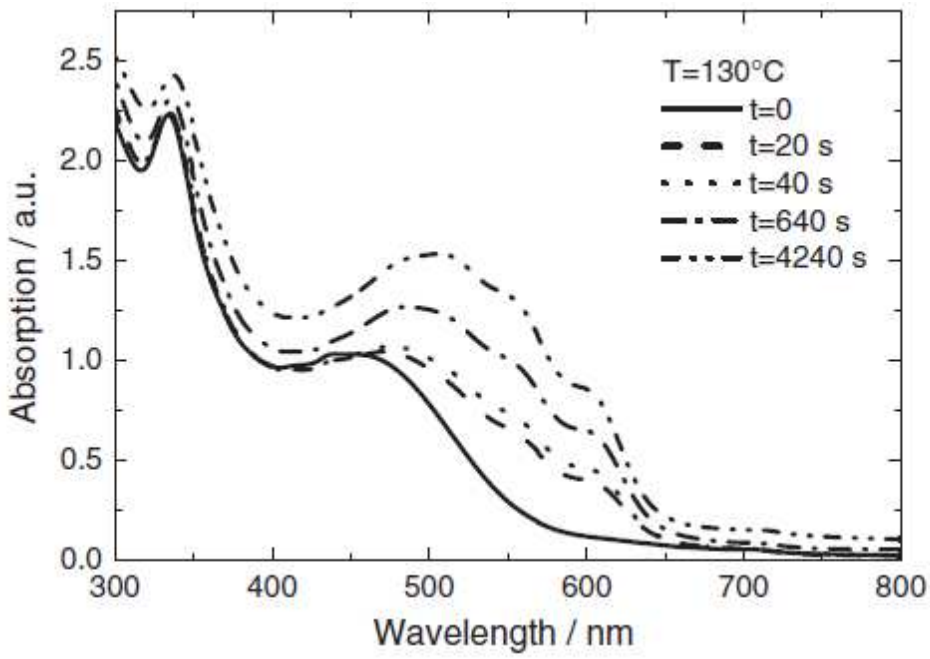

Figure 1.8 Example of the effect of thermal annealing on the optical signature of P3HT in films. The increased length of time results in more favorable polymer alignment allowing for reformation of the vibronic structure. Figure from Chirvase *et al.*[67]

Controlling the optical characteristics of CP thin films is not limited to annealing and can be completed through a wide range of techniques similar to those of the solution phase. Techniques such as altering the polymer solvent composition and polarity of solution used for thin film casting, and varying the casting parameters used, have been shown to have large effects on both the morphologies[68] of the film

and the optical characteristics.[20] This giving rise to not only optical control, but also physical characteristic control of CPs via these techniques.

CPE films are slightly different to that of CP films. With CPs, there is a large disorder in the structure of films when first cast, this is not the case for CPEs. When CPEs are cast into thin films, there is an inherent polarisation of the system due to the backbone preferentially aligning to other organic species, resulting in the ionic side chains pointing away from the backbone giving the polarisation effect.[69] This effect becomes significant when the CPE is used in conjunction with a CP. In this case the CPE backbone will directly interact with the CP layer and the side chains are forced away causing the film to become polarized with the charged side chains pointing towards the electrodes and the backbone interacting with the CP. This effect was shown by Seo *et al.* where the CPE was used as a charge transport layer. Due to the polarisation of the CPE ions within the film, ions become accumulated at the electrode causing the effective work function of the gold electrode used to be raised. The increased work function of the electrode allowed for more efficient electron injection into the device fabricated from stable gold electrodes allowing for increased device efficiency.[70]

The polarization of the thin films of CPE also allows for strong interactions with other charges species when in close proximity. The surface of the film is slightly polar resulting in favorable electrostatic interactions with oppositely charged species such as other CPEs. This results in the potential to create layers of CPE on top of each other through simple electrostatic processes. This technique is known as layer-by-layer (LBL) assembly and can be used to create thin film multi-layer systems using charged species.[71] The layering can be repeated many times and with a wide range of anionic and cationic species resulting in a multi-component layered system with each layer increasing the overall film thickness. The electrostatic force alone does not guarantee the formation of multi-layered assemblies. Studies summarized by Kotov *et al.* have shown the requirement of electrostatic, hydrophobic, and solvent rearrangement interactions for successful layering of PE or CPE systems.[72]

Typically, the LBL technique is composed of four or more steps where an initial CPE or PE layer is deposited (1), washed (2), then a second CPE or PE layer is added of opposing charge (3) and again washed (4). This results in a easy approach to film coating, however the internal structure of the layers created is not uniform or ordered.[72] The layers are also often not unique with the layers often forming interdigitated systems at the intersections between layers with the layers becoming less uniform with each new layer.[73]

The LBL effect is not limited to PE–PE or CPE–CPE systems with the electrostatic binding process having found use in many applications such as creating nanoparticle–polymer assembled device fabrication,[74,75] surfactant based assemblies of PE films[76,77] and biosensor/bioactive type applications.[78]

1.4 Förster Resonance Energy Transfer with CPEs

The implementation of the layer-by-layer technique with CPEs allows for direct layering of optically active polymer chains. Particular CPEs are chosen that have a high optical overlap, so there is potential for Förester resonance energy transfer (FRET) to occur within CPE films.

FRET is a process where energy is transfered from a high energy donor chromopore to a lower energy acceptor chromopore. The transfer of energy is through dipole–dipole resonance interactions through space (not direct electron cloud interactions), resulting in coupled transitions between donor and acceptor pairs provided the optical overlap of the system is favorable. This results in an excitation of the donor species with coupled emission from the acceptor species.[79] A basic Jablonski diagram for this process is shown in Figure 1.9.

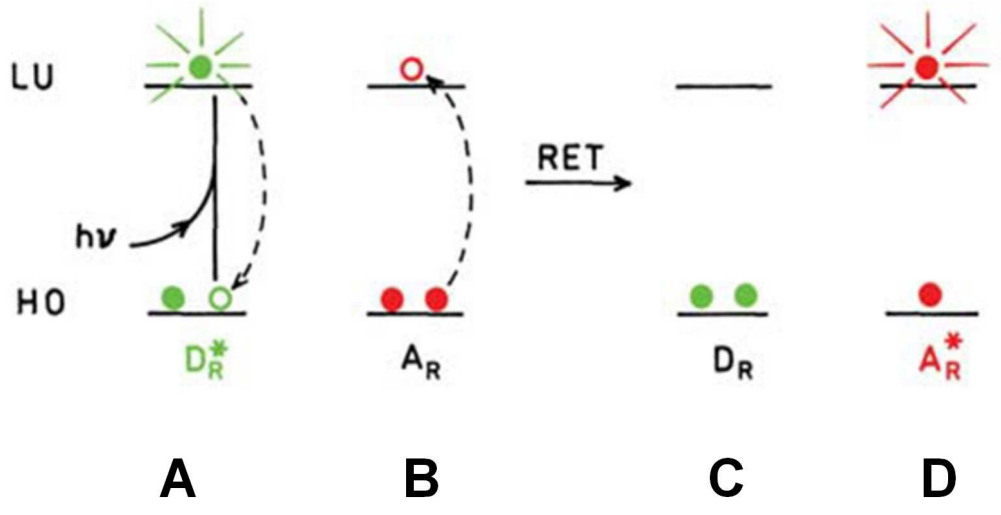

Figure 1.9 Jablonski diagram showing FRET based energy transfer between a donor (green, $D_R{}^*$) and acceptor (red, A_R molecules. A shows the initial excitation of the donor to the excited state followed by non-radiative relaxation. B shows the dipole induced excitation of the acceptor to the excited state. C shows the donor molecule back in the ground state with subsequent excited state acceptor (D). Figure adapted from Lakowitz[79]

The Förster equation for the rate of energy transfer between donor and acceptor chromophores ($\kappa_{D^* \to A}$) is shown as equation 1.1. From this equation it can be seen that the FRET efficiency is strongly dependant on the distance between donor and acceptor chromophores ($R_0{}^6$), and the optical overlap of the emission and absorbance spectra of the donor and acceptor chromophores ($f_D(\nu)$). Other factors include the quantum yield of fluorescence (Ψ_f), the mean lifetime of fluorescence of donor species (τ), Avagardos number (N), the solvent refractive index (n), orientation factor (κ^2), and the molar extinction coefficient (ϵ_A).[80]

$$\kappa_{D^* \to A} = \frac{9000ln(10)\kappa^2\varphi_f}{128\pi^6 n^4 N\tau_D R^6_{DA}} \int_0^\infty f_D(\nu)\epsilon_A(\nu)\frac{dv}{v^4} \tag{1.1}$$

The term "optical overlap" refers to the overlap of the donor chromophore emission spectra with the absorption spectra of the acceptor chromophore. The rate of energy transfer between the donor and acceptor should be faster than the donor fluorescence lifetime (τ). Given this, the higher the optical overlap the greater the amount of energy transfered to the acceptor rather than lost as donor fluorescence or other non-radiative decays.[79,80]

Throughout the literature, FRET is often utilized for recognition of fluorescent dye labelled single stranded DNA (ssDNA) molecules when complexed to CPEs. The use of a dye and ssDNA is used to allow for the efficient energy transfer when in close proximity. The ssDNA is composed of many base pairs allowing for electrostatic interactions with the CPE with subsequent aggregation. The direct coupling and associated aggregation of the ssDNA and CPE allows for increased proximity of the donor (CPE) and acceptor (labelled DNA strands) chromophores allowing for FRET recognition. The FRET between the CPE and dye occurs allowing for fluorescence of the labelled DNA structures when in contact with the CPE.[81,82]

Aggregation of CPEs in aqueous media can be both a hindrance and help with biosensor applications. Due to the amphiphilic nature of the CPEs, the polymers are highly susceptible to aggregation with subsequent fluorescence quenching. This results in less fluorescence emission (reduced $f_D(\nu)$) and shorter fluorescence lifetimes (reduced τ)[83] decreasing the potential FRET efficiency. However, the aggregation also aids the FRET due to the complementary electrostatic interactions. The fluorescent molecules are brought close together in the aggregate state resulting in greatly reduced separation distances (reduced $R_0{}^6$) and hence increased FRET efficiency when the acceptor and donor chromophores are within the aggregates.

Work published by Bazan *et al.*[84,85] have attempted to use this effect for specific

sensing opportunities. The work completed by this group has shown that altering the structure of the polymer backbone allows for mutli-colored labeling properties when the chain is in an aggregated state (not complexed to ssDNA) or in aggregates containing dye labeled ssDNA media. The authors created a CPE/CP copolymer based on two fluorescent units (5% 1,2,3-benzothiadiazole (BT) 95% cationic poly(fluorene-co-phenylene) (PF)), and tested the system with aggregation[85] and ssDNA.[84] Of note, the emission spectra of the BT monomer units had poor optical overlap with the dye labelled ssDNA, while having a large optical overlap with PF, which in turn had an increased optical overlap with the ssDNA. When aggregated, the blue emitting PF monomers come into close proximity allowing for FRET between the two units. This resulted in the large emission of the PF monomers being quenched with the growth of the green emission intensity of the smaller concentration BT monomers. When this monomer is then aggregated to dye labelled ssDNA, due to the more favorable spectral overlap of the BT monomers with the dye labelled ssDNA, an increased emission from the ssDNA was observed. This shows that the reduction in distance between the monomer units allowed for more efficent energy transfer from the PF to the BT sites increasing the observed BT fluorescnece, which allows for a further FRET cascade to dye labelled ssDNA which resulted in the emission of the labelled ssDNA complex.

1.5 CPEs in Organic Electronic Devices

A large effort throughout CP and CPE research is to fabricate and improve photovoltaic devices for solid state, lighting, lab on a chip devices, biosensors, and solar energy harvesting. Initially, CPEs were devised to allow for device fabrication through more favorable polar solvent systems.[6] These efforts were quickly hindered however due to the poor film casting solvents, unevenness of resulting films, and poor efficiency of the created devices.[86–88]

The interest in CPEs for device application then turned to the polymers being used in conjunction with CP systems as charge injection layers. CPEs have been widely shown to be very efficient as both hole or electron injectors based on the structure of the CPE used. These layers have become increasingly important in device fabrication due to the presence of the mobile ions and the natural dipole created by CPEs when cast into thin films on top of organic layers.[70] With applied bias, the mobile ions have the potential to accumulate at the electrodes resulting in a reduction in the internal electric field of the device. This along with the CPE film internal dipole, results in more efficient devices with CPE layers, and also for

the use of more stable high work function electrodes without hampering device performance.[89,90] An example of a PLED device incorporating CPEs as transport layers is shown in Figure 1.10

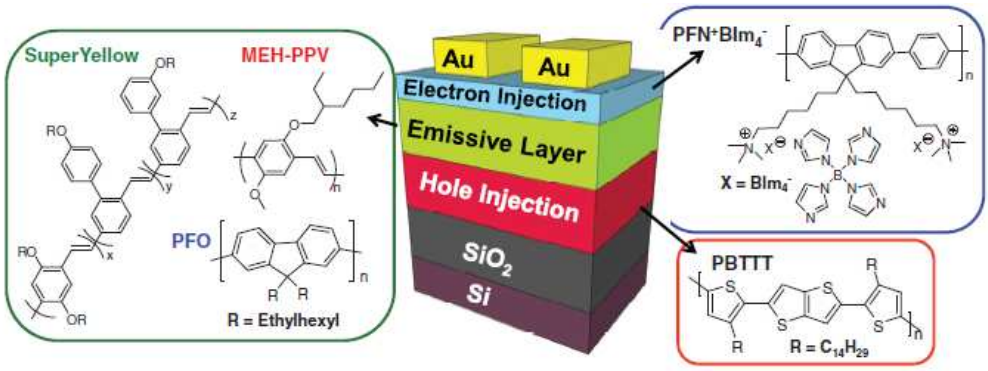

Figure 1.10 An example of an efficient PLED device created by Heeger *et al.*[70]. The device uses a CPE transport layer to alter the work function of the gold electrodes allowing for effective electron injection into the device.

A publication by Ma *et al.*[91] showed the effect of electron transport in device efficiency. The authors of this publication created three sets of polymer light emitting diodes (PLEDS) of different colors with and without CPE electron transport layers. It was found that with all three emissive layers, there were significant increases in the luminescence and reduction in turn-on voltages. Both the increased luminescence and lowered turn on voltages are highly desirable effects in PLED devices. Example plots of the comparisons between devices with and without electron transport layers presented in the publication are shown in Figure 1.11.

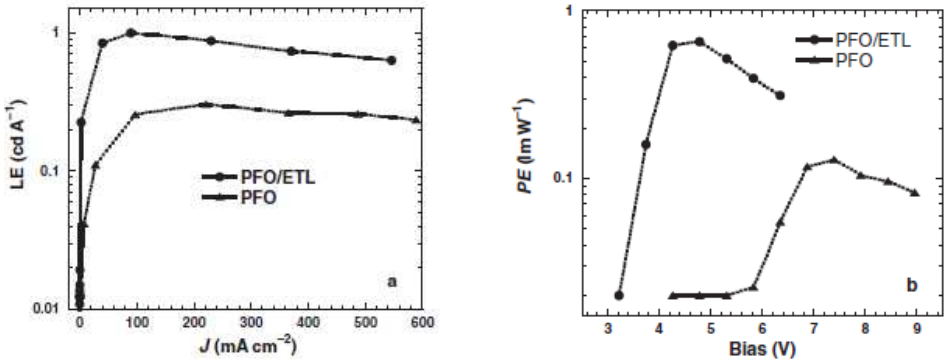

Figure 1.11 Plots published by Ma *et al.*[91] showing the effect of CPE electron transport layers (ETL) on the luminescence (left, a) and turn on voltages (right, b) of a PLED device

Similar effects have been noted in other publications[92,93] with the authors of these studies attributing the increased luminescence to the improved electron injection and the hole blocking potential of the transport layer. The reduced-turn on voltage is a result of the enhancement of the built-in potential of the electron transport layer resulting in effective lowering of the injection barrier and hence work function of the electrodes.

Studies of the CPE electron transport layers have yielded interesting results. It has been shown that the structure of backbone, charge, and choice of counter ion have effects on the charge injection character of single component CPE devices.[92] Systematic experiments completed by deMello *et al.* have shown that the concentration of mobile ions within the system is also important and provided a large enough charge density, the mobile ions accumulate at electrodes resulting in screening of the electric fields, which resulted in changes in the work function of the electrodes.[94] Thus, charge mobility also has a large effect on the charge injection layer properties.

Charge injection layers are not limited to CPEs however. A common hole injector used in organic photovoltaics is PEDOT:PSS while thin film inorganic materials such as LiF have been shown to have highly efficient electron injecting capabilities. These injection layers work through reducing the energy level offset between the polymers and electrodes. These systems lack mobile ions however, resulting in no change in the effective work function of the electrodes.[95]

1.6 Research Aims

The primary aim of this research project is to control the optical and physical characteristics of two conjugated polyelectrolytes PTEBS and FPQ-Br in the solution phase. This was to be completed by controlling the self assembled structures of the CPEs through the use of solvents, electrostatic interactions with the side chains, and surfactant induced self-assembly.

The secondary aim of the project is to transfer the solution phase characteristics through to the solid phase via spin or spray coating. Due to the highly unfavorable casting solvent (water) being the primary solvent being used, this was expected to be a highly challenging stage of the research.

The final aim of this research is to fabricate devices from the CPE–extrinsic ion complexes and utilize the ion mobility to create asymmetric devices (devices of unequal work function electrodes) from symmetric electrodes. The field effect transistor (FET) configuration was to be used for this device fabrication to allow for ion movement between the gate and source electrodes while being able to measure the change in FET character and hence ion movement through analyzing the source–drain voltage *vs.* current curves.

Chapter 2

Experimental

2.1 Materials

2.1.1 Conjugated Polyelectrolytes and Conjugated Polymers

Four CPEs and one non-ionic CP have been used for optical and physical characterization. Three versions of cationic poly(9,9-bis[6-(N,N,N-trimethylammonium)hexyl]fluorine-co-alt-phenylene] (FPQ) where the stabilizing anions are bromide (FPQ-Br), tetrakis(1–imidazolyl–)borate (FPQ-IB), and tetraphenylborate (FPQ-PB) were analyzed. Sodium poly [2-(3-thienyl)-ethoxy-4-butyl-sulfonate]) (PTEBS) was used an anionic CPE where the anionic sulfates are stabilized by a sodium counterion. The non-ionic CP used was poly(3-hexylthiophene) (P3HT) was used for comparison and device purposes. See Figure 2.1 for structures of CPEs used.

CPEs FPQ-Br, FPQ-IB, and FPQ-PB were provided by Professor Han Woo and coworkers from the Department of Nanofusion Technology, Pusan National University, South Korea. Molecular masses were shown to be 25836 g mol^{-1} with a polydispersity index of 1.78. Samples were used as provided without any further purification.

PTEBS was purchased from the American Dye Source with a molecular weight of 840000–1000000 g mol^{-1}. Polydispersity index data for this compound was not provided however purity data was shown to have no metal content. PTEBS was

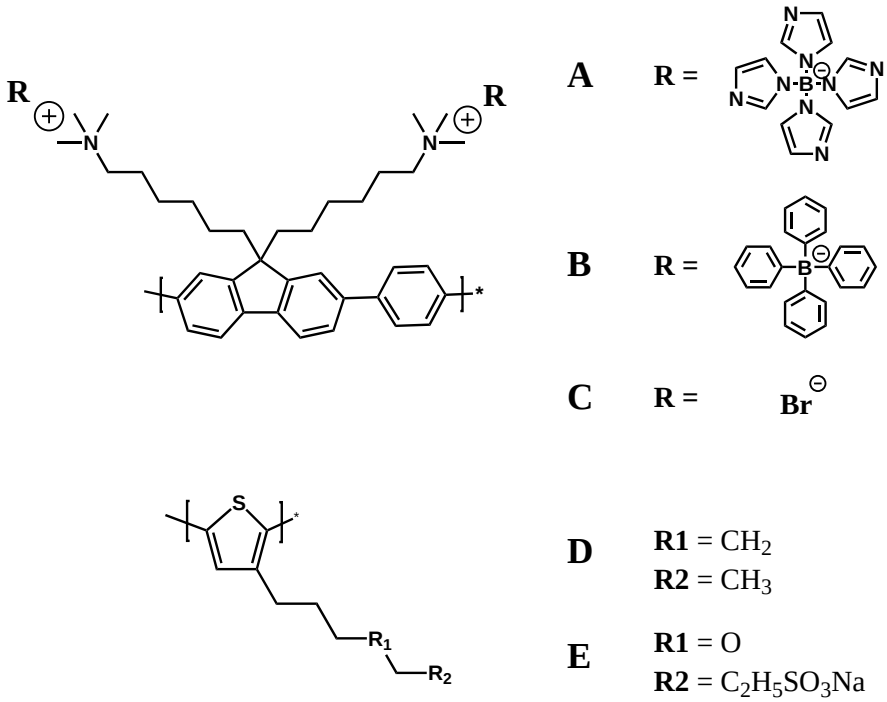

Figure 2.1 Structures of CPEs used. A-C show the structure FPQ-X series (A is FPQ-IB, B is FPQ-PB, and C is FPQ-Br). D shows the structure of P3HT, and E shows the structure of PTEBS

used without further purification. Four batches of PTEBS were purchased with the first three having similar optical properties. These three batches were later found to be contaminated with large insoluble particles. The fourth was received near the end of this work and had slightly blue shifted absorbance characteristics with no contaminant. Table 2.1 below shows the characteristics of the batches used throughout this work. Of note, the fourth batch was only used for the solvent characterization effect in the following chapter and select repeat experiments of extrinsic ion addition being completed to show that the interactions are the same.

Table 2.1 PTEBS batch details

Batch Number	$\lambda_{abs}/\lambda_{PL}$ (nm)	MW (g mol^{-1})
1	462 / 587	1000000
2	453 / 587	840000
3	453 / 587	840000
4	401 / 587	1000000

P3HT was used in two different types of experiments. For base optical and physical characterization, lower grade (lower molecular weight and purity) P3HT was used due to the comparatively large volumes required whereas with device production and characterization, a much higher grade P3HT is required.

P3HT for optical characterization was ordered from the American Dye Source with

a molecular weight of 45000 g mol^{-1} and polydispersity index of 2.0. Purification analysis shows nickel content of 62.0 ppm showing high levels of purity. P3HT was used without further purification.

P3HT for device fabrication is a higher grade and higher molecular weight conjugated polymer. P3HT for device fabrication was ordered from Sigma Aldrich with a molecular weight of 250000 g mol^{-1} and purification analysis showed high levels of purity. No polydispersity index was provided for this polymer. P3HT for device fabrication was used without further purification

All solid state optical characterization was completed on 12 mm diameter fused silica spec2000 substrates purchased from UQG Optics Limited.

2.1.2 Extrinsic Ions and Surfactants

Metal salts and salts of surfactants such as calcium (Ca^{2+}) and potassium (K^{+}), trimethyldodecylammonium bromide (DOD), sodium methyl sulfate (SMS), sodium propyl sulfate (SPS), and sodium dodecylsulfate (SDS) were ordered from Sigma Aldrich at high purity (>98 %) and used as provided.

Salts of surfactants tetramethylammonium bromide (TMA), tetraethylammonium bromide (TEA), tetrapropylammonium bromide (TPA), and sodium dodecylsulfate (SDS) and decylamine (DEC) were obtained from stocks within the VUW science department, pre-ordered from Acros Organics at high purity (>98 %) and used as provided.

2.2 Solution Preparation

2.2.1 Conjugated Polyelectrolytes

Conjugated polyelectrolyte FPQ-Br is soluble in methanol at relatively high concentrations. For solution phase characterization, stock solutions were created at 3.6×10^{-4} M and stirred overnight to dissolve. Once fully dissolved, the stock solutions were diluted down to twice the optical concentration (0.2 absorbance, 7.2×10^{-5} M) in distilled water and used as required. Unless otherwise stated, all solutions were mixed at a 1:1 ratio with additive solutions resulting in a 3.6×10^{-5} M FPQ-Br

solution. For solid phase characterization FPQ-Br was dissolved at 2.2×10^{-4} M in methanol. No further dilution or solvent change was required.

FPQ-IB and FPQ-PB are not soluble in highly polar solvents but can be dissolved directly into DMSO at high concentrations and then dispersed into polar solvents such as water and methanol. For solution phase characterization, stock solutions of 0.079 (FPQ-IB) and 0.085 (FPQ-PB) mg mL^{-1} were placed in DMSO and stirred at 600rpm overnight until dissolved. Stock solutions were then diluted to twice the optical concentration (7.2×10^{-5} M) in distilled water and used as required. Unless otherwise stated, all solutions were mixed at a 1:1 ratio with additive solutions resulting in a 3.6×10^{-5} M FPQ-IB and PB solution. For solid phase characterization FPQ-IB and FPQ-PB were both dissolved at 3 mg mL^{-1} in a 1:5 DMSO:methanol mixture. No further dilution or solvent change was required.

PTEBS is directly soluble in distilled water at high concentrations. For solution phase characterization a stock solutions of 3.6×10^{-3} M in distilled water was stirred overnight at 600rpm to dissolve. Once fully dissolved, the solution was diluted with distilled water to twice the optical concentration (3.6×10^{-5} M) and used as required. Unless otherwise stated, all solutions were mixed at a 1:1 ratio with additive solution resulting in a 1.8×10^{-5} M PTEBS solution. For solid phase characterization PTEBS was dissolved at 1.1×10^{-2} M in a 3:1 distilled water : methanol mixture. No further dilution was required.

P3HT is not soluble in polar solvents due to the lack of any ionic character. When used for solution phase characterization, a stock solution of 2 mg mL^{-1} was placed in chloroform and left to dissolve overnight with magnetic stirring. Once fully dissolved, the stock solution was diluted in chloroform to twice the optical concentration and used as required. For solid phase, 2.5 mg mL^{-1} solutions were created in chloroform and stirred overnight to dissolve. For solid phase device use, a 10 mg mL^{-1} solution of P3HT in chloroform was made and stirred over three days to fully dissolve. No further dilution was required.

For all above stock solutions, new stock solutions were created for each new batch of samples.

2.2.2 Extrinsic Ions and Surfactants

All ions and surfactants used are directly soluble in distilled water to within the concentrations required. The following is split into the different types of additives

used; micelluar surfactants, non-micellular surfactants, and ionic salts. When these solutions were made, 1:1 mixtures were created with the desired CPE to create a solution suitable for optical spectroscopy (0.1 peak absorbance) and desired extrinsic ion concentration. All solutions are made up separately in individual clean glass vials. Structures of all ionic salts and surfactants used are shown in Figure 2.2 below.

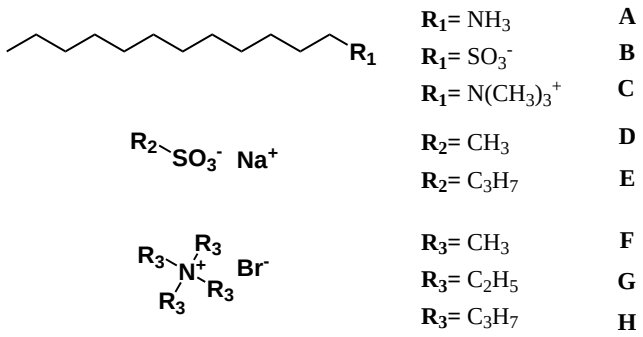

Figure 2.2 Structures of Surfactants and Ionic salts. A is Decylamine (DEC), B is Sodium dodecylsulfonate (SDS), C is trimethyldodecylammonium bormide (DOD), D is sodium methylsulfonate (SMS), E is sodium propylsulfonate (SPS), F is tetramethylammonium bromide (TMA), G is tetraethylammonium bromide (TEA), and H is tetrapropylammonium bromide (TPA)

Micellular Surfactants

Micellular surfactants are a class of compounds that are amphiphilic in nature due to the hydrophilic ionic head group and hydrophobic long chain aliphatic tail. This results in the surfactants having the ability to self assemble in specific solvent types when at a critical concentration. For the surfactants below, when dissolved in a highly polar solvent such as distilled water above the critical concentration (CMC), the materials group together and form micelles.

Trimethyldodecylammonium bromide (DOD) is a cationic micellular surfactant and has a CMC of 0.012 M[96] in distilled water. Sodium dodecylsulfate (SDS) is an anionic micellular surfactant and has a CMC of 0.008 M[97] in distilled water. Decylamine (DEC) is a neutral micellular surfactant and has a CMC of 0.005 M[98] in distilled water. For all of the above cases, stock solutions were created at the CMC and at half the CMC of the micellular surfactant and dissolved in distilled water overnight via magnetic stirring. Once dissolved, 10 further solutions were created via quantative dilution from the 0.5×CMC solution creating 12 solutions in total ranging from 1×CMC through to $\frac{1}{2048}$×CMC concentration.

Ionic Salts and Non-micellular Surfactants

Ionic salts of non-miceulluar surfactants such as cationic TMA, TEA, TPA, were used all used at the same concentration as that of cationic DOD above while the anionic SMS and SPS were used at the same concentration as anionic SDS above. This was done to help eliminate any potential concentration effects that may occur from excess ions in solution or swamping effects. As with the micellular surfactants, a total of 12 solutions were prepared, however, in this case 11 solutions were created by quantative dilution from the largest concentration as there are no micellular equilibria to avoid.

Table 2.2 below shows a summary of the characteristics of all extrinsic ion used within this work.

Table 2.2 Characteristics of extrinsic ions used

Extrinsic Ion	CMC (M)	Carbon Chain	Concentration Range (M)
$CaCl_2$	—	—	6×10^{-5} – 0.012
K^+	—	—	6×10^{-5} – 0.012
DOD	0.012	$C_{12}H_{27}$	6×10^{-5} – 0.012
SDS	0.008	$C_{12}H_{27}$	4×10^{-5} – 0.008
DEC	0.005	$C_{10}H_{23}$	2×10^{-5} – 0.005
TMA	—	CH_3	6×10^{-5} – 0.012
TEA	—	C_2H_5	6×10^{-5} – 0.012
TPA	—	C_3H_7	6×10^{-5} – 0.012
SMS	—	CH_3	4×10^{-5} – 0.008
SPS	—	C_3H_7	4×10^{-5} – 0.008

2.3 Thin Film Preparation

Thin solid films of CPEs and CPE with additives were created through spin coating concentrated solutions at various speeds, volumes, and accelerations dependant upon the CPE being spun. For a material to be spin coated effectively, the CPE itself needs to be reasonably viscous so it can spread evenly across the surface and also needs to be in a volatile solvent for rapid evaporation. This allows materials such as P3HT in chloroform and FPQ-Br in methanol mixtures to be easily cast through single step spin coating due to the increased volatility of the solvent mixtures. Materials such as PTEBS in distilled water however require much more effort and multiple step casting programs. The following will detail the process in which thin films of all CPEs were cast and give detail on the programs used for casting. In all cases

below, solutions requiring additives were prepared at least 1 hour before casting to allow time for equilibriation between CPE and additive.

2.3.1 General Methods for Thin Film Casting

All thin solid films are cast onto precleaned substrates. The substrates are cleaned throughly via sonication for 15 minutes in acetone followed by isopropanol (IPA) and then air dried. Substrates used for thin films are fused silica (spec2000) for optical characterization and silicon dioxide on silica for transistor devices. The cleaned substrates are then placed onto the spinning chuck and held in position via a vacuum. A high pressure stream of nitrogen is then passed over the substrate to remove any remaining dust or particulates that may have settled on the substrates.

All films were cast out of solutions as described above in the "Solution Preparation" section. Volumes and spin speeds of solutions used are specific to the polymers used and shown below. Accelerations used were such that the desired spin speed was reached within 1 second. All solutions were left to spin until all the solvent was evaporated. In some cases this required multiple step spin processes. The films are stored in a clean container which was wrapped in foil and placed under vacuum until required in order to minimize any possible degradation that may occur before analysis could be completed. The conditions for spin coating of each polymer was kept constant for each polymer analyzed and is summarized below in Table 2.3

Table 2.3 Spin coating parameters used for casting thin films of polymers

Polymer	Conc.(mg mL^{-1})	Vol. (μL)	Spin Speed (rpm)	Time (s)
PTEBS	3	120	8000	30
FPQ-Br	3	70	5000	30
FPQ-PB	3	100	3000 / 8000[a]	30 / 30[a]
FPQ-IB	3	100	3000 / 8000[a]	30 / 30[a]
P3HT	2.5	80	2500	40
P3HT[b]	10	80	2500	40

[a]Two spin modes were required for casting. Initially the thin film was cast at 3000 rpm for 30 seconds. The speed was then increased to 8000 rpm for 30 seconds to allow for drying/removal of excess DMSO.

[b]The increased concentration of P3HT was used in device fabrication.

2.3.2 Device Fabrication

Transistor type devices were fabricated using P3HT at 10 mg mL^{-1} in chloroform and directly adding various concentrations of additives (also in chloroform) to the P3HT stocks. The substrates used were silicon with a 100 nm silicon dioxide dielectric directly grown on top of the silicon substrate. P3HT films were cast onto the precleaned substrates using 80 microlitres of solution at 2500 rpm with an acceleration of 2450 m s^{-2}. The films then had 50 nm gold electrodes deposited onto the film via thermal evaporation with an Angstrom Engineering Nexdep evaporator. The fabricated devices were then stored separately, away from sunlight, and under vacuum.

The devices were composed of a silicon bottom gate with silicon dioxide dielectric, P3HT with DOD surfactant conducting media, and 50 nm gold source and drain electrodes separated by a 100 μm channel. Three different devices were created with different concentrations of DOD added. All devices were fabricated at the same time using the same batch of polymer and surfactant solutions. The properties of created devices is summarized below in Table 2.4

Table 2.4 Properties of fabricated P3HT devices

Polymer Layer	Back Gate	Source / Drain	Dielectric	Channel
P3HT	Si	50 nm Au	100 nm SiO_2	100 μm
P3HT-DOD 0.02 w%[a]	Si	50 nm Au	100 nm SiO_2	100 μm
P3HT-DOD 0.0002 w%	Si	50 nm Au	100 nm SiO_2	100 μm

[a] w% refers to weight percent of polymer in solution.

2.4 Characterization Techniques

2.4.1 Optical Characterization

Optical characterization was completed using absorbance and fluorescence measurements. All solution phase measurements were taken using the standard equipment provided with the instrument. Solid phase measurements were completed using in house absorbance and fluorescence mounts to position the thin film substrates. Where possible, all optical characterization was completed on the same day to avoid degradation.

Absorbance Measurements

All absorbance (UV-Vis) measurements were taken on an Agilent 8453 UV-Visible spectrophotometer scanning over the range 220-1100 nm. Samples were analyzed using 4 mL quartz cuvettes with 1 cm path length. In all cases, blanks of solvents were run as backgrounds and stored as necessary. Optical data was normalized by setting an inital zero absorbance point where the CPEs have minimum absorbance.

Fluorescence Measurements

Fluorescence spectroscopy was performed with a Shimadzu RF-5301PC spectrofluorophotometer using a quartz cuvette with a 1 cm path length and four polished sides. The slit widths on the spectrofluorophotometer were set differently for each CPE due to differences in the quantum efficiencies of the polymers. For PTEBS the slit widths were set to 5 nm, 1.5 nm for the FPQ-X series, and 5 nm for P3HT (for both excitation and emission). In some cases, emission intensities became too large for the initial slit widths with increased additive addition. In these cases a reference point was taken at the initial slit width and normalized to the new slit width. For the samples, in all cases the excitation wavelength was set to the maximum measured absorbance wavelength and all samples were normalized by dividing the emission intensity by the absorbance to remove any variation due to changes in absorbance.

2.4.2 Physical Characterization

Dynamic Light Scattering Measurements

Dynamic light scattering (DLS) measurements were recorded on a Malvern Zetasizer Nano-ZS. Samples were measured in a 4 polished side quartz cell with a 1 cm path length at 25°C. Absorbance at 632 nm and refractive indices were set accordingly for each CPE to allow for accurate size calculations. The size for each sample was recorded 4 times per run and each run repeated at least three times until concordant good quality reports were achieved. Any poor quality report measurements were ignored and the samples were re-run. The variation in the particle size measurements for each sample was taken as the uncertainty in the measurements.

Surface Tension Measurements

All surface tension measurements were taken on a NIWA technology surface pressure sensor type PS4 surface tension meter. Double distilled deionized water was used as the reference and zero point. All samples that were analyzed through surface tension were created in double distilled deionized water as a substitute for distilled water and made in the same fashion described in the "solution creation" section. 25 mL solutions of CPE and CPE with additive solutions were prepared individually in clean glass vials at the optical concentration. All samples were repeated 3 times with the variation in surface tension taken as the uncertainty in the measurement.

2.4.3 Transistor Characterization

All fabricated transistor device characterization was completed using an Agilent 4156C semiconductor analyzer with probe station in the VUW clean room. Devices were loaded onto the sampling stage and held in position via vacuum. The analysis used the organic field effect transistor (OFET) type configuration with a source, drain, and gate probe attached to the source, drain, and conducting gate stages respectively. All measurements were repeated multiple times to test for variations in the measurements and all samples were compared directly to a control sample prepared at the same time as the test samples.

All base transistor measurements were completed by scanning the samples over a 15- -50V range source/drain range with gate voltages ranging from 0-50 V. All samples were tested at all 6 sets of electrodes on each fabricated device allowing for multiple data sets to be taken for a single sample. non-operational electrode sets were ignored when comparing data.

Measurements taken over time at a set source and gate voltage were completed using the repeat scan function and a stop watch for timing. The repeat scan was allowed to run for a set length of time (1-2 minutes) then single scans were taken and saved and repeat runs were allowed to continue again for the required time. All single runs are directly compared to each other and that of the control.

Chapter 3

Dependence of CPE Photophysics on Solvent Composition and Salt Content

3.1 Introduction

Aggregation and modification of the backbone configuration within aggregates is shown to have large effects on the characteristics of CPs, PEs, and CPEs alike. Unlike PEs, CPs and CPEs have the added benefit of a π-conjugated backbone allowing for further characterization through optical spectroscopy. The resulting spectra are highly sensitive to changes in the aggregation state of the CPs or CPEs[33] thus allow for probes into aggregation states of CPEs in solution.

A very powerful tool for inducing inter- and intra-molecular changes in the aggregation state of CP and CPE systems is through changes in solvent or solvent composition. In both CP and CPE cases, addition of a favorable solvent (good solvent) will result in high level of solubility of both the side chains and the backbone of the polymer resulting in isolated, free chains in solution with little inter- and intra-molecular interactions.[99,100] In contrast, addition of a less favorable solvent or a solvent that favors side chain solubility in preference to the backbone (a poor or bad solvent) results in self-assembly of the backbone into aggregates via polymer folding to form intra-molecular aggregates, and stacking of neighboring polymer chains results in inter-molecular aggregates.[101,102] Thus, changes in the solvent used has large effects on the optical and physical character of the CP or CPE in solution.

CPEs are structures that have both ionic side chains and a hydrophobic conjugated backbone. The dual ionic and hydrocarbon character of CPEs allows for both hydrophobic (CPE backbone) and hydrophilic (CPE ionic side chains) interactions when dissolved into a solvent. This results in a single solvent being unable to favorably solvate both the hydrophilic (ionisable side chains) and hydrophobic (π-conjugated backbone) components of CPEs. Thus, solvent composition effects have interesting results on CPE solutions due to high concentrations of a good (or bad) solvent resulting in unfavorable interactions to one component results in unfavorable interactions with the other.[31]

Changes in the ionic strength of solutions through metal ion addition have also been shown to result in changes in the optical nature of CPE solutions. Low concentration metal ion addition results in the solvent environment becoming increasingly polar causing the solvation of the CPE backbone to be reduced. This results in CPEs inter- and intra-molecular π-interactions to increase in order to reduce the number of interactions with the increasingly unfavorable environment with subsequent changes in the optical character previously discussed.[103]

The introduction of metal salts has been shown to result in distinct changes in the optical character of the CPEs depending on the valency of salt (monovalent or divalent) and the specific salt used. Kuar *et al.* have shown that monovalent salts such as sodium chloride (NaCl) have varying degrees of interaction with CPEs based on the absolute concentration of salt used. In the low concentration ($\leq$100 mM) range little effect on the optical character of the systems is seen due to low levels of ionic screening of the CPE side chains. Small levels of fluorescence quenching are seen due to changes in the ionic strength of the solvent causing increased unfavorable interactions and subsequent increase of the π-orbital overlap of CPE aggregates. Increased concentration ($\geq$100 mM) has been shown to induce aggregation of the systems due to high levels of electrostatic screening of the charge. The subsequent accumulation of ions with the CPE causes changes to the CPE chain configuration and stiffening of the polymer chain.[34]

Multi-valent metal ions have the potential to induce aggregation differently than their monovalent counterparts. The divalent nature is shown to be able to cross-link neighboring aggregates resulting in bridged aggregate structures.[37,39] Tests with a wide range of divalent metal salts have been completed with the concentration and type of ion again being shown to have large effects on the interactions seen with the general trend of increased valency of the salts, induces larger aggregates.[104] The nature of the salt used is also shown to have potential to alter the aggregate structure itself (disordered, H-type, J-type). Specific salts have been shown to induce

H-aggregates in peptide tethered perylene bisimide due to the bridging effect of the divalent metal ion causing compaction of the aggregate system.[105]

This chapter investigates the effect of solvent composition and ion addition on the optical characteristics of the CPE PTEBS. Four different solvents are tested at various solvent compositions in water through absorbance and fluorescence spectroscopy. Both monovalent and divalent metal ion additions are also examined over a range of concentrations with varying effects. Further experiments using organic ionic salts to combine favorable electrostatic and van der Waals forces are also completed with three different organic salts. Finally, a model for the interactions of the organic salts with PTEBS is proposed to explain the observed changes in the optical character of PTEBS.

3.2 Effect of Solvent Composition and Polarity on the Optical Characteristics of PTEBS

The normalized absorption and emission spectra of 1.8×10^{-5} M PTEBS in distilled water is shown in Figure 3.1. The black peak shows the broad absorption spectra of PTEBS in water. The absorption wavelength maximum of PTEBS is shown to be 401 nm in distilled water with the lack of any thiophene vibrionic features indicating the presence of aggregation throughout the solution. The fluorescence spectra peaks at 587 nm in distilled water and is featureless with the small shoulder at approximately 520 nm being due to scattering from the excitation lamp.

The effect of solvents on the optical characteristics of PTEBS was examined through UV/Vis and fluorescence spectroscopy. Solutions of 1.8×10^{-5} M PTEBS with ethanol (EtOH), acetone (Me_2O), acetonitrile (MeCN), and tetrahydrofuran (THF) were analyzed with at 0, 10, 20, 30, 40 and 50% solvent compositions in distilled water. EtOH, Me_2O, MeCN, and THF were chosen as solvent additives due to their high miscibilty in water and differences in both structure and polarity. Direct comparisons between the PTEBS in distilled water and that of the solvent compositions are made with conclusions of interactions causing the observed changes.

A plot of the absorption maximum of PTEBS with different solvent compositions is shown in Figure 3.2. The absorption spectra show the same line shape throughout all solvent compositions with little change in the absorption intensity. Significant red shifts of the peak maximum with increased solvent composition were observed in the range of 10–30% for MeCN, Me_2CO, and EtOH and 10–40% for THF. The higher

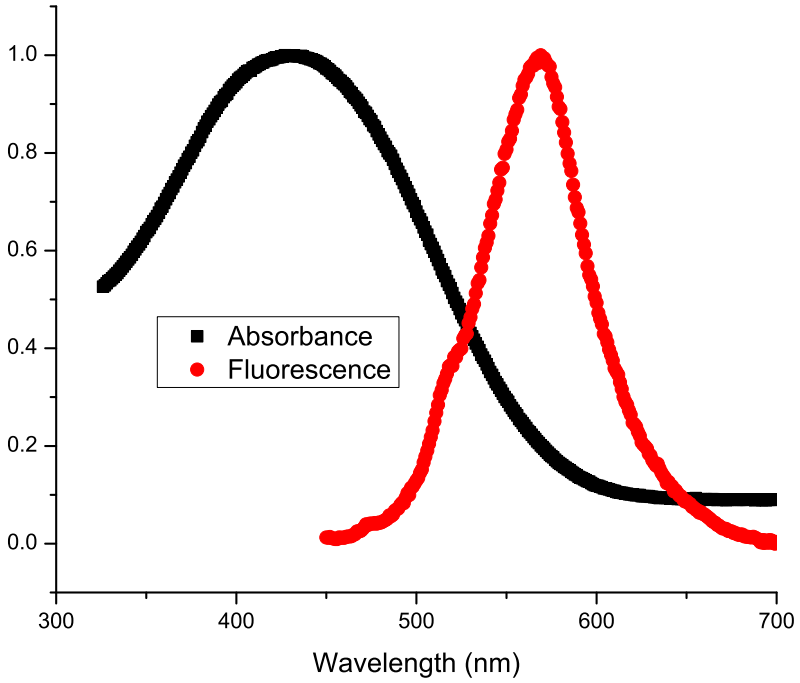

Figure 3.1 Normalized absorbance and fluorescence spectra of PTEBS in distilled water.

30–50% solvent composition (40–50% for THF) showed a plateau in absorption wavelength coresponding to 427 nm for Me_2CO, MeCN, and EtOH and 420nm for THF. A blue shift to 420 nm was observed with EtOH solvent additions at 50% solvent composition matching that of THF. The 10 and 20% THF composition ranges are not shown in the plots due to clouding of the solutions causing scattering in the optical measurements.

Fluorescence emission spectra of all above mentioned solutions were obtained with the excitation wavelength set at the recorded absorption maximum for each solution. Excitation slit widths and scan ranges were kept the same throughout all experiments to allow for direct comparison between the original PTEBS solutions and the different solvent compositions. The collected emission intensity (I) is plotted in reference to the intensity of PTEBS in pure water (I_0) in order to show magnitude increases with solvent composition.

A plot of the maximum fluorescence emission for all solvent compositions is shown in Figure 3.3. The emission intensities for all solvent compositions were observed to have a large increase with increased percentage composition of each solvent tested, peaking at varying levels. All solvents showed similar early range effects however with little variation in emission intensities <20% solvent composition range and only

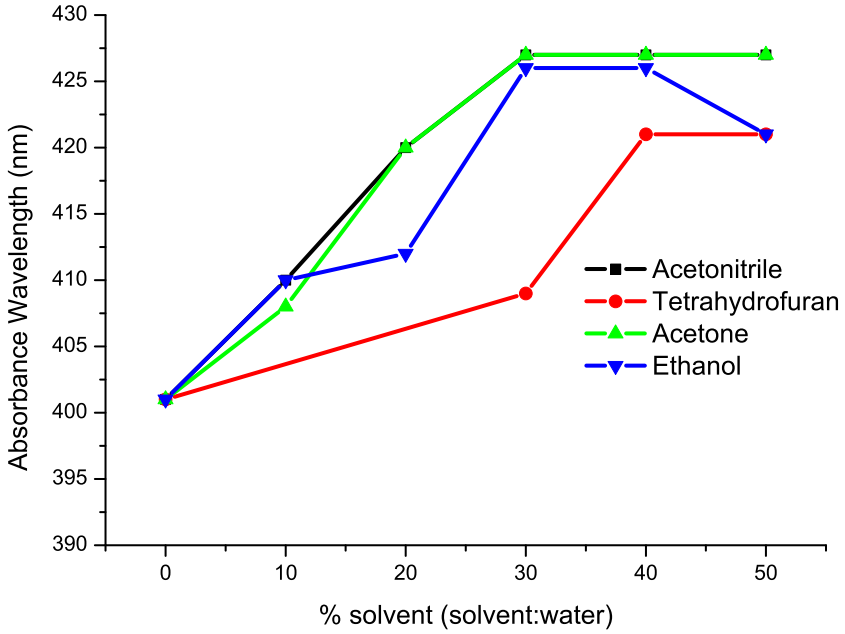

Figure 3.2 Plot of PTEBS absorbance wavelength with changes in solvent environment. All solvent addition results in large redshifts showing changes in the aggregate structure of the CPE backbone.

small deviations (I/I_0 between 4.5 and 5.5) at the 30% solvent compoisition point.

Large deviations in fluorescence emission intensity between the solvent compositions examined occurred within the 30–50% composition range. MeCN and Me_2O had the smallest increase over this range (I/I_0 of 4.5 and 6 respectively) with the bulk of the intensity increase being within the 10-30% solvent composition. A general plataeu in emission intensity with the final 40 and 50% solvent compositions with a slight rise in intensity was seen for Me_2O (I/I_0 increases from 4.5–6). EtOH and THF both exhibited both larger overall emission intensity increases (I/I_0 of 7.5 and 9.5 respectively) and longer composition range interactions (10–40%) in comparison to the Me_2O and MeCN indicating increased effect with these solvent compositions. Little change was observed in the line shape or emission wavelength in the spectra of the examined samples.

The observed red shift to 427 nm of absorption wavelength for Me_2O, MeCN, and EtOH over the compositions between 10–30% regardless of type of solvent indicated a change in ordering of the CPE hydrophobic backbone within the aggregates resulting in formation of π-π interactions. The common nature of this shift observed with all solvents within the range further indicated that the effect reaching an equilibrium ordering of the backbone at 30% solvent composition solutions. This effect is further evident in the fluorescence emission spectra. The observable increase in emission

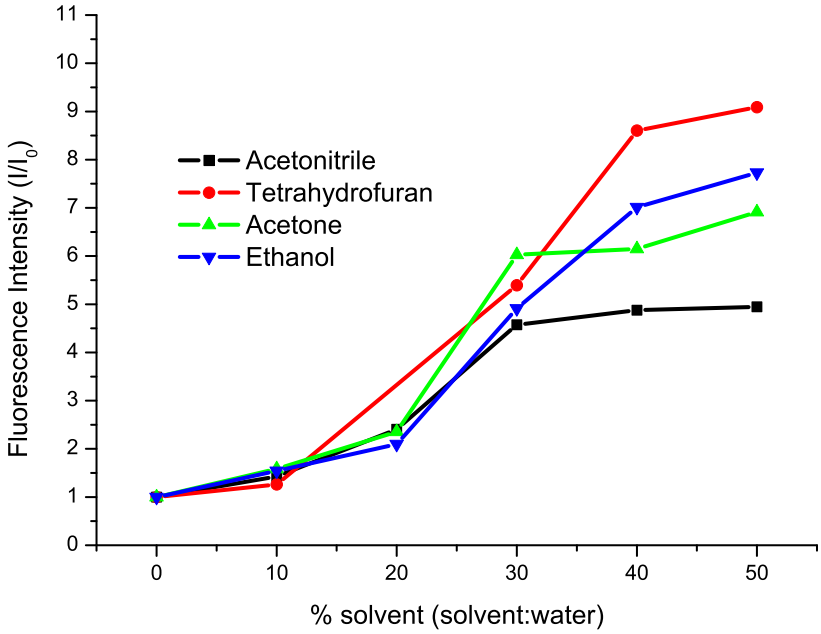

Figure 3.3 Plot of PTEBS fluorescence intensity with changes in solvent environment.

intensity to approximately 1.5 times PTEBS in pristine distilled water over the 10–20% solvent composition range, regardless of solvent analyzed shows that during this stage, reinforces the π-conjugated backbone reordering proposed. The observed increased fluorescence itensity over all solvent compositions also with associated red shift shows that there is also likely two different interactions occuring within the solvent addition system.

The large deviations in observed fluorescence intensity above 30% solvent composition between the diffferent solvents indicates a deviation of the equilibrium structure due to the type of solvent added. This effect is probably due to the differences in polarity between the solvents studied and their relative ability to solvate the CPE backbone. MeCN and Me_2O are the most polar of the solvents added with dipole moments of 3.92 and 2.91 respectively. The relatively high dipole character of these solvents results in little favourable interaction of the CPE backbone past the proposed reorganisation with little changes in the π–π interactions past this point. This results in the observed plateau in emission intensities and absorption wavelength.

THF and EtOH both have comparatively low dipole moments of 1.61 and 1.69 respectively, greatly reducing the overall hydrophobicity of the solvent system. The low dipolar and hydrocarbon nature of these solvents allows for the CPE backbone to begin to be partially solvated within the higher (30-50%) solvent:water composition ranges. With increased solvation of the backbone, the inter- and intra-molecular

π–π interactions are reduced resulting in a greatly increased emission intensity and blue shift in absorption wavelength.

This leads to the tentative proposal that the initial solvent interactions between the 10–20% solvent regime are likely due to the relaxation of the intra-molecular aggregation states within the system coupled with formation of favorable inter-molecular π-interactions to reduce the remaining hydrophobic effect. The combination of these effects would account for the red shifted absorption due to the formation of the inter-molecular π-interactions while also limiting the fluorescence intensity increase due to the relaxation of the coiled intra-molecular π-interactions. Due to the limited evidence, this cannot be accurately assigned however.

Given that the above proposal is correct, the higher solvent concentration effect are likely due to the partial solvation of the backbone to differing levels dependant on the polarity of the solvent. Partial solvation allows for the backbone inter-molecular interactions to be reduced allowing for a reduction in the inter-molecular fluorescence quenching. The lower polarity solvents (EtOH and THF) allow for increased relaxation of the backbone thus reducing the inter-molecular interactions the greatest resulting in the observed large fluorescence increase and blue shifted absorption at higher concentrations.

Both low (0-30%) and high (30-50%) solvent composition, as well as the polarity of solvent being utilised, has been shown to have large effects on the optical characteristics of CPEs. The low solvent composition range of all solvents results in a reorganisation of the CPE backbone within the aggregate causing an approximate 4.5 fold rise in fluorescence intensity with an associated red shift in absorption wavelength. Higher solvent composition effects have been shown to be linked to the polarity of the solvents used where the lower polarity allows for partial solvation of the CPE backbone causing further increases in fluorescence intensities and blue shifts in absorption wavelength.

This section has shown that controlling the structure of the CPE backbone through reorganization and solvation allows for effective control of the optical characteristics of CPEs in aqueous environments. Throughout this section the main focus has been on the interactions of the backbone within aggregates due to the optical nature of CPEs coming from this system. The following section investigates these ionic side chain interactions and the effects ionic salt addition has on the optical and physical characteristics of CPEs.

3.3 Effect of metal ion addition on the optical and physical characteristics of PTEBS

The effect of metal ions on the optical and physical characteristics of PTEBS was examined through UV/Vis absorption and fluorescence spectroscopy. Solutions of 1.8×10^{-5} M PTEBS with monovalent potassium bromide (KBr), and divalent sodium sulfate (Na_2SO_4) and calcium chloride ($CaCl_2$) additions were analyzed over a range of additive concentrations (0–1.2×10^{-2} M). For ease of comparison, the following section will be split into PTEBS with monovalent cation and divalent cation additions.

3.3.1 PTEBS with Monovalent Salt Additions

Solutions of PTEBS with KBr addition of 0–1.2×10^{-2} M were prepared and analyzed individually through UV/Vis absorption and fluorescence emission spectroscopy. All emission spectra were excited at the absorption peak maximum and all data normalized for variation in the absorption intensity. Only the fluorescence emission intensity is presented due to little changes seen in absorption and fluorescence wavelengths with the addition of these cations.

The relative fluorescence emission intensity of PTEBS for a range of KBr additions is shown in Figure 3.4. From this figure it can be seen that there was an initial drop in fluorescence intensity with 4×10^{-5} M KBr addition to approximately 80% that of the PTEBS in distilled water. This is followed by a plateau in emission intensity across the range of 1×10^{-4} M through to 1.1×10^{-3} M concentration of KBr. There was then a further drop in fluorescence emission intensity to approximately 72% at 2×10^{-3} M KBr addition followed by a further plateau in emission intensity over the remaining KBr addition (to 1.2×10^{-2} M).

The addition of KBr has a two fold effect. Direct addition or substitution of the K^+ ion with the natural PTEBS sodium counter-ion causing changes in the counter-ion effects and/or ion condensation type effects, and secondly, a solvent ionic strength effect similar to that described in the solvent composition section above where the increased ionic strength of solvent causes changes in the CPE backbone aggregate structure. Both of these effects are seen with KBr addition and are related to the two quenches and subsequent plateau in fluorescence intensity seen in Figure 3.4.

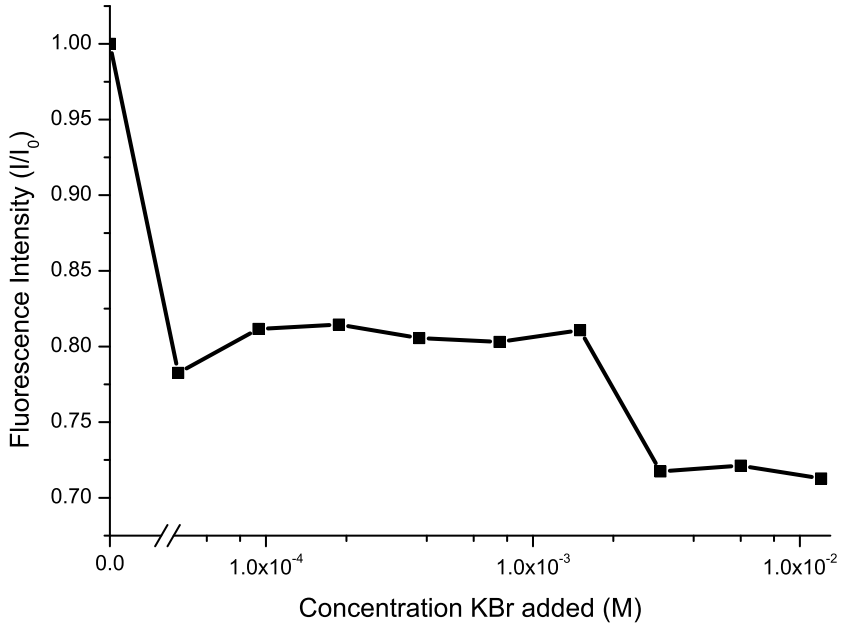

Figure 3.4 Plot of PTEBS relative (I/I_0) fluorescence intensity with varying concentration of monovalent KBr addition.

Due to the lack of any further information obtained, it is impossible to assign the two interactions directly to their relative plateau. It is known however that in PE systems with salt addition, there are distinct interactions with increased salt concentrations. Dobrynin, and M. Rubinstein,[106] detail the competition between the entropic and electrostatic interactions with salts and PEs. The authors show examples where there is direct competition between the electrostatic attraction between PEs and salts and the resulting increased entropy due to the localization about the side chains. This effect is shown to be directly related to the concentration of PE with low concentration PE resulting in the preference for the entropy favored free counter ions in solution and high PE concentration favoring the electrostatic attraction causing a stiffening of the polymer chain and eventual coiling and collapse of the chain upon itself increasing the intra-chain interactions.

Applying the theory from Dobrynin *et al.* and that of the ionic strength changes discussed in the introduction[103] to the current KBr salt and PTEBS system, the PTEBS is at a concentration of 1.8×10^{-5} M which can be considered to be in the low concentration regime. This shows that there is likely to be little electrostatic interactions between the CPE and salt during the early (1×10^{-4}–1.1×10^{-3} M) salt concentration addition. The initial drop in observed fluorescence intensity can be attributed to the increased ionic strength of solution effect. The increased ionic strength of solution would cause an increased level of unfavorable interactions of the hydrophobic CPE backbone resulting in increased inter- and intra-molecular π–π

interactions with subsequent fluorescence quenching.

The high concentration 2×10^{-3}–1.2×10^{-2} M salt addition fluorescence intensity decrease must be due to the direct addition of ions to the CPE caused by electrostatic interactions between the CPE side chains and the salt. This effect causes stiffening of the polymer chain and further cooperative ion attraction to the CPE. This causes rapid ion addition to the CPE once some ions are bound, causing the CPE to stiffen and then collapse into changes in the coiled structure. The tighter coiling results in further increases in the inter- and intra-molecular fluorescence quenching causing the observed decrease in fluorescence intensity. This effect has shown to be both CPE chain length, and salt concentration dependant.[36,107] As the fluorescence quenching observed is only 10%, it is likely that only the initial stages of this effect is observed.

This shows that altering the side chains through monovalent ion addition can result in subtle (with potential for much larger) alterations of the optical and physical characteristics of CPEs via solvent like ionic strength effects and direct electrostatic coupling to the CPE. These effects are not limited to monovalent ions however. Divalent have the potential to bind to multiple monomer units giving rise to the potential to further alter the characteristics of CPEs. Divalent ionic salt addition is studied in the next section.

3.3.2 PTEBS with Divalent Salt Additions

Solutions of PTEBS with $CaCl_2$ and Na_2SO_4 additions (0–1.2×10^{-2} M) were prepared and analyzed individually through UV/Vis absorption and fluorescence emission spectroscopy for optical characteristics. All emission spectra were excited at the absorption peak maximum and all data normalized for variation in the absorption intensity.

The relative emission intensities of solutions of PTEBS with $CaCl_2$ and Na_2SO_4 can be seen in Figure 3.5. Na_2SO_4 additions showed a gradual decrease in fluorescence intensity to approximately 80% that of PTEBS in distilled water over the 0–6×10^{-4} M Na_2SO_4 concentration range. A plateau in fluorescence emission intensity then follows accross the remaining concentration range (6×10^{-4}–1.2×10^{-2} M). $CaCl_2$ showed a much more abrupt decrease in emission intensity comparable to that of the KBr additions (Figure 3.4). Initial addition of $CaCl_2$ resulted in a decrease in PTEBS emission intensity to approximately 70% that of PTEBS in distilled water followed by a linear decrease in emission intensity to approximately 55% over the remaining salt concentration range (1×10^{-4}–1.2×10^{-2} M).

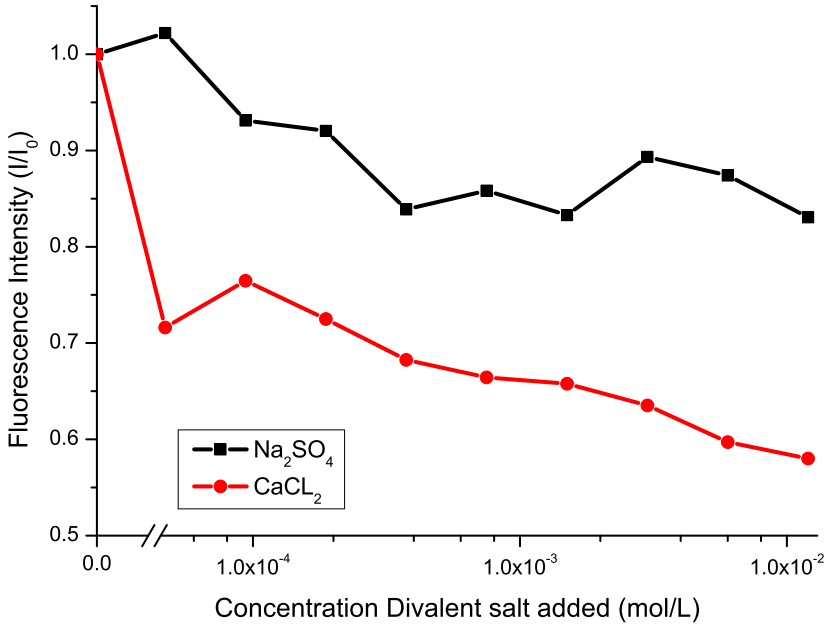

Figure 3.5 Plot of PTEBS relative (I/I_0) fluorescence intensity with varying concentration of divalent $CaCl_2$ (red circles) and Na_2SO_4 (black squares) addition.

As can be seen, there are clear differences in interactions between the two divalent salt additions. The initial decrease in emission intensity over the 1×10^{-4}–1×10^{-3} M Na_2SO_4 concentration range is comparable to that of the initial fluorescence quenching seen with KBr addition. This indicated that the fluorescence intensity quench with Na_2SO_4 can be attributed to the increased ionic strength of solution causing increased inter- and intra-molecular π-interactions.

Increasing concentration of Na_2SO_4 in the PTEBS solution results in little change in the fluorescence intensity with the intensity fluctuating about the 80-85% region. This shows that unlike the K^+ ion additions with Br^- as the anion, there is no further electrostatic interactions of the $SO_4{}^{2-}$ ions with PTEBS in solution. This can be attributed to the noncomplementary charge of the $SO_4{}^{2-}$ ion resulting in electrostatic repulsion.

$CaCl_2$ additions resulted in a different effect in comparison to both KBr and Na_2SO_4. The instantaneous decrease in emission intensity is similar to that of KBr, however the linear decrease in intensity past this point is not similar to either Na_2SO_4 or KBr. This indicates the presence of competing interactions occurring with $CaCl_2$ additions to PTEBS solutions.

The initial quench to 80% can again be attributed to the change in conformation of the CPE polymer chain due to increased ionic strength as seen with both KBr

additions and Na_2SO_4 additions. This change in emission intensity is now common to all three studied salts showing that the ionic strength of solution has a large effect on the CPE optical characteristics regardless of salt added.

The linear decrease in emission intensity cannot be explained through ionic strength effects. This effect is hypothesized to be a cross-linking effect caused by the Ca^{2+} ions. This effect is a concentration dependant effect where the divalent ion cross-links two neighboring aggregates (Scheme 3.1) resulting in either larger aggregate formation causing increased fluorescence quenching pathways,[108] or cross-linking induced compaction of CPE aggregates resulting in reduced particle size but greatly increased inter- and intra-molecular fluorescence quenching[38] Particle size studies would need to be completed in order to distinguish the effect seen here. A further experiment that could be completed to test this effect is to add a trivalent cation such as Al^{3+} to the solutions. The increased valency of the ions would allow for further cross-linking of CPE chains resulting in a further quenching of the fluorescence intensity.

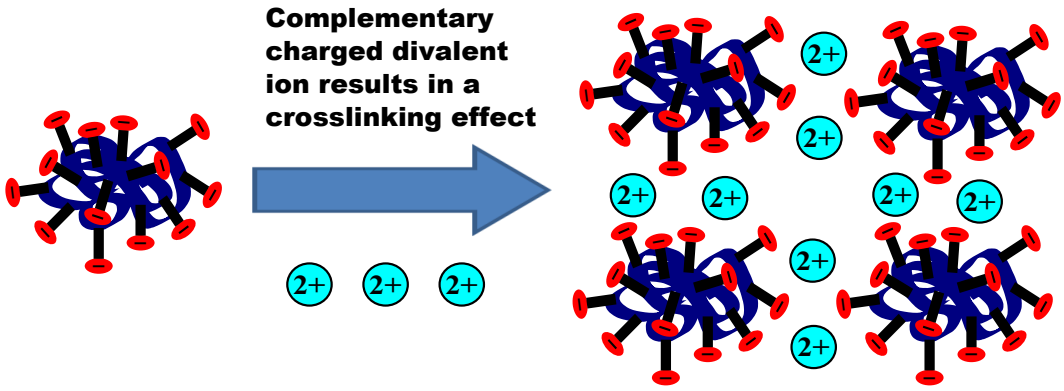

Scheme 3.1 Schematic of divalent metal ions on CPE aggregates. Addition of complementary charged ions results in cross-linking of aggregates with associated loss of fluorescence intensity.

The addition of ionic salts and solvents has been shown to have great effect in altering the relative fluorescence intensity of CPEs. The observed effects have been due to direct interactions with the CPE side chains through electrostatic attraction and through altering the ionic strength or polarity of the solvent causing changes to the CPE backbone. The following section discusses interactions with CPEs where the ion added has a combination of both favorable electrostatic interactions and hydrophobic interactions of side chains through studying the effects of PTEBS with non-micellular organic ionic salts additives.

3.4 PTEBS with Non-Micellular Organic Ionic Salt Additions

Solutions of PTEBS with tetramethyl ammonium bromide (TMA), tetraethyl ammonium bromide (TEA) and tetrapropyl ammonium bromide (TPA) additions (0–1.2×10^{-2} M) were prepared and analyzed individually through UV/Vis absorption and fluorescence emission spectroscopy for optical characteristics and dynamic light scattering (DLS) techniques for physical characteristics. All emission spectra were excited at the absorption peak maximum and all data normalized for variation in the absorption intensity. DLS measurements were tested multiple times each with testing being composed of three scans to account for variations in particle size calculations. Data shown are the relative emission intensities of all measured solutions and particle size and emission of TPA for comparative purposes. Little change was observed in absorption and emission wavelengths.

The emission intensities of TMA, TEA, and TPA are shown in Figure 3.6. As can be seen, with all additions there was an observable increase in fluorescence emission intensity to varying degrees. TMA was shown to have a small increase in fluorescence intensity to 1.2 times that of PTEBS in distilled water with the greater majority of the increase observed with the initial TMA addition (1×10^{-4} M). TEA was shown to have a greater effect with an initial increase to 1.3 times that of PTEBS in distilled water followed by an increase to 1.8 times that of PTEBS in distilled water with increased TEA concentration (2×10^{-4}–1.2×10^{-2} M). TPA was shown to have a much stronger effect than that of TMA and TEA with the emission intensities again rising to approximately 1.3 times that of the original followed by a superlinear increase to 3.5 times the emission intensity of PTEBS in distilled water with increased TPA concentration (2×10^{-4}–1.2×10^{-2} M).

As shown in the Introduction chapter, with increased emission it can be expected that there is a decrease in particle size due to the loss of the inter- and intra-molecular quenching states. As the greatest fluorescence emission intensity increase effect is seen with TPA additions, these samples were then further analyzed for changes in particle size. It is expected that with increased TPA concentration there will be an observed decrease in particle size due to a loss of inter- and intra-molecular π–π interactions (and associated fluorescence quenching) reducing aggregate size.

The particle size of PTEBS with TPA additions is directly compared to the observed fluorescence increase in Figure 3.7. It can be seen that there was scatter about the 9 ± 4 nm aggregate size with increased TPA concentration. This shows that there was

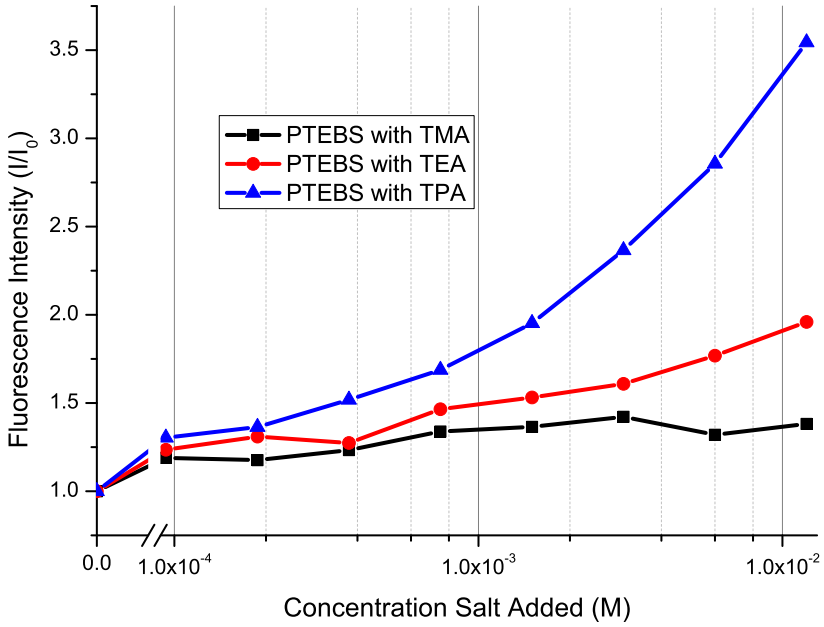

Figure 3.6 Plot of PTEBS fluorescence intensity with organic ionic salts TMA, TEA, and TPA

little change in the observed aggregate size with increased concentration while the associated fluorescence intensity increase remains showing that the two parameters are not linked in this case. The uncertainty about the PTEBS particle size in distilled water (approximately 9 nm) is due to the instrument and experimental error when measuring small particle sizes.

The distinct changes in emission intensity maxima with increased chain length (TPA>TEA>TMA) showed the interactions between the salt and CPE are alkyl chain length dependent with larger chain lengths resulting in increased fluorescence enhancement. Throughout the literature, this effect was commonly attributed to changes in the overall particle size of the aggregates and the degree of which the side chains can interrupt the CPE aggregate π-π interactions.[109,110] Again, this theory does not apply in this case due to the lack of particle size change, thus the bulk of the inter- and intra-moleculat interactions of the CPE–TPA aggregate remain. Cabarcos *et. al.* have completed a similar experiment using PTEBS and tetrabutylammonium perchlorate (TBA). The fluorescence intensity was shown to increase rapidly (faster than TPA), then plateau with increased concentration.[111] As the main focus of this study was superquenching, no explanation of the fluorescence intensity mechanism was discussed.

This leads to the proposal here of an effect localized to the surface of CPE aggregates without altering the physical size of the system. The complementary charged ionic

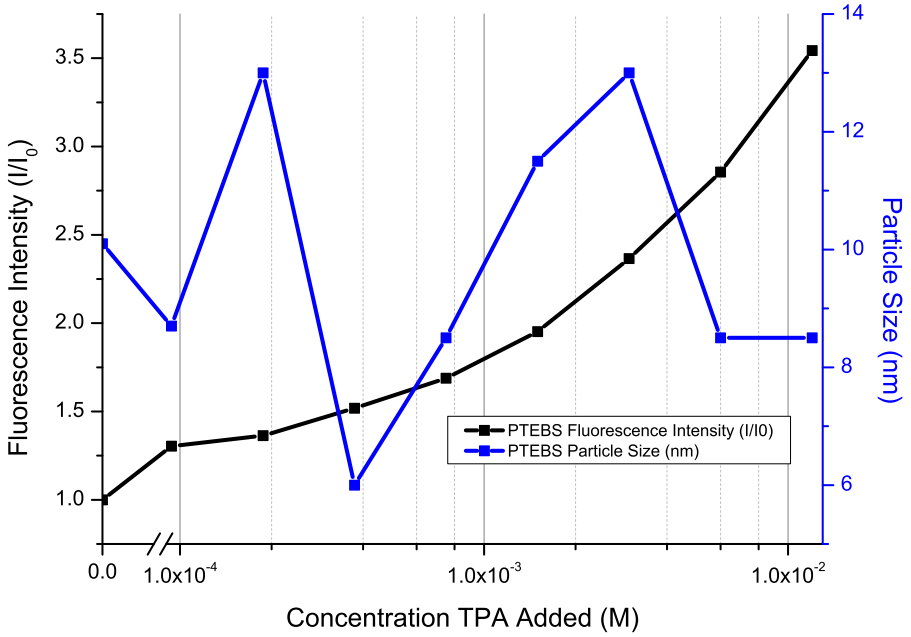

Figure 3.7 Plot of PTEBS fluorescence intensity and particle size with increased TPA concentration.

salts are driven to electrostatically associate to the CPE side chains at concentrations lower than expected for ion condensation via the hydrophobic effect of the salts alkyl chains. Once bound with the CPE side chains, the alkyl chains of the salt begin to sterically force the side chains of the CPE aggregates apart inducing a twisting of the CPE backbone. The twisting occurs via a "crowbar-like" steric effect of the salt pushing the CPE side chains away due to the size of the ionic salt being electrostatically bound. The effect is greater with increased ionic salt chain length due to the larger side chains of the salt having a larger steric demand thus forcing the side chains of the CPE further apart and increasing the twisting and associated disruption of the CPE backbone. The effect is proposed to be localized to the surface of the CPE aggregates causing only a small increase in the fluorescence intensity due to only a small portion of the CPE monomers being affected with little changes in the observed aggregate size. The localization to the surface of the aggregate would also result in a maximum achievable result, which may explain the plateau seen with TBA addition by Cabarcos *et. al.*. Scheme 3.2 shows a schematic of this effect with TPA and PTEBS causing the twisting of the PTEBS backbone.

Concentration and chain length dependant fluorescence enhancement effects were also seen when using the FPQ-X series of polyelectrolytes with the small alkyl chain organic salt sodium propyl sulfate (SPS), however, fluctuations about 10% quenching and mild fluorescence enhancement was noted with sodium methyl sulfate (SMS). The changes in the concentration based effects are not comparable as these salts

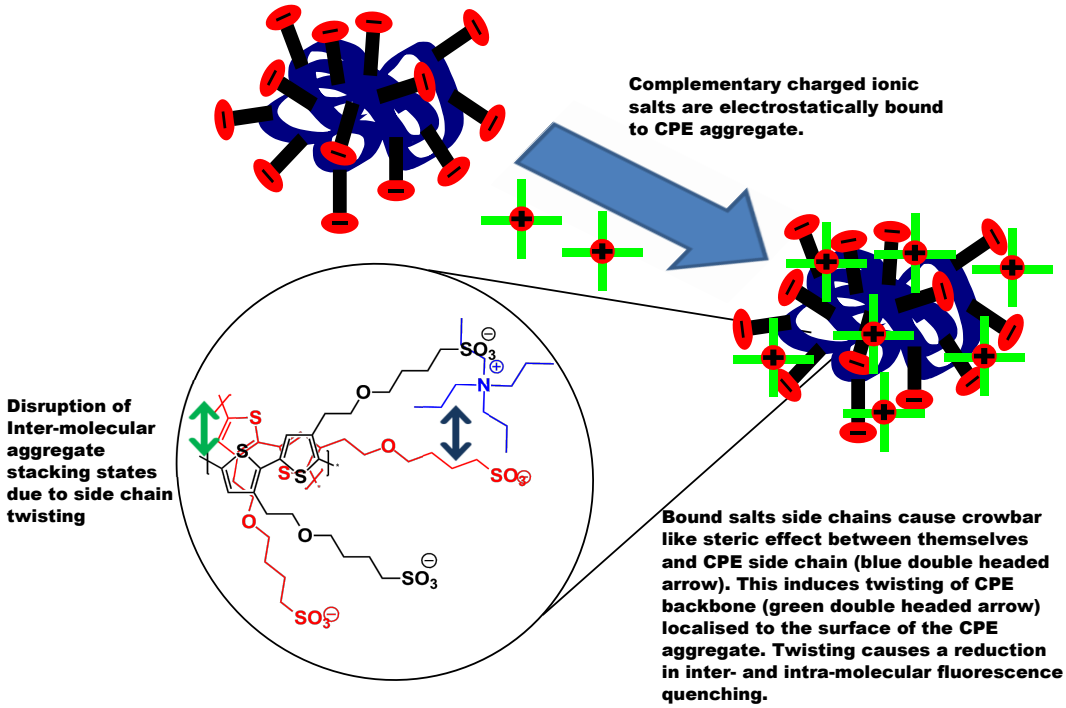

Scheme 3.2 Schematic of the proposed model showing non-micellular ions creating localized disruptions of π–π interactions due to crowbar-like steric prying of CPE aggregates.

do not have the same tetraalkyl configuration as the TMA-TPA series proposed to induce the steric effect. This further exemplifies the steric contribution to the fluorescence enhancement however. The plots of the FPQ-organic salts are shown in the appendix as Figure 9.1 and Figure 9.2.

3.5 Summary

This section has shown the changes in optical characteristics of PTEBS with different solvent compositions and differing concentrations of monovalent and divalent metal ions with proposals of interactions for the observed interactions. Optical and physical characteristics have been detailed for interactions of non-micellular organic salts with a proposed model for the observed interactions provided.

It was shown that relative solvent composition as well as polarity have a large effect on PTEBS absorption wavelength and emission intensity. The effect of PE to salt electrostatics and entropic forces have been linked to the observed data showing that the initial increase in both emission intensity and absorption wavelength are due to a change in polarity of the solvent causing the backbone of the CPE to rearrange regardless of solvent added. Further increases in emission intensity with higher solvent compositions have been linked to changes in solvation of the CPE

backbone due to the differing polarity of the solvents used.

The addition of metal salts have been shown to be have differing levels of effect on the optical characteristics of PTEBS also. All metal salts both monovalent and divalent have been shown to initially quench the fluorescence intensity due the increased ionic strength of the solution. Complementary charged ions have also been shown to bind and accumulate onto the CPE at higher concentrations resulting in increased intra-chain fluorescence quenching (monovalent salts) and inter-aggregate cross linking (divalent salts).

Non-micellular organic ion salts have been shown to have an interesting effect on the characteristics of PTEBS not explainable by conventional PE or CPE-salt interactions. Addition of these salts has been shown to have a large chain length dependent effect on the optical characteristics of the CPE without altering the particle size of aggregates in solution. A model of interactions has been proposed where the ionic salts induce changes to the CPE backbones localized to the surface of the aggregates.

Chapter 4

Dependence of CPE Photophysics on Surfactant Head Group and Concentration

4.1 Introduction

The process of surfactant addition to CPEs is a well studied phenomenon with numerous publications showing the effects of oppositely charged surfactants interacting with CPE systems over a wide range of surfactant concentration additions.[14,112] The observed change in the optical spectra induced by surfactant addition to CPE systems is known as "surfactochromicity", where the optical spectra of the CPE is dependant on the concentration of surfactant within the system.[113,114]

Due to the chromophoric nature of the CPE, the changes induced by the addition of surfactant can be effectively monitored through simple spectroscopic techniques such as UV/Vis absorption and fluorescence spectroscopy. These techniques are highly advantageous within these systems due to the optical properties of the backbone being highly sensitive to the local environment and aggregation state of the CPE systems.

Throughout the literature, there are many examples of surfactant complexes altering the optical signature of the CPE through inducing and reducing aggregation and/or chain collapse with various concentrations of surfactant addition. Commonly, the introduction of surfactant to CPE systems results in observed fluorescence enhancement or fluorescence quenching depending on the concentration of surfactant added

and the CPE used. These effects are discussed below.

Publications showing large scale fluorescence enhancement attribute the increase to effects due to surfactants having direct interactions with the side chains of the CPE. In these cases, the most common description of interactions involves the alkyl chain of the surfactant causing a reduction in the coil state of the backbone due to interrupting the π-interactions of the backbone within the aggregates. This causes rapid decreases in the inter- and intra-molecular fluorescence quenching states due to the uncoiling of the CPE aggregates.[110,115]

Publications that show highly quenched fluorescence intensity often also report the appearance of increased particle size,[116] excimer emission,[117] and decreased fluorescence lifetimes,[118] all of which indicate the presence of surfactant induced aggregation throughout the systems. Some speculation has been given as to the cause of such aggregates with authors attributing the aggregation to charge neutralization of the CPEs at what is known as the critical association concentration (CAC) where the surfactants replace the counter ions of the CPE resulting in a charge neutral polymer. With the lack of charge, the electrostatic repulsion between chains is decreased and hydrophobicity is increased thus further aggregation commences.[117,118]

The type of surfactant used is shown to have a significant effect on the interactions seen when complexed to CPEs. The use of non-ionic surfactants with CPE solutions such as Triton X[114] or polar alkyl chains[119,120] is shown to have little effect on the optical or physical characteristics in the concentration regime below the CMC of the surfactant. Post-CMC additions are seen to cause large enhancements of fluorescence intensities and dynamic blue shifts in the optical spectra. Small angle neutron scattering (SANS) or small angle x-ray scattering (SAXS) studies show long cylindrical micelles within the solution with the CPE embedded within the micelles with both charged and non-ionic surfactant addition.[114,120,121]

The changes in the optical characteristics are due to the changes in CPE environment once embedded inside the micelle structure. In this state, there are little to no unfavorable water–CPE backbone interactions resulting in the inter- and intramolecular interactions of these systems becoming greatly reduced. This results in a reduction in the inter- and intra-molecular red shifted fluorescence defect sites causing an observed blue shift in peak maxima and free CPE fluorescence emission enhancement.[114,120]

The differences in reports produced with different polymers can largely be attributed to the changes in polymer molecular weight and structure. A report by Kim and

et al. have shown that changes in the structure of the CPE has large effects on the way the polymer itself interacts at the air–water interface which may have large effects on further interactions with extrinsic ion addition.[122]

The high surfactant concentration (while remaining in the pre-CMC concentration) is often shown to result in increases in fluorescence intensity and has been then been shown to be at levels near (or at the CMC) of the surfactant used. For this reason, the authors of the studies then attribute a dramatic change in backbone structure of the CPE due to micelle formation which separates the neighboring polymer chains.[115,123] This effect is also further detailed with authors ascribing the electrostatic attraction of the CPEs to the micelles resulting in the CPE wrapping around spherical[115,124] or cylindrical micelles[125,126] resulting in highly elongated CPE backbones with little inter- and intra-molecular CPE-CPE interactions.

The surfactant alkyl chain length has also been shown to significantly alter the optical and physical spectra of CPEs. Monteserin *et al.*[109] has shown the effective fluorescence quenching is directly related to the alkyl tail length of the surfactant with the larger tails quenching fluorescence at a much greater rate. In all cases, the fluorescence quenching is at its lowest once the CMC of the surfactant is reached. Conversely, Laurenti *et al.*[110] has shown that the rate and level of fluorescence enhancement is increased by the alkyl tail length. These authors tested four surfactants of 8, 9, 10, and 12 carbon chain length and showed that the fluorescence intensity enhancement is greater than with the longer chain length surfactants.

Further research studies by Ruppelt *et al.*[127] have been completed within these types of structures where the amphiphilic type structure of the surfactant has been used as the counter-ion of the CPEs itself. The publication showed that the chain length and size of the surfactant counter ion can significantly alter the optical signature of films and devices made from these systems with variations in the spectra maxima being reported between 430 and 515 nm, depending on the surfactant counter ion used. Other publications have also shown that surfactant complexation also allows for much more sensitive sensor type applications.[78,128]

The general confusion of interactions seen within literature of CPE–surfactant assemblies and lack of investigation into the driving forces behind the specific interactions needs attention. The following sections attempt to give further insight into the driving forces behind CPE–surfactant assemblies and propose a model for interactions of complementary charged surfactants with both a cationic and anionic CPE. This is achieved by analysis and comparison of a range of surfactants that are complementary, non-complementary, and neutral in nature with both anionic

and cationic polyelectrolytes. In order to remove any pre and post-CMC surfactant concentration problems and chain length issues, all surfactants are used in the low (pre-CMC) concentration through to CMC concentration regime and have 10-12 carbon units in their alkyl tail.

The following chapter will detail the interactions between surfactants and the CPEs PTEBS, and FPQ-Br with a P3HT CP control sample also being used. For clarity and due to the length and complexity of direct comparisons between sections, the chapter will be split into the following sections:

- PTEBS with complementary charged dodecylammonium bromide (DOD) additions
- PTEBS with non-complementary charged sodium dodecylsulfate (SDS) additions
- FPQ-Br with non-complementary charged dodecylammonium bromide (DOD) additions
- FPQ-Br with complementary charged sodium dodecylsulfate (SDS) additions
- PTEBS with non-ionic decylamine (DEC) additions
- P3HT with non-ionic decylamine (DEC) and charged dodecylammonium bromide (DOD) additions
- Proposed model of full range of interactions
- Summary of the chapter.

4.2 PTEBS with Complementary Charged Surfactant DOD

The effect of trimethyldodecylammonium bromide (DOD) additions on the optical and physical characteristics of PTEBS was examined by UV/Vis absorption and fluorescence spectroscopy (optical characteristics) and DLS and surface tension measurements (physical characteristics). All emission spectra were excited at the absorption peak maximum and all data normalized for variation in the absorption intensity. All surface tension measurements were completed using a new whelmy plate for each new batch of solutions. Little change was seen in the peak shape for both absorbance and fluorescence spectroscopy with only small changes ($\pm$10 nm)

in wavelengths. For these reasons, only the fluorescence intensity, particle size, and surface tension plots of PTEBS with DOD additions are shown.

The fluorescence intensity, particle size, and surface tension measurements of PTEBS with DOD additions is shown in Figure 4.1. From this figure it can be seen that there were large variations in all three types of measurements undertaken and that they are strongly correlated. The data shown from each of the techniques will be described individually.

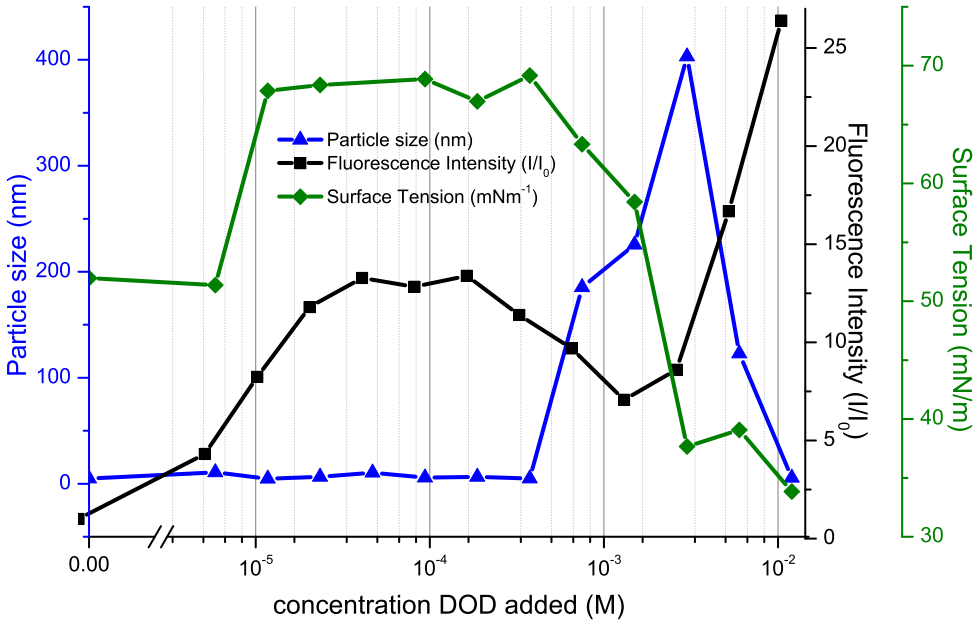

Figure 4.1 Plot of PTEBS fluorescence intensities, surface tensions, and particle sizes with increased DOD concentration. Shown are the normalized representative points from each spectra at each concentration of DOD analyzed.

The fluorescence intensity of solutions of PTEBS with DOD additions (I) (as a ratio of PTEBS in distilled water (I_0)) across the range of (0–1.2×10^{-2} M) is shown as the black squares in Figure 4.1. As can be seen, in the low concentration DOD addition (0–1.2×10^{-4} M) there was an observable 13 fold increase in PTEBS fluorescence intensity. This was followed by a pronounced decrease in PTEBS emission intensity across the range of 1×10^{-4}–1×10^{-3} M DOD addition. There was then a dramatic increase in fluorescence intensity over the 1×10^{-3}–1.2×10^{-2} M DOD addition range with the fluorescence intensity peaking at a 28 fold increase with the final analyzed DOD addition.

DLS particle size analysis is shown as the blue triangles on the same figure. Due to the scale of the plot, the initial change in particle size cannot be accurately viewed. During the initial 1×10^{-5}–4×10^{-4} M concentration range of DOD addition, the ob-

served particle size of PTEBS aggregates decreases from 22±5 nm through to 8±4 nm with the majority of the decrease occurring over the 0–5×10^{-5} M concentration range. There was then a large increase in aggregate size across the 4×10^{-4}–5×10^{-3} M DOD addition with aggregate particle size measurements peaking at approximately 400 nm. This was followed by a rapid decline in particle size across the remaining 5×10^{-4}–1.2×10^{-2} M DOD with particle sizes going back to 8±4 nm for PTEBS in distilled water.

The green diamond surface tension data initially showed little change with the first two solutions (PTEBS with 0 and 7×10^{-6} M DOD) surface tension remaining at approximately 50 mN m^{-1}. This was followed by an increase in surface tension to approximately 70 mN m^{-1} between 0–1×10^{-5} M DOD with subsequent plateau across the 1×10^{-5}–8×10^{-4} M DOD addition range. There was then a gradual decrease in surface tension to approximately 35 m Nm^{-1} with DOD addition across the 8×10^{-4}–4×10^{-3} M concentration range followed by fluctuations in measurements about this level through to the final 1.2×10^{-2} M DOD concentration analyzed. Comparisons to the DOD control are can be in the appendix as viewed as Figure 9.4.

In order to test the aggregation and general internal structure of the aggregates, time correlated single photon counting (TCSPC) experiments were completed on select solutions of PTEBS with DOD additions. The solutions chosen were PTEBS with no additives as a control, and solutions at 0.012, 0.06, and 0.03 M DOD concentration; relating to the solutions with large aggregates (0.03 M), decreasing aggregate size (0.06 M) and the solution with the highest fluorescence intensity (0.012 M). The fluorescence decays of these solutions are shown as Figure 4.2.

The fluorescence lifetimes of PTEBS with and without surfactant addition are very different with the lifetime measurements of the PTEBS–surfactant solutions resulting in non-exponential decays regardless of concentration of surfactant in the solutions. However, it can be seen that the lifetimes are dramatically accelerated with DOD additions in comparison to that of PTEBS in pristine distilled water due to the greatly increased gradient of the non-exponential (dispersive) fluorescence decay. This dispersive decay is also consistent with PTEBS chromophores occupying a wide range of environments within the aggregates which indicates a high level of disorder of the CPE backbone. The accelerated decays indicate increased inter- and intra-molecular interactions of the π-conjugated backbone indicative of PTEBS in an increased aggregate state.

The following discusses the observed data with comparisons to literature in order to attempt to decouple some potential interactions being observed. For ease of

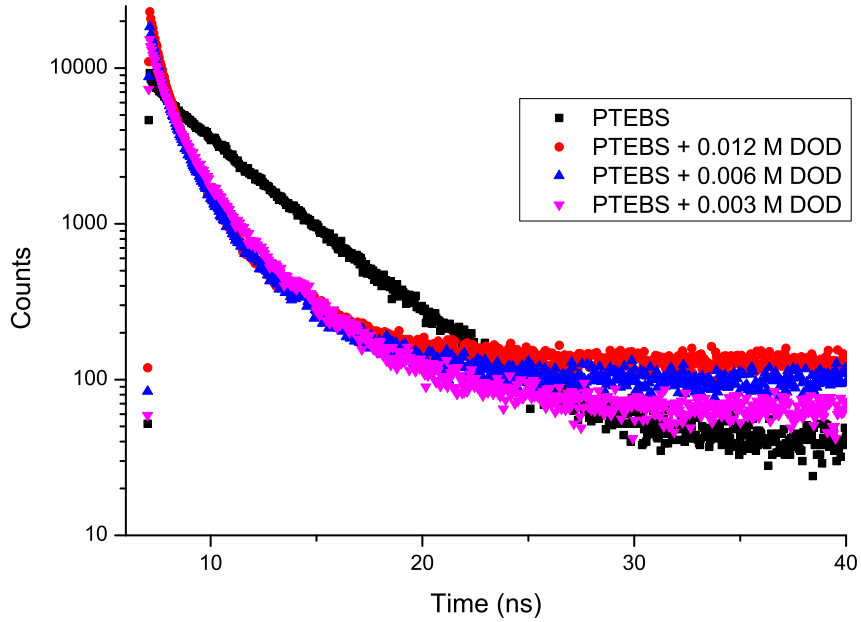

Figure 4.2 TCSPC data showing the change in fluorescence lifetime of aggregated PTEBS-DOD and unaggregated PTEBS without surfactant addition.

discussion, the data will be discussed in three sections with respect to DOD concentration. The first is that of the low concentration DOD addition (0–1×10^{-5} M) followed by the mid level DOD concentration (1×10^{-5}–8×10^{-4} M) and finally the high concentration level DOD addition (8×10^{-4}–1.2×10^{-2} M).

4.2.1 PTEBS with Low Concentration DOD Additions

The driving force and cause of the initial (0–1×10^{-5} M) changes of PTEBS optical and physical characteristics with DOD additions are not immediately obvious. The data show an observed increase in fluorescence intensity with only slight decreases in particle size. From chapter 3, it is known that low concentration additives result in effects that can be attributed to increased ionic strength which decreases the fluorescence intensity, while other changes such as favorable solvent composition alters the bulk solvent environment causing increases in the observed emission intensity.

From an ionic strength perspective, addition of DOD would result in an increased ionic strength due to the ionic character of the surfactant head group and counterion. This has been shown to induce further π orbital overlaps within CPE aggregates resulting in an expected decrease in emission intensity. As the PTEBS emission intensity is shown to be greatly enhanced, the ionic strength effects specific to DOD

addition must therefore be minor. The surface tension data also show a rapid rise in surface tension over the low concentration DOD addition range. This shows that the majority of DOD added is preferentially associated to the air–water interface rather than the bulk solution with the polymer. Thus in the initial additions of DOD having limited effects on the bulk solvent composition within this range.

Comparing the complementary DOD addition to other previously discussed systems, the only similar ion pairing interaction previously completed with PTEBS is that of PTEBS with TPA. As previously described in chapter 3, the comparatively large size of tetrapropylammonium bromide (TPA) molecule in all dimensions results in a twisting and steric disruption of CPE aggregates resulting in increased fluorescence intensity with no change in particle size due to the localized effect. The twisting and steric effect has been attributed to the side chains of the added salt forcing the side chains of the CPE apart with the increased length of chain causing increased steric disruption. With this is mind, DOD is composed of three methyl groups and a single dodecyl group. The hydrophobic demands of the long alkyl chain would result in the long chain preferentially being pointed towards (or embedded in) the aggregate resulting in any steric disruption effect of the aggregate (like those proposed in chapter 3) being a result of the remaining methyl side chains. This makes the structural and steric effects of DOD more related to that of tetramethylammonium bromide (TMA) than TPA, with TMA having a relatively low steric effect. Consequently, the observed initial increase in emission intensity cannot be directly attributed to this steric disruption effect proposed in chapter 3.

Similar surfactant concentration dependant fluorescence intensity plots have been shown throughout the literature. Johal *et al.* have published a study on the interactions of surfactant complexation with a cationic CPE derivative of poly(p-phenylenevinylene) (PPV). Within this study, the authors attribute the comparatively low fluorescence emission of the CPE without additives, to twisting of the aggregate backbone due to monomer–monomer ionic side chain repulsion. The authors then show that the initial increase in fluorescence intensity is due to ion pairing of the CPE and surfactant. This allows for relaxation of the twisting of the backbone due to reducing the repulsive CPE side chain interactions. The reduction in twisting of the backbone increases the inter-molecular π-π interactions with an associated red-shift in absorption wavelength.[77] It is important to note that PPV type monomers also have two side chains pointing in both directions whereas PTEBS only has one. This allows for PTEBS to effectively twist reducing any unfavorable electrostatic effects. Therefore electrostatic induced twisting is not being expected to be important in PTEBS systems.

With the above twisting and surfactant binding in mind, and applying these interactions to our system, with additions of DOD to PTEBS, blue shifts in absorption peak maxima were observed (see appendix Figure 9.3) indicating a disordering of the CPE aggregates in this case, rather than an increased ordering proposed by Johal *et al.*. This indicates that there is likely a different interaction mechanism occurring within our work with further information being required to be able to accurately state the means of these interactions.

4.2.2 PTEBS with Mid Concentration DOD Additions

Dramatic changes in both the optical and physical characteristics of PTEBS with DOD additions occurs over the 1×10^{-5}–8×10^{-4} M DOD addition range of Figure 4.1. Within this concentration range, there was an increase in particle size directly related to a decreased fluorescence intensity, indicating aggregation/bridging of the smaller CPE aggregates into larger aggregate systems.

Aggregation is known to result in fluorescence quenching due to the increased inter- and intra-molecular fluorescence quenching due to the favorable π-π overlaps being formed when CP and CPE backbones become closely associated.[108] This aggregation and quenching effect is further exemplified with the TCSPC data (Figure 4.2). The dramatic decrease in the fluorescence lifetime with aggregated solutions effectively showed the increased inter- and intra-molecular quenching within these systems.

The TCSPC data also provided an insight to the comparative structure of the CPE backbone within the aggregates of this regime. The loss of exponential line shape of TCSPC plots of aggregated PTEBS solutions indicated a dramatic loss of ordering within the CPE aggregate systems, and decays from many different emissive phases resulting in the dispersive line shape. This shows that the aggregation event is not due to the CPE backbone configuration alone, but rather a CPE–surfactant complex.

4.2.3 PTEBS with High Concentration DOD Additions

The high concentration regime (4×10^{-3}–1.2×10^{-2}) of DOD addition showed the most dramatic and sudden changes of the three effects discussed. Within this region there was a large decrease in particle size with a corresponding increase in fluorescence intensity. A decrease in surface tension to levels corresponding to micelle

formation was also observed in this regime.

The rapid decrease in particle size over this concentration range with a dramatic increase in fluorescence intensity is the result of surfactant induced disruption of aggregation and subsequent loss of inter- and intra-molecular fluorescence quenching. The general magnitude of the increase shows that this effect is not only a simple aggregate dispersion effect (inter-molecular) but is also likely altering the PTEBS backbone conformation (intra-molecular) further increasing the observed fluorescence intensity. At this point, the surfactant was already bound to the CPE resulting in increased surfactant–surfactant density which would indicate that at high surfactant concentrations, surfactant–surfactant self-assembly is likely to be present.

Laurenti *et al.* has studied interactions of PTEBS with DOD over this concentration region and has shown very similar results. As the titrations completed within this publication did not show the large particle (>400 nm) size of the low concentration regime, the authors have attributed the reasonably small increase in particle size to electrostatic screening of charges. The authors then suggested that whilst this screening would slightly increasing the particle size (10–30 nm), the surfactant tails embedding into the core reducing inter- and intra-chain fluorescence quenching, allowing for relaxation of the CPE π-conjugated backbone.[110] This explanation does not agree with the shown in Figure 4.1 however, and the proposed interactions cannot explain the large aggregate structure or initial large fluorescence enhancement seen in the low concentration levels.

The data collected in with respect to PTEBS with DOD additions showed that with high concentration surfactant addition, the particle size rapidly decreases to sizes comparable to low concentration surfactant addition, showing that the previously created CPE aggregates have been dispersed. The large fluorescence increase at this point indicates that the aggregates are not in the same state/phase as the low concentration regime however. If the small aggregates formed after the large aggregation event (high concentration DOD addition) were in the same structural configuration as they were before the large aggregate formation (low concentration DOD addition), it can be assumed that the fluorescence intensity is likely to be approximately the same with the same backbone configuration, at the same particle size. The data show that this is not the case with the fluorescence intensities being recorded at levels 15 times higher than the aggregates of comparable size in the low concentration regime. This shows that the CPEs are in a much more extended and uncoiled state in the high surfactant CPE-surfactant complex.

The main point of difference between the data published by Laurenti *et al.* and observed data in Figure 4.1 comes with the surface tension measurements. These measurements are shown to fall to approximately 40 m Nm^{-1} at 3×10^{-3} M DOD addition. This indicates micelle formation at concentration almost an order of magnitude lower than that of the CMC alone (1.2×10^{-2} M, control surface tension measurements are shown in the appendix as Figure 9.4). This point also coincides with the surfactant concentration where the large (400 nm) particles and lowest PTEBS-DOD fluorescence intensity are recorded. These results indicate that the CPE is templating the micelle growth within the large aggregates with the micelle formation potentially resulting in the aforementioned changes in backbone conformation where bending of the polymer chain allows for favorable van der Waals interactions of the surfactants bound to the side chains. This also indicates that surfactants are likely playing a large role in the aggregation event causing the observed large particles. Again, the surface tension data clearly show that the micelle formation plays a role in the fluorescence enhancement and aggregate dispersion in the high concentration regime.

As stated in chapter 1, CMC micelle growth caused by the polyelectrolyte (PE) templating surfactant self-assembly has precedence in the PE and CPE literature with many studies referring to this effect. When surfactants are complexed to the PE at high concentration, short range van der Waals attractive forces between surfactants bound to the PE side chains causing a bending of the polymer chain so surfactant-surfactant self-assembly can occur. This causes the templating of micelles at concentrations below that of the surfactant CMC with the polymer being wrapped around and electrostatically bound to the micelles.[121] The resulting complex is known as the "ball and chain" or "string of pearls" structure and has been noted with PE and surfactant complexes,[129] but is not limited to surfactant induced systems.[130,131] Figure 4.3 shows a pictorial representation of the ball and chain structure.

In order to decouple and analyze specific ionic/electrostatic, hydrophobic, van der Waals, and self-assembly effects that are observed and determine their relative strengths, specific interactions are removed and analyzed while keeping others constant. The following section analyzes the effect of the non-complementary charge of the surfactant to test the role of complementary electrostatic interactions in the CPE-surfactant complexes.

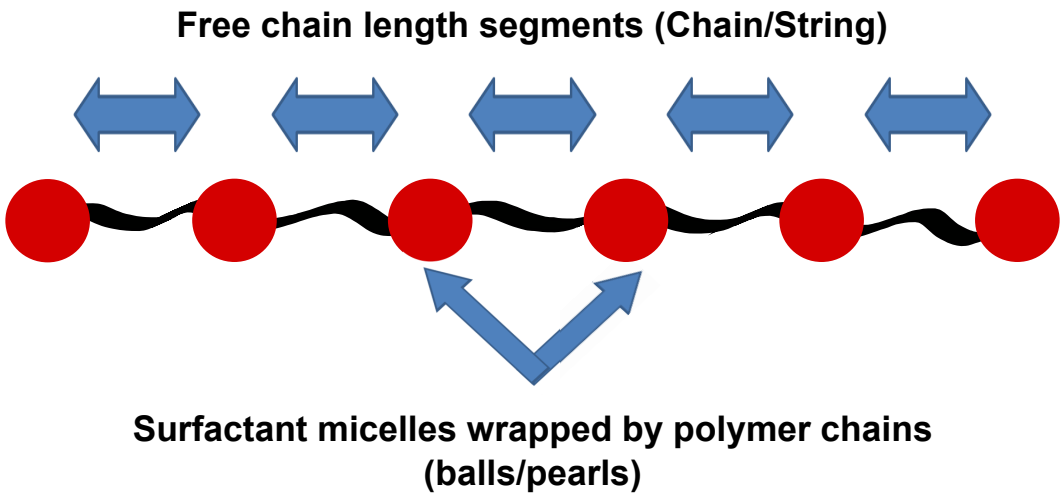

Figure 4.3 Depiction of the ball and chain structure common in PE and CPE system. The black line represents the free polymer backbone chains while the red balls represent the points where the polymer chain has become wrapped around a micelle.

4.3 PTEBS with Non-complementary Charged Surfactant SDS

The effect of SDS additions on the optical and physical characteristics of PTEBS was examined through UV/Vis absorption and fluorescence spectroscopy and DLS and surface tension measurements. All emission spectra were excited at the absorption peak maximum and all data normalized for variation in the absorption intensity. All surface tension measurements were completed using a new whelmy plate for each new batch of solutions. The small change in concentration range at which the samples are analyzed over in comparison to PTEBS with DOD additions, is due to the changes in the CMC of SDS and DOD (0.8×10^{-2} and 1.2×10^{-2} M respectively). All samples are prepared in the same fashion as with PTEBS with DOD additions and analyzed across the same fraction of the CMC concentrations. Little change is seen in the peak shape for both absorbance and fluorescence spectroscopy with only small changes ($\pm$10 nm) in maxima peak wavelengths. For these reasons, only the fluorescence intensity, particle size, and surface tension plots of PTEBS with SDS additions are shown.

The optical and physical characteristics of PTEBS with the non-complementary charged surfactant SDS over a range of concentrations (0–0.8×10^{-2} M) is shown in Figure 4.4. It can be seen that there are variations in all three types of measurements undertaken. The data shown from each of the techniques will be described individually. Of note however, is the dramatically reduced overall effect of SDS in comparison to DOD in all measurement cases.

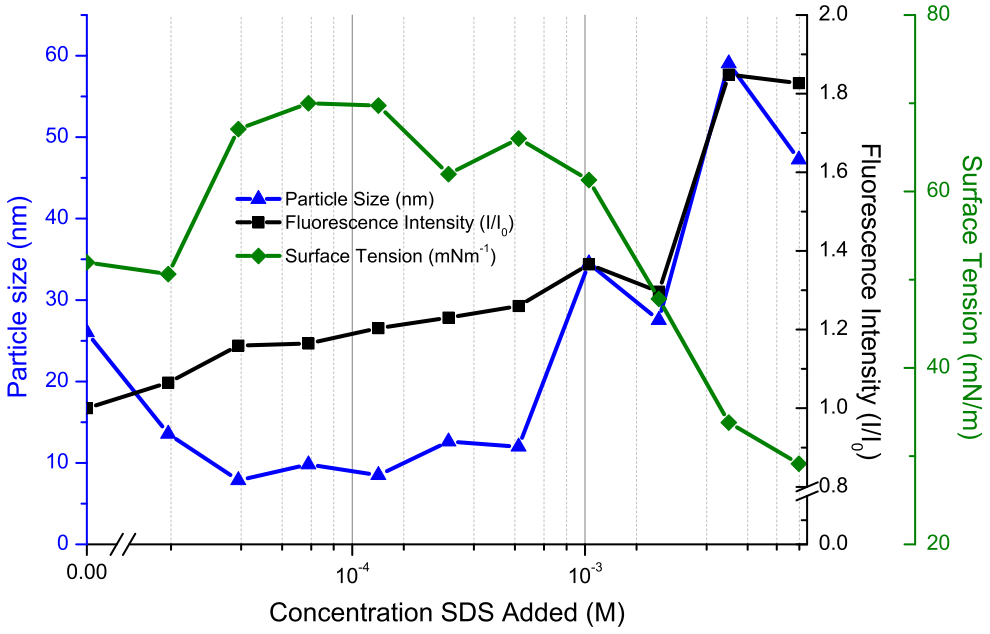

Figure 4.4 Plot of PTEBS fluorescence intensity, surface tension, and particle size, with increased SDS concentration. Shown are the normalized representative points from each spectra at each concentration of SDS analyzed.

The fluorescence intensity of PTEBS with SDS additions was shown to have a greatly reduced overall effect in comparison to that of PTEBS with DOD. The initial additions of SDS resulted in a gradual increase in emission intensity to approximately 1.4 times that of PTEBS in distilled water across the range of 0–1×10^{-3} M SDS. This was followed by a larger increase over the later concentration range (1×10^{-2}–0.8×10^{-2} M) with emission intensities increasing by 1.8 times that of PTEBS in distilled water at concentrations relating to the CMC of SDS (0.8×10^{-2} M).

The particle size of PTEBS with SDS showed an initial decrease in particle size similar to that of PTEBS with DOD. Additions across the 0–4×10^{-5} M SDS resulted in a gradual decrease in particle size from 24±5 nm to approximately 8±4 nm followed by a plateau across the 4×10^{-3}–6×10^{-3} M SDS additions. The aggregate size of PTEBS in solution then increases to approximately 55±5 nm over the remaining SDS concentration additions 6×10^{-3}–0.8×10^{-2} M).

The surface tension data is shown to have little variation from that of SDS without any CPE addition (see appendix Figure 9.5 for comparison to the control plot). Initial additions of SDS across the 0–1×10^{-4} M concentration range showed a climb in surface tension to approximately 70 m Nm^{-1}. This was followed by a slight decrease in surface tension to approximately 60 m Nm^{-1} over the 1×10^{-4}–1×10^{-3} M SDS concentration range. A further gradual decrease to 30 m Nm^{-1} over the

1×10^{-3}–0.8×10^{-2} M SDS addition was then observed for the remaining analyzed PTEBS with SDS solutions.

When comparing these data with the complementary charged DOD additions, distinct differences become visible. The first is the magnitude of change in the emission and particle size with all changes of PTEBS with SDS being a fraction of what they were when SDS is used instead of DOD. With DOD additions there was a clear increase-decrease-increase structure in emission intensities corresponding to changes in a decrease-increase-decrease structure in particle sizes. With SDS additions, the same initial interactions are not seen, indicating that electrostatic (and potentially hydrophobic) interactions drive the mid–high concentration interactions of PTEBS with DOD.

There is an observable change in the optical and physical characteristics however. This shows that it is not simply complementary electrostatic interactions driving the changes seen with complementary surfactant addition. Addition of a non-complementary surfactant is shown to increase the fluorescence intensity of PTEBS to approximately twice that of the original solution over the analyzed range with particle sizes climbing in the high concentration SDS regime. While not as dramatic as that of PTEBS with DOD, this scale of increase cannot be attributed to uncertainty within measurements and is thus a real effect.

The changes in both aggregate size and fluorescence intensity of PTEBS with SDS cannot be driven by electrostatics due to the overall charge repulsion of the two components. This shows that there is a hydrophobic and/or van der Waals driving force resulting in changes in aggregate conformation. It is likely that the particle size reduction and associated fluorescence enhancement effects seen with SDS addition are due to similar interactions as the early concentration range of PTEBS with DOD additions. This is where the surfactant tails are hydrophobically driven to embed themselves into the CPE aggregate core causing disruptions to the inter- and intra-molecular π system of the CPE. The reduced magnitude of change in both the particle size and fluorescence intensity is therefore attributed to ionic repulsion of the like charges of the surfactant head and CPE side chain reducing the embedding ability of the side chain and any subsequent interactions.

The little variation in surface tension measurements with SDS additions also show that the surfactant molecules remain in their monomer form at concentrations up to the CMC in the PTEBS solutions. At this stage similar effects as those discussed in the introduction of this chapter with non-ionic and/or charged surfactant micelles with PEs and CPEs could be occurring. Recall from the introduction section,

SAXS and SANS studies have shown that micelles can encapsulate CPE aggregates allowing for changes in the backbone conformation due to the effective change in environment.[114,120] Given this, the CPE may be able to become encapsulated by the micelles at high surfactant concentration, however this is unlikely due to the electrostatic repulsion between the CPE and micelle. Thus slow increases in PTEBS particle size with the onset of natural SDS micellation is likely due to a similar effect as with PTEBS with DOD at a greatly reduced effect due to the electrostatic repulsion between the SDS and PTEBS molecules.

In order to further test this hypothesis and to test if this effect is not unique to the anionic PTEBS, both non-complementary and complementary charged surfactant additions are added to cationic CPE based on polyfluorene with ammonium side chains, FPQ-Br (see Figure 2.1 C for molecular structure). Provided that the above hypothesis of interactions is correct, similar results to PTEBS with DOD and SDS should be seen in reverse due to the opposite charges of the CPEs. The following section analyzes the non-complementary surfactant (DOD) with FPQ-Br to further test the role of ionic charge on the physical and optical characteristics of CPEs.

4.4 FPQ-Br with Non-complementary Charged Surfactant DOD

The normalized absorption and emission spectra of 1.8×10^{-5} M FPQ-Br in a highly diluted methanol:distilled water is shown in Figure 4.5. The black peak shows the broad absorption spectra of FPQ-Br in water. The absorption wavelength maximum of FPQ-Br is shown to be 380 nm in distilled water with the lack of any vibrionic features indicating the presence of aggregation throughout the solution. The red fluorescence spectra shows a vibronic structure peaking at 425, 452, and 484 nm in distilled water with each transition being assigned to the 0-3, 0-2, and 0-1 excitations respectively. Conversions of the peaks to wavenumber yields transitions of approximately 1400 cm^{-1} indicating excitations from C=C transitions within the π system of the backbone. Unlike PTEBS, FPQ-Br is a low molecular weight CPE and highly fluorescent with a quantum efficiency shown to be 0.48 in DMSO[132] while PTEBS quantum yield was calculated to be approximately 0.05 using the dye coumarin 6 as a standard.

The effect of DOD additions on the optical and physical characteristics of FPQ-Br was examined individually through UV/Vis absorption and fluorescence spectroscopy and DLS and surface tension measurements. All measurements were taken

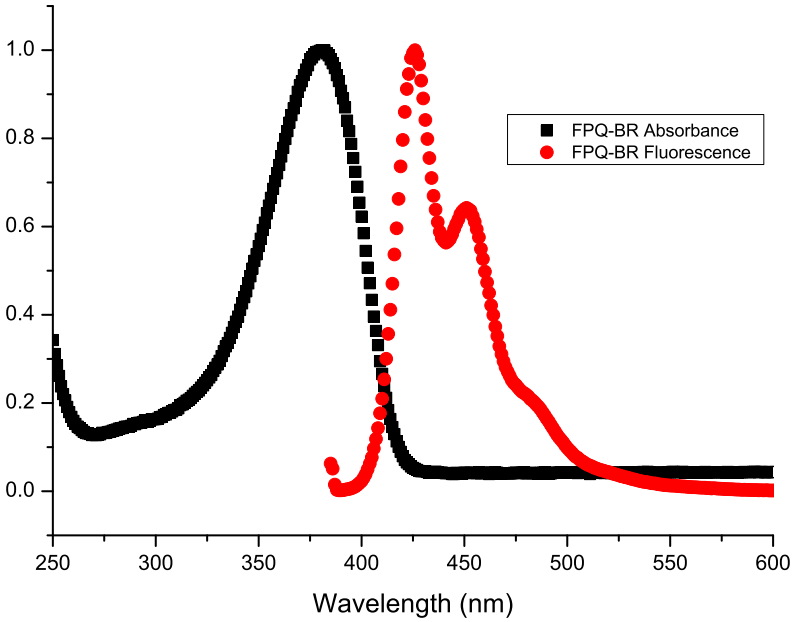

Figure 4.5 Normalized absorbance and fluorescence spectra of FPQ-Br in distilled water.

in the same fashion as with PTEBS above. The concentration of the polymer used was again set to 0.1 absorbance however it was more concentrated (3.6×10^{-5} M) than its PTEBS counterpart. Of importance however is that the FPQ-X is not directly soluble in distilled water and is initially dissolved in either methanol (FPQ-Br) or DMSO (FPQ-PB/IB) then dispersed in distilled water.

The fluorescence emission intensity, particle size, and surface tension measurements of FPQ-Br with DOD additions are shown in Figure 4.6. As can be seen from this plot, there are many similarities in the changes in optical and physical characteristics of FPQ-Br with increased concentration of non-complementary surfactant DOD, and that of PTEBS with non-complementary surfactant SDS.

The fluorescence intensity of FPQ-Br with DOD additions was shown to increase with non-complementary charged DOD addition. As can be seen there are fluctuations in the overall increase, however, additions of DOD across the 0–4×10^{-5} M concentration range resulted in the emission intensity of FPQ-Br increasing to approximately 1.5 times that of FPQ-Br without additives. A gradual further increase in emission intensity with DOD concentration across the remaining concentration additions (4×10^{-5}–1.2×10^{-2} M) yielded an overall fluorescence emission intensity increase of approximately 2.3 times that of FPQ-Br without any additives.

FPQ-Br without additives in distilled water was found to have particle sizes of

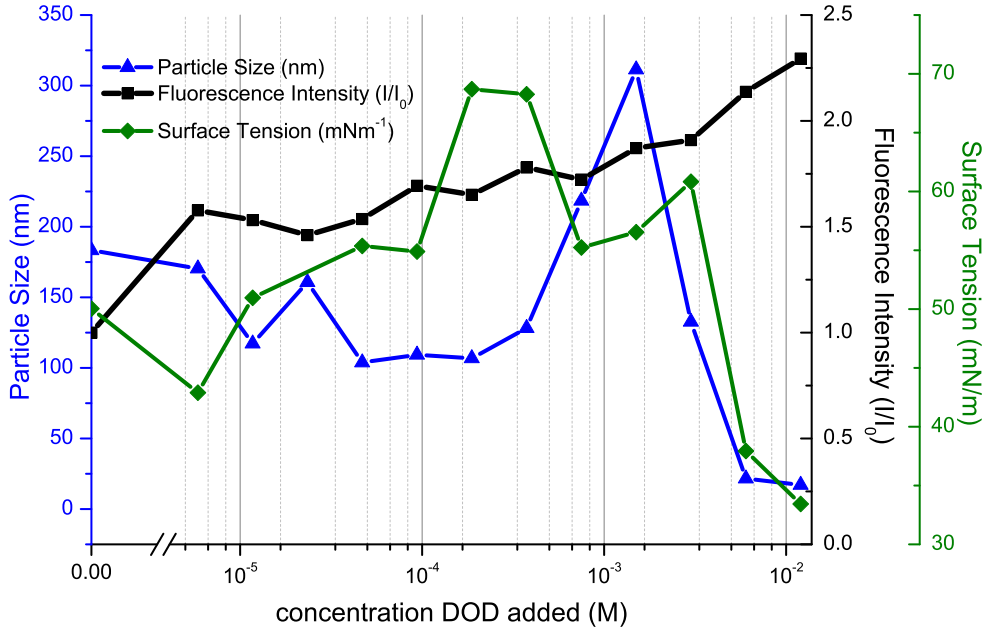

Figure 4.6 Plot of FPQ-Br fluorescence intensity, surface tension, and particle size, with increased DOD concentration. Shown are the normalized representative points from each spectra at each concentration of DOD analyzed.

approximately 180 nm, nearly 10 times larger than that of PTEBS. Initial additions of DOD across the 0–1×10^{-4} M concentration range to the FPQ-Br solutions was shown to decrease the particle size to approximately 100 nm. This was followed by an increase in aggregate size to approximately 300 nm with further DOD addition over the 1×10^{-4}–2×10^{-3} M concentration range. There was then a decrease in observed aggregate size over the remaining DOD additions (2×10^{-3}–12×10^{-2} M) with aggregates decreasing to approximately 50 nm in size.

With initial 0–1×10^{-4} M DOD additions, the surface tension measurements remained roughly constant at approximately 50 m Nm^{-1} within the fluctuations shown. There was then an observable increase in surface tension across the 1×10^{-4}–6×10^{-4} M DOD addition concentration to approximately 70 m Nm^{-1}. Increased DOD concentration resulted in a decrease in surface tension to approximately 30 m Nm^{-1} over the remaining 6×10^{-4}–1.2×10^{-2} M DOD concentration range. The odd results in comparison to that of PTEBS with DOD or SDS additions is likely due to the dispersion of methanol within the solutions altering the surface tension results.

The particle size measurement changes are much more dramatic with the FPQ-Br CPE however with CPE aggregates without surfactant addition being approximately 180 nm in size. The increased initial size allows for an increase DLS measurement sensitivity allowing for the measurements to more effectively show the changes in

particle size within the low concentration regime. As with PTEBS with DOD, there is an observable increased in FPQ-Br fluorescence intensity and a decrease in particle size with increase DOD addition. This suggests that even with unfavorable electrostatic forces, the hydrophobic effect is large enough to result in the tails of the surfactant embedding into the CPE core and effectively altering the CPE backbone aggregate conformation.

As can be seen from these results, the interactions of the non-complementary charged surfactant DOD with FPQ-Br show similar results to those of PTEBS with non-complementary charged surfactant SDS. In the current FPQ-Br case, the same effects discussed in the previous section can be applied again here. There is a change in particle size with associated mild increase in fluorescence intensity. This indicates that the DOD tails are embedding into aggregates cores causing aggregate dispersion through disruption of the backbone π-interactions. Due to the changes in both measurements being mild, the effects can be assumed to be limited to the backbone reordering effects rather than micellation and free polymer chains as with PTEBS with DOD. This is likely due to the electrostatic repulsion of the FPQ-Br and DOD ionic groups causing competition between the hydrophobic forces causing the tails to insert into the polymer and the ionic repulsion forcing the two molecules apart. The lack of backbone ordering is further evident in the lack of change of absorbance measurements of the FPQ-Br-DOD and PTEBS-SDS solutions with increased surfactant concentration. As the solutions have a methanol content, the surface tension measurements are unreliable.

It is proposed that the initial interactions between surfactants (both complementary and noncomplementary) are hydrophobically driven resulting in the alkyl tails of the surfactants embedding into the core of the aggregate in order to reduce the hydrophobic effect. In the case of noncomplementary surfactants, while the hydrophobic effect drives the surfactant tails into the CPE aggregates core disrupting inter-molecular π-interactions, the electrostatic repulsion between the CPE side chains and surfactant reduce the potential for further changes in backbone conformation. Scheme 4.1 shows a representation of this CPE–non-complementary charge surfactant effect.

When directly comparing the observed interactions of both the non-complementary surfactant addition data plots (PTEBS with SDS and FPQ-Br with DOD) with that of the complementary charged surfactant addition (PTEBS with DOD), it can be seen that the mid–high concentration surfactant interactions of the complementary charged system (PTEBS with DOD large particle sizes and large fluorescence intensity increase) is not visible in the non-complementary charged surfactant addition case. This indicates that the complementary electrostatic interactions of CPE and

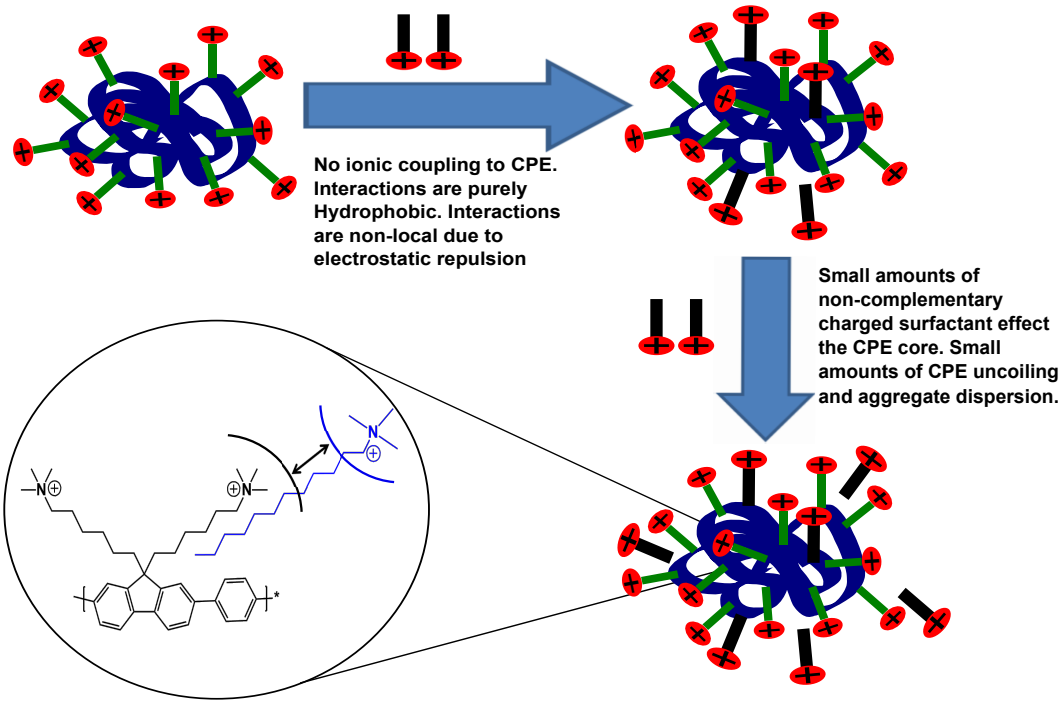

Scheme 4.1 Schematic of interactions of non-complementary charged surfactants with CPEs. Initial interactions show little effect from the surfactant due to electrostatic repulsion between like charged surfactant head group and CPE side chain. High concentration of surfactant results in hydrophobic effect dominance allowing for surfactant tails to embed into CPE aggregate causing mild disruptions to CPE aggregates resulting in aggregate dispersion.

surfactant are likely the cause of the mid-high surfactant–CPE interactions.

This illustrates that while the CPEs are of opposing charge and differ in both molecular weight and structure, the interactions with surfactants remain constant. The lack of large changes in both the optical and physical characteristics of FPQ-Br with DOD additions also reinforces the proposal of the need for complementary change of the CPE for significant changes to be seen. With this information in mind, addition of the complementary charged surfactant (*i.e.* SDS) to FPQ-Br should result in similar effects as seen with PTEBS and DOD additions. This experiment is discussed in the following section.

4.5 FPQ-Br with Complementary Charged Surfactant SDS

The effect of additions of the complementary charged SDS on the optical and physical characteristics of FPQ-Br was examined individually through UV/Vis absorption and fluorescence spectroscopy (optical) and DLS and surface tension measurements

(physical). All measurement techniques were kept the same as with FPQ-Br with DOD additions above.

The fluorescence emission, particle size, and surface tension measurements plotted against concentration of SDS added is shown in Figure 4.7. As can be seen, there are again large variations in the particle size and fluorescence intensities with surfactant addition which are similar to those seen with PTEBS and DOD.

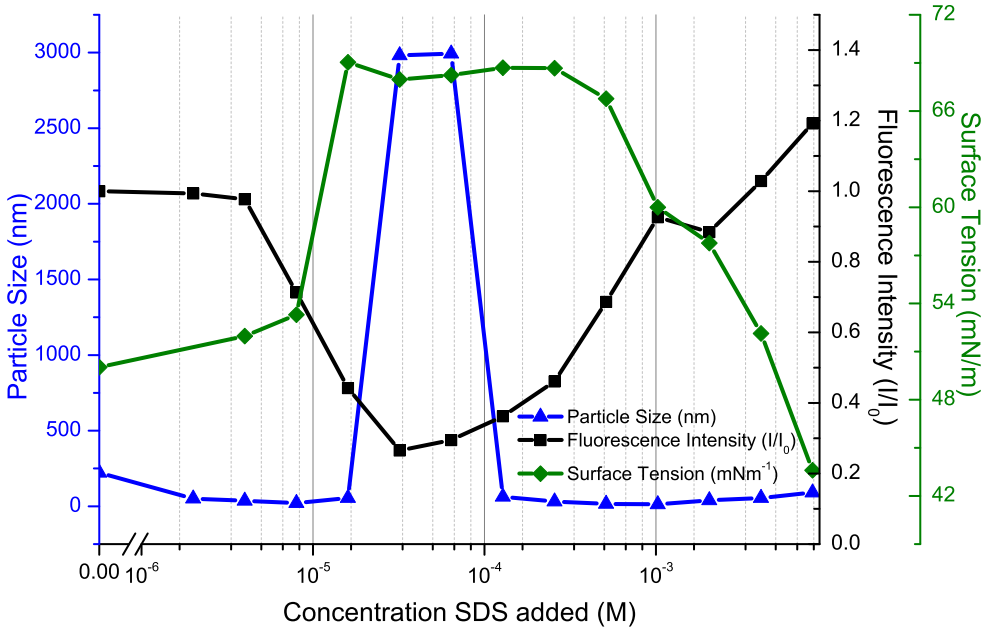

Figure 4.7 Plot of FPQ-BR fluorescence intensity, surface tension, and particle size with increased SDS concentration.

The observed fluorescence emission intensity of FPQ-Br with SDS additions is shown as black squares in Figure 4.7. It can be seen that there was little change in the observed emission intensity over the initial 0–4×10^{-6} M SDS addition. This was followed by a large gradual decrease in emission intensity to 0.3 times that of FPQ-Br alone over the 4×10^{-6}–3×10^{-5} M SDS addition range. This intensity then returned to the level of FPQ-Br without additives. The intensity then increased gradually over the remaining 3×10^{-5}–0.8×10^{-2} M SDS additions, with the emission intensity peaking at 1.2 times that of the FPQ-Br without additives solution.

The particle size data shows the most dramatic effects of the observed FPQ-Br with SDS addition series. Initial SDS additions over the 0–2×10^{-5} M concentration range resulted in the particle size decreasing from approximately 200 though to 70 nm with increased SDS concentration. There was then a dramatic increase in particle size of FPQ-Br solutions with particle sizes peaking at approximately 3000 nm over the 2×10^{-5}–1×10^{-4} M SDS addition concentration. This was followed by a dramatic

decrease in particle size over the 1×10^{-4}–2×10^{-4} M SDS addition concentration with particle sizes being reduced to approximately 50 nm in size. The aggregate size then returned to approximately 100 nm over the remaining 2×10^{-4}–0.8×10^{-2} M SDS addition concentration.

The surface tension data showed an initial plateau over the initial concentration range with measurements remaining at approximately 55 m Nm^{-1} over the 0–1×10^{-5} M SDS concentration range. There was then a climb in surface tension to approximately 70 m Nm^{-1} with SDS additions of 1×10^{-5} M followed by a plateau at this point through to 3×10^{-4} M SDS addition concentration. The plateau was then followed by a decrease in surface tension to approximately 45 m Nm^{-1} over the remaining 3×10^{-4}–0.8×10^{-2} M SDS addition range. Again, due to the methanol content of these solutions, these results cannot be taken as reliable.

As expected, the interactions of FPQ-Br with SDS additions are reasonably similar to that of PTEBS with DOD additions. The large change in particle size coupled with fluorescence quenching observed is due to complementary electrostatic interactions of the surfactant. This is also true with the rise in fluorescence intensity with decreased particle size in the late concentration complementary surfactant additions showing that this too is linked to the complementary charge of the surfactant addition. Consequently, the interactions of the CPEs with the complementary charged surfactants can be attributed to the same effects as discussed in the PTEBS with DOD section. To reiterate, the initial decrease in particle size is associated with the disruption of the π-π interactions of CPE aggregates resulting in the loss of inter- and intra-molecular interactions. The favorable electrostatics allow the surfactant to be bound to the smaller aggregates. Aggregation then ensues with suspected micelle templation, with the following decrease in aggregation being linked to pre-CMC micelle formation.

The interactions of FPQ-Br and SDS and that of PTEBS with DOD do vary subtly. The first variation of note is that there is no initial low concentration enhancement in the fluorescence intensity while the particle size of CPE aggregates does decrease. A potential explanation for this effect can be attributed the CPE itself. FPQ-Br has a molecular weight of approximately 25000 g mol^{-1} relating to approximately 40 monomer units, where as PTEBS molecular weight is over 1000000 g mol^{-1} relating to over 3500 monomer units. The greatly reduced number of monomer units in the FPQ-Br case results in the aggregates having little intra-molecular fluorescence quenching contribution without additives where as the much larger PTEBS system will have a much larger intra-molecular fluorescence quenching contribution. This results in the surfactant addition to FPQ-Br only reducing the inter-molecular

aggregation effects as the CPE chains are already in an extended state thus cannot be enhanced through this means.

This explanation also applies to the enhanced fluorescence quenching effect seen with FPQ-Br in comparison to PTEBS. With increased surfactant addition, the bound surfactant molecules induce bending in the polymer chain due to forming favorable van der Waals interactions of the surfactant tails. In the PTEBS system, the low concentration surfactant addition reduction in intra-molecular fluorescence quenching greatly outweighs the induced intra-molecular interactions caused by the bending thus the fluorescence intensity remains high. In the case of FPQ-Br, in order to accommodate the van der Waals interactions of the electrostatically coupled surfactants, significant twisting of the backbone is required resulting in reductions of the fluorescence intensity of the complexes.

The micro scale particle size aggregates (3000 nm) also result in a much larger than expected fluorescence quenching effect. Again, the particle size data and mid–high concentration SDS addition fluorescence intensity changes remain consistent with those of PTEBS with DOD additions further reinforcing the proposal that the large scale physical and optical characteristic changes require both the hydrophobic effect and complementary electrostatics between CPE and surfactant to be present.

These data clearly show that direct complementary charge ionic interactions between the CPE and surfactant is responsible for the large changes in optical and physical characteristics of CPE-surfactant complexes. The particle size data also exemplify the physical character of initial low concentration interactions of complementary charged surfactants with CPEs aiding in the explanation of the initial rise in fluorescence intensity seen in PTEBS with DOD additions. In order to further test the role of electrostatics with surfactant-CPE complexation, non-ionic surfactants can be tested with CPE solutions as a potential control. These effects are discussed in the following section.

4.6 PTEBS with Non-ionic Surfactant DEC

The role of hydrophobic and van der Waals interactions on the optical and physical characteristics of PTEBS was examined through additions of the non-ionic surfactant decylamine (DEC) to solutions of PTEBS over a range of concentrations (0–3×10^{-4} M). The range of concentrations is limited due to the CMC of DEC (0.005 M) and further limited by slight precipitation (clouding) of solutions due to poor

solubility of the DEC surfactant. All clouded solution areas are removed from the plots with only reliable data being presented. Full plots are shown in the appendix as Figure 9.6. All solutions were analyzed individually through UV/Vis absorption and fluorescence spectroscopy (optical) and DLS and surface tension measurements (physical). All further analysis techniques were completed in the same fashion as with PTEBS and DOD/SDS.

The particle size, fluorescence intensity, and surface tension measurements of the non-clouded FPQ-Br are shown plotted against DEC concentration in Figure 4.8. Due to the high levels of scattering, only the initial interactions of the non-ionic surfactant with PTEBS is shown.

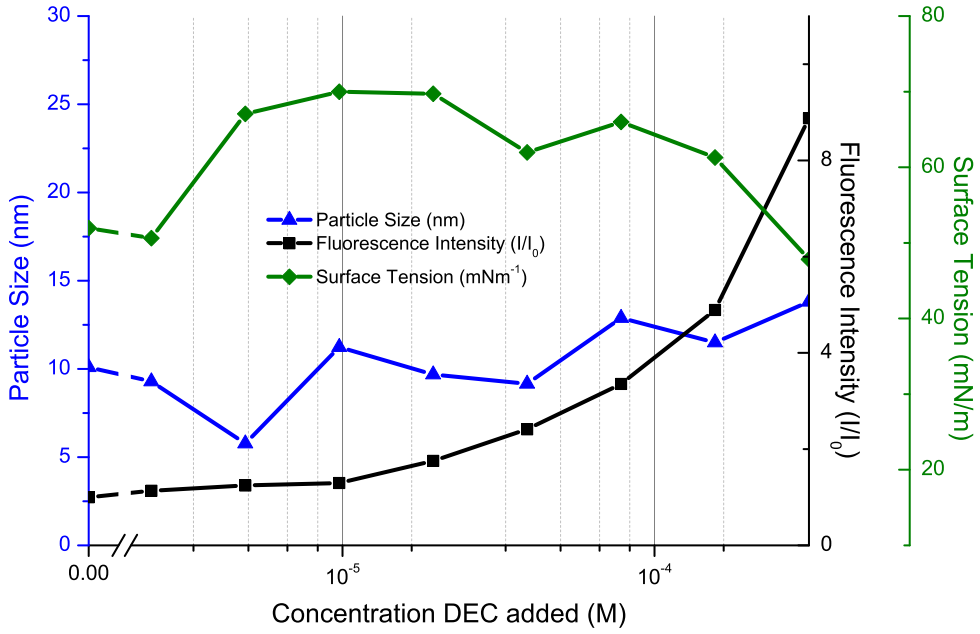

Figure 4.8 Plot of PTEBS fluorescence intensity, surface tension, and particle size, with increased DEC concentration. Shown are the normalized representative points from each spectra at each concentration of DEC analyzed.

The fluorescence intensity of PTEBS with DEC additions was shown as a gradual curve rising to approximately 10 times that of PTEBS in distilled water over the analyzed 0–3×10^{-4} M DEC concentration range. The fluorescence intensity increases most towards the point of clouding and subsequent scattering indicating the possibility of scattering throughout these solutions also.

The particle size of PTEBS aggregates in the analyzed solutions with DEC additions was shown to have little variation. Over the entire analyzed range (0–3×10^{-4} M), the particle size of PTEBS aggregates remains at approximately 9 nm with fluctuations of approximately 3 nm.

The surface tension data of PTEBS with DEC solutions was observed to have an initial increase from approximately 55 m Nm^{-1} though to approximately 70 mN m^{-1} over the 0–1×10^{-5} M DEC concentration additions. This is followed by a gradual decrease (with fluctuations) to approximately 60 m Nm^{-1} over the 1×10^{-5}–2×10^{-4} M DEC concentration addition range. There was then beginnings of a decrease in surface tension with the next data point decreasing to approximately 50 m Nm^{-1}. Due to scattering and clouding, the remaining data points are unreliable.

Over the reliable concentration range, there is an observable increase in fluorescence intensity to levels higher than that of PTEBS with SDS additions but lower than that of PTEBS with DOD additions. There is also no large increase and subsequent quench of fluorescence intensity as seen with the complementary charged DOD additions over the low–mid concentration range. The observed fluorescence enhancement is consistent with the proposed interactions discussed in the previous sections. With non-complementary surfactant addition, the rise in fluorescence intensity was hindered by the electrostatic repulsion which caused a comparatively low increase in fluorescence intensity (2 fold increase). Addition of complementary charged DOD allowed for electrostatic binding give rise to the dramatic increase in fluorescence intensity (28 fold) observed. Due to the lack of charge of DEC, it is expected that this surfactant should lie between these two systems. The results showed an observable approximate 10 fold increase in fluorescence intensity showing that this surfactant is again consistent with the expectations of the proposed scheme of interactions.

The significant change in fluorescence intensity of the PTEBS solutions with DEC additions also reinforces the proposed hydrophobic driven initial interactions effectively increasing the short range electrostatic interactions. If the driving force for CPE-surfactant complexes was purely electrostatically driven, there would be no change in PTEBS characteristic as DEC has no formal charge. The converse of this, if the effects were purely hydrophobically driven, all three surfactant sets would remain the same due to the electrostatics playing no role. As there is significant changes with all three surfactant additions, the interactions must therefore be initially hydrophobically driven causing the surfactant tails interact with the CPE aggregate core. This increases the proximity of the CPE side chains and surfactant head groups allowing for the electrostatic forces to then dominate the system.

Experiments were completed with FPQ-Br, FPQ-IB, and FPQ-PB with DEC additions in order to further test these effects, however the samples showed high levels of scattering, with solutions at the same concentration showing absorbance measurements ranging from 0.06–0.15. These results were assumed to be unreliable. The plot containing the physical and optical data normalized as best as possible for

the variation in absorption of FPQ-Br with SDS can be seen in the appendix as Figure 9.7. Data for FPQ-IB and FPQ-PB is not shown.

The data presented in this section show that there are significant effects due to hydrophobic and/or van der Waals interactions on aggregates of CPEs in aqueous environments. In order to further show the interactions due to these effects, experiments of surfactant addition to a non-ionic conjugated polymer (a CP) in an organic solvent (chloroform) environment. These experiments in these environments reduces ionic and hydrophobic interactions resulting in the study of pure van der Waals interactions between the CP and surfactant. The details of these experiments are discussed in the following section.

4.7 P3HT with non-ionic (DEC) and charged (DOD) surfactants

The role of van der Waals interactions on the optical and physical characteristics of the conjugated polymer (CP) P3HT was examined through additions of non-ionic decylamine (DEC) and ionic dodecylammonium bromide (DOD) over a range of concentrations (0–5×10^{-3} and 0–1.2×10^{-2} M, respectively) in chloroform ($CHCl_3$). The range of concentrations is not limited by clouding of solutions with DEC, due to the high solubility of the surfactant in chloroform. All solutions were analyzed individually through UV/Vis absorption and fluorescence spectroscopy (optical). The non-aqueous environment and high solubility of P3HT in chloroform results in surface tension and DLS measurements being irrelevant. All optical spectroscopy techniques were completed in the same fashion as in all other cases. Due to the only significant changes being seen with surfactant addition to P3HT being in the emission intensities, only the fluorescence emission data is shown in the following chapter.

The fluorescence intensity of P3HT with DOD and DEC additions in chloroform are shown in Figure 4.9 with PTEBS and DOD additions in distilled water plotted on the same graph for comparison purposes. Inset is the fluorescence intensity of P3HT with DOD and DEC showing the level of variation due to van der Waal interactions.

The fluorescence data of Figure 4.9 showed that there was little variation in the fluorescence intensity of P3HT with either DOD or DEC additions in comparison to that of PTEBS with DOD additions. The scale of the main plot enhances this effect due to the changes being significantly smaller than that of PTEBS with DOD

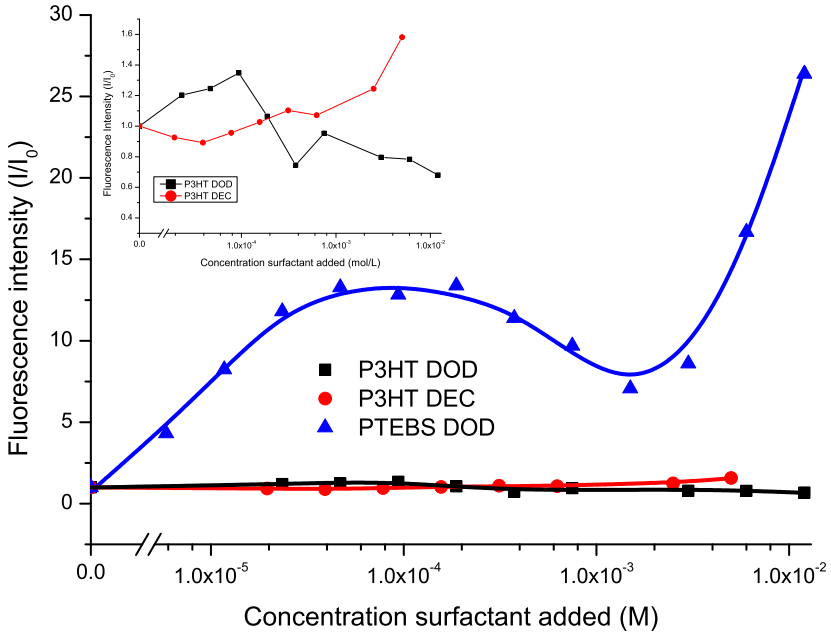

Figure 4.9 Plot of P3HT fluorescence intensity with DOD, DEC, and PTEBS with DOD additions. Inset is a plot of the fluorescence intensity of P3HT with DEC and DOD over the range of analyzed concentrations.

additions.

The inset plot of P3HT with both DEC and DOD shows that the fluorescence intensity of P3HT with both DOD and DEC fluctuates about the the same intensity as P3HT in chloroform. DEC additions was observed to fluctuate between 0.9 and 1.1 times that of the original fluorescence intensity over the 0–1×10^{-3} M DEC addition concentration followed by a rise to approximately 1.6 times that of P3HT in pristine chloroform over the remaining DEC additions (1×10^{-3}–5×10^{-3} M). DOD additions were also shown to originally fluctuate over the initial concentration 0–1×10^{-3} M range with intensities measuring between 0.8 and 1.2 times that of P3HT in pristine chloroform. This was then followed by fluctuations in fluorescence intensity at approximately 0.8 times that of P3HT alone over the remaining DOD additions (1×10^{-3}–1.2×10^{-2} M).

The plots show little effects from the surfactants for two reasons, the first is that P3HT is very well dissolved in chloroform resulting in little aggregation. This is evident with the DLS measurements showing no particles and hence no reliable readings were achieved with this technique (data not shown). The second and possibly most important is the distinct lack of hydrophobic interactions driving the surfactants to interact with the CP. Due to the hydrophobic effect being the driving force for the initial interactions, removing this force resulted in little to no direct

CP–surfactant interactions.

The small changes in fluorescence intensity observed are likely due to changing the solvent environment. As seen in chapter 2, changing the solvent environment through solvent composition or ionic strength can change the optical characteristics of CPEs. In this case, addition of the ionic surfactant DOD increases the ionic strength of the solvent system resulting in the observed fluorescence quenching, while the addition of the non-ionic surfactant DEC results in increased solubility of the CP due to increasing the non-polar character of the solvent.

This reinforces that the initial driving force for CPE–surfactant is the hydrophobic interactions of the aqueous environment. Without this force, no direct CP/CPE-surfactant interactions are seen. Therefore the initial interactions are dominated by the hydrophobic interactions.

4.8 Model of Favorable Interactions of CPEs and Surfactants

The following section proposes a model of interactions for CPEs with complementary charged long chain surfactants. The model is split into three regions on interactions relating to the low, mid, and high concentration surfactant additions regimes. The model proposed is based around known interactions found in the PE literature with the specifics and reasonings for the assignments stated in the relevant sections above. For the following section, PTEBS with DOD and FPQ-Br with SDS additions is used as examples for described interactions.

4.8.1 CPEs with Low Concentration Surfactant Addition

The low concentration surfactant addition regime is that of 0–1×10^{-4} DOD addition to PTEBS solutions. The initial interactions of complementary charged surfactants with CPEs is proposed to be driven by a combination of the hydrophobic effect and electrostatic interactions. Addition of surfactant to distilled water systems is known to result in natural self-assembly with the large majority of surfactant molecules being located at the air-water interface.[41] When the solution becomes charged via the addition of a CPE, competition between electrostatic forces of the surfactant head groups and CPE side chains, and surfactant alkyl tails hydrophobic effects begins

to take effect. The competition between the two reasonably strong electrostatic and hydrophobic forces provides the driving force for the initial interactions.

In the formation of CPE-surfactant complexes, it is proposed that the hydrophobic effect induced onto surfactants in the bulk results in the surfactant molecules interacting with, and embedding in, the core of the CPE aggregate in order to reduce the unfavorable interactions of the aqueous environment. This results in partial disruption of the π-interactions of the CPE backbone resulting in aggregate dispersion and small fluorescence enhancement. The alkyl tails interacting with the core results in a reduced distance between the charged CPE side chains and the surfactant head group allowing for the electrostatic forces provided by the complementary charges to dominate the system. This would result in a small portion of surfactant molecules becoming electrostatically bound to the CPE side chains.

Given that the size of the alkyl tail of the surfactant is significantly longer than that of the CPE side chains, it is proposed that the when the tails of the surfactant embeds deeply into the CPE aggregate, the tails intersect inter- and intra-molecular π-interactions resulting in a loss of stability of CPE aggregates. This causes further aggregate dispersion and the backbone configuration uncoils, resulting in an initial loss in aggregate size (Figure 4.7 particle size) and increased fluorescence intensity (Figure 4.1 fluorescence intensity). This effect is depicted in Scheme 4.2.

4.8.2 CPEs with Mid Concentration Surfactant Addition

The mid concentration regime covers the range of 1×10^{-4}–1×10^{-3} M DOD additions to PTEBS solutions. This range involves the decrease in fluorescence intensity coupled with rapid increase in particle size for both PTEBS with DOD and FPQ-Br with SDS. The beginnings of a decrease in observed surface tension is also noted in this regime for PTEBS with DOD.

As previously stated, there is an observable decrease in fluorescence intensity with increasing particle size indicating an increase in inter- and intra-molecular fluorescence quenching which is due to increased π-π interactions of the hydrophobic backbone. Whilst true, the very small magnitude of decrease in fluorescence intensity compared to the magnitude of the increase in particle size of CPE aggregates suggests that this is the only interaction occurring. The greatly reduced fluorescence quenching compared to what is expected shows that previous alterations of the backbone remain with the aggregation event and that the interactions of the CPE backbone are limited.

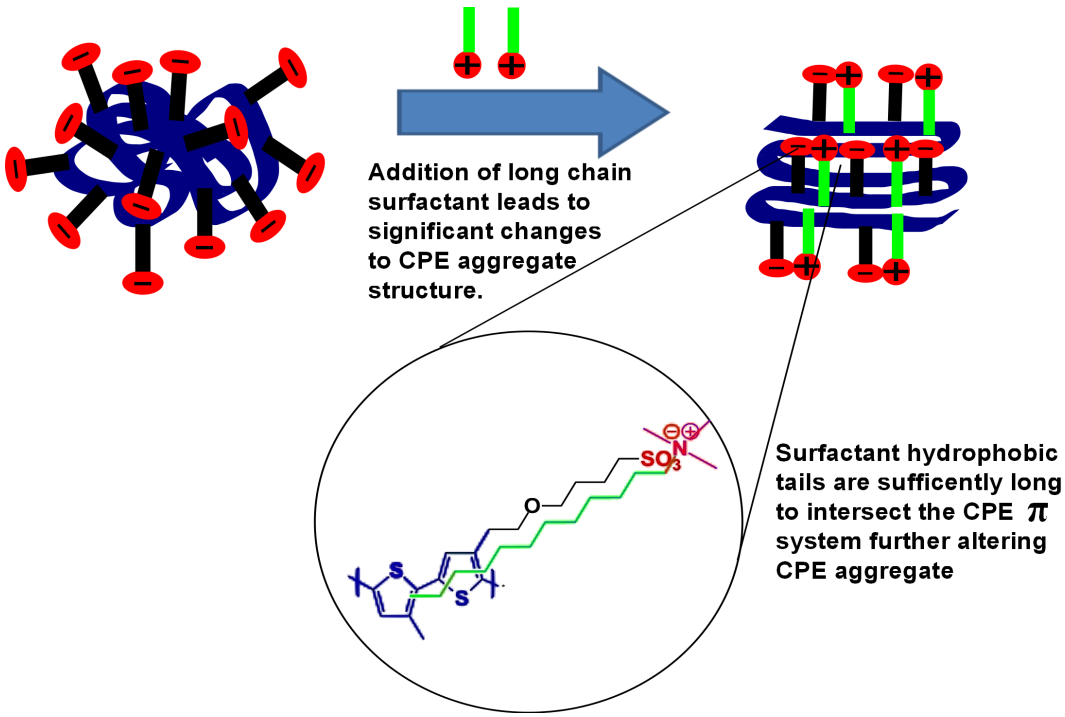

Scheme 4.2 Scheme showing interactions of surfactants and CPE aggregates. The CPE backbone is represented by the blue thick line, CPE side chains are black with red negative heads, and surfactant hydrocarbon tails are green with red positive heads. Hydrophobic effect initially dominates the system causing the alkyl tails of surfactants to interact with CPE aggregates. This induces the comparatively short range ionic interactions between CPE side chains and surfactant head group resulting in surfactant tails disrupting the CPE aggregate π system.

To fully explain this set of interactions we propose an effect that is again often seen in polyelectrolyte with surfactant systems. This effect draws on the fact that the surfactants have a natural self-assembly that is driven by the hydrophobic effect and favorable van der Waals interactions with non-polar aliphatic chains in order to reduce the hydrophobic effect. Both the CPE and surfactant tails contain non-polar aliphatic chains, thus within aggregated systems with nearby surfactant molecules, there is little preference for an electrostatically bound surfactant to van der Waals couple with the CPE side chain, or another surfactant molecule to reduce the felt hydrophobic effect. Provided a high enough surfactant density within the solution, this results in a combination of surfactant–surfactant and surfactant–CPE side chain van der Waals interactions.

The surfactant–surfactant coupling of molecules electrostatically bound to neighboring CPE aggregates resulting in twisting of the polymer chains with reformation of intra-molecular fluorescence quenching states, while a bridging or cross-linking effect of smaller aggregates through bound surfactants results in the reformation of some inter-molecular fluorescence quenching states. This would result in a rapid increase in aggregate size due to the surfactant cross-linking but a less than expected intra-

molecular fluorescence quenching (PTEBS-DOD) due to the changes in backbone coiling being limited. A pictorial representation of this effect is shown in Scheme 4.3 below.

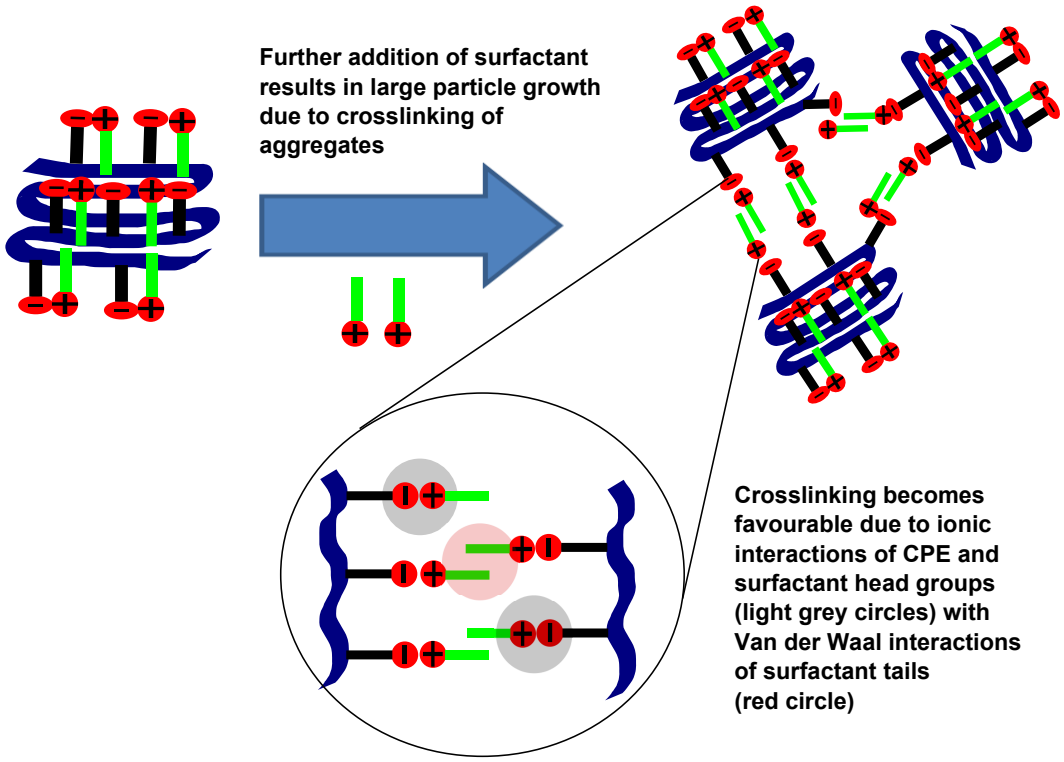

Scheme 4.3 Schematic of cross-linking effect observed with increased surfactant concentration. Surfactant self-assembly results in surfactants cross-linking with one-another on neighboring aggregates. Surfactant molecules are shown as either black or lime green lines with red heads. The lime green tails of surfactants indicate the cross-linked surfactant molecules causing the aggregation. Black tailed surfactant molecules indicate the surfactants that are responsible for the observed increased fluorescence intensity with large aggregates.

This point is the beginning of the proposed micelle templating which is also shown in the surface tension data. At this point, the surfactants bound to the polymer chain begin to create cooperative surfactant binding through van der Waals and self-assembly effects. The cooperative effect coupled with drive for self-assembly results in the surfactants binding to both neighboring surfactant units through van der Waals coupling of the side chains while remaining electrostatically bound to the CPE side chains.

4.8.3 CPEs with High Concentration Surfactant Addition

Region three consists of interactions between 1×10^{-3}–1.2×10^{-2} M DOD additions to PTEBS solutions. The data seen within this range consist of a rapid decrease in

both particle size and surface tension with associated 28 fold increase in fluorescence intensity.

As previously stated, the change in fluorescence intensity is associated with the change in particle size due to the reduction in inter- and intra-molecular fluorescence quenching. This however cannot only be attributed to the change in aggregation state due to the dramatic increase in intensity from the emissive aggregates and that of PTEBS in pristine distilled water.

At this point the polymer is still in a three dimensional aggregate with surfactant molecules piercing into the aggregate from all directions. The bending of the polymer chains within this three dimensional structure coupled with the increased drive for self-assembly of surfactants due to cooperative attraction of molecules from the air-water interface, results in the surfactant to begin to assemble into a spherical or cylindrical micelle type structure with the polymer backbone wrapping around the outside surface. At this point the micelle structure has been formed with steric interactions pushing the polymer into a highly uncoiled structure greatly reducing any intra-molecular π-interactions.

Once the micelle has been formed with the polymer chain extended, the ball and chain structure is completed. Further addition of surfactant beyond this point results in rapid micelle formation bound to the polymer chains with further increases in the polymer uncoiling. The result of this is the previously described ball and chain type structure where the polymer is at full extension wrapped around surfactant micelles. This effect would not be expected with non-complementary, non-ionic, or non-micellular surfactants due to the favorable electrostatics, and micellular nature being required for this effect. The micelle templating and pre-CMC formation proposed is consistent with our observed surface tension data with PTEBS and DOD addition with micelles being shown to be formed (35 mN m^{-1}) an order of magnitude before the CMC of DOD and is an effect noted in PE literature.[59] Scheme 4.4 shows a representation of this transition with the monomer surfactant molecules shown as lime green tails while the templated micelle structures shown as light blue tails.

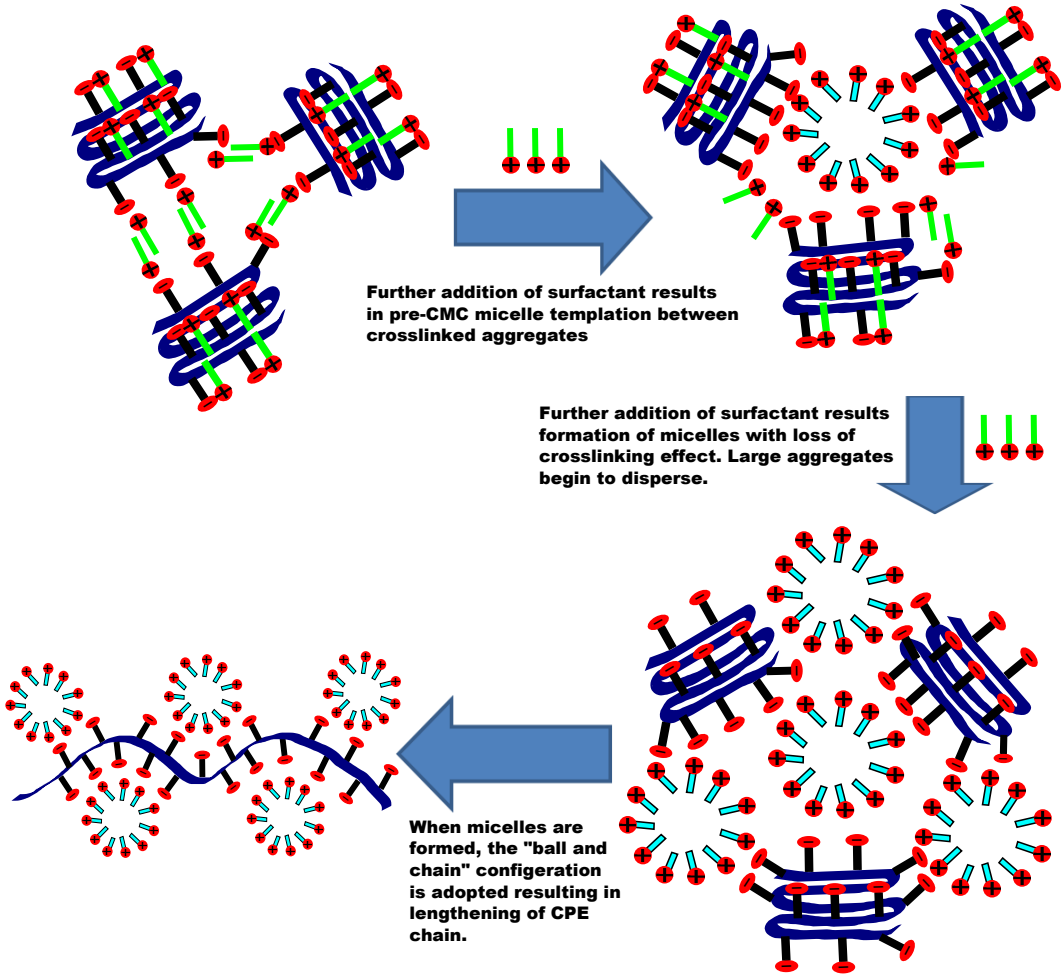

Scheme 4.4 Schematic of the micelle templating effect caused by the CPEs. Bound surfactants in micelle form are shown with light blue tails whilst the bound but not templated are shown with green tails. As with other figures, the CPE backbone is shown as the thick dark blue line, CPE side chains as black, and charged head groups as red circles.

4.9 Summary of Chapter

This chapter has detailed the interactions of complementary charged, non-ionic, and non-complementary charged surfactants with two CPEs and a CP. The systematic testing of the various surfactants has allowed for studies of the different forces seen in CPE–surfactant systems with the resulting data directly compared to both literature and other surfactant systems. The resulting data has shown the specific interactions and associated changes in optical and physical characteristics due to the different forces with the resulting analysis providing a proposed new model of interactions of CPEs and surfactant systems.

It has been shown that the initial low concentration surfactant changes in optical and physical properties are hydrophobically driven with the hydrophobic effect then inducing the electrostatic interactions of the CPE side chains and surfactant

head groups. These two forces have been shown to result in loss of aggregation and increased fluorescence intensity due to the tails of the surfactant molecules interrupting the π system of CPE aggregates.
The mid concentration range interactions are shown to be driven by complementary electrostatic binding of the surfactant molecules to the CPE and the natural self-assembly of surfactant molecules in aqueous environments. Due to the lack of preference of van der Waals interactions of surfactant molecules, self-assembly of surfactant tails on neighboring aggregates results in a cross-linking effect between small CPE aggregates causing large aggregates to be formed. The larges aggregates are shown to be highly disordered with the formation being surfactant induced rather than due to increased π-π interactions of the CPE backbone. This results in the high molecular weight aggregates remaining reasonably emissive due to poor inter-molecular π orbital overlap.

Further self-assembly and cooperative binding of surfactant molecules has been shown to drive the final stage of interactions with the surfactant molecules natural self-assembly causing CPE backbone bending and uncoiling. Micelle templating has then been shown to cause rapid loss of aggregation with the further change in CPE backbone conformation resulting in ball and chain type structures being formed causing rapid increases in fluorescence intensity.

Chapter 5

Transitions of CPEs–Surfactant Complexes to the Solid Phase

5.1 Introduction

One of the main goals of most CP or CPE research is to create and optimize organic electronic devices. For this to occur, the solution phase CP or CPE is cast into a film through a variety of techniques such as spin or spray coating, thereby a transition from solution phase to solid phase is completed.

A film is the solid form of the polymer previously in solution and hence can be seen as a large aggregate. As a consequence of this, the optical signature of the solid phase film is often highly red shifted and it lacks vibronic structure indicating that the film is disordered in character. This means that when casting is occurring, the rapid loss of solvent results in the polymer becoming randomly dispersed over the surface of the substrate. As previously shown in the introduction chapter (Figure 1.8), annealing processes have been shown to allow for some diffusion controlled reorganization into a favorable π-backbone interactions.[65,133]

The bulk solution phase characteristics can be transfered to the solid phase however. Using the solvent effects discussed in chapter 3 as an example, changes in the solvent and/or solvent composition are shown to have large effects on the optical signature of the resulting solution. These solvent induced effects are also seen in the solid state where films cast from solutions of highly aggregated or highly solvated systems are shown to transfer that characteristic to the solid phase. In these cases, the vibronic features of the highly solvated systems are quenched, however, they remain much

more apparent than films cast from less favorable solvent compositions. This effect is shown in detail below in Figure 5.1 where the aggregation induced solvents in the solution phase leads to changes enhancement of 0-1 and 0-2 states in the solid phase aggregates.[32,134]

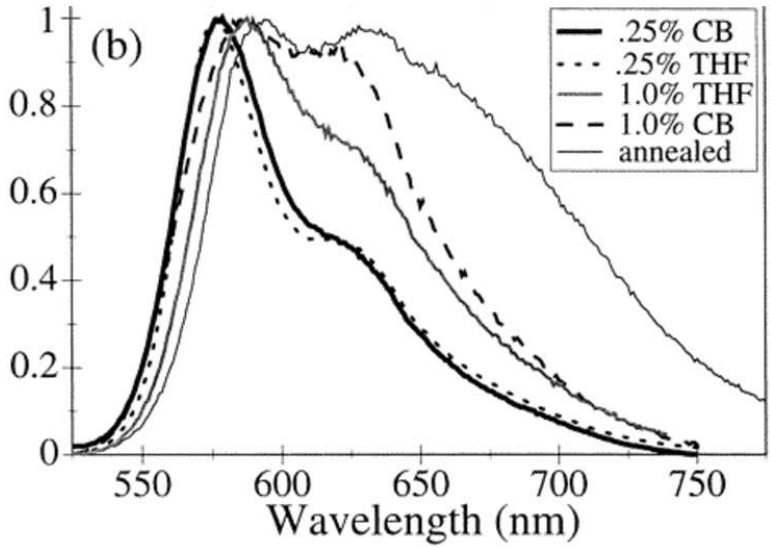

Figure 5.1 Solvent effects in films of MEH-PPV. The casting solvents are shown to significantly alter the vibronic structure of the films when cast with different solvents and/or solvent compositions. CB is chlorobenzene, and THF is tetrahydrofuran. Figure adapted from Nguyen *et al.*[134]

The state of aggregates within a solution being cast into the solid state is not limited to solvent phase effects. Recent publications by Pace *et al.*[135] has shown the surfactant based structure of a CPE–zwiterionic surfactant complex in the solid phase. Within this study, the authors noted the appearance of a lamellar phase when solutions of CPE and zwitterionic surfactant were drop cast onto the substrate. This shows that surfactant based control of the solution phase has the potential to be transferred to the solid phase with film casting. The formation of lamellar phases within a film has also been noted within PE and CPE–surfactant systems in the solid phase with many studies showing this effect.[136–138]

The electrostatic interactions of CPEs allows for an easy casting process for ultra-thin films known as the layer-by-layer (LBL) techniques. Once a single CPE layer is cast onto a substrate, direct layering of oppositely charged CPEs can be completed through simple dip processes into a solution of the oppositely charged CPE. Electrostatic attraction of the opposing charges results in the second layer adhering to the cast layer with multiple dips into solutions allowing for building up of the CPE layers. A more detailed description is discussed later. This process allows for an easy and successful means of depositing multiple CPEs onto a single substrate affording opportunities to make multi-layered devices tailored for multi-layer assemblies[139] for various applications and/or Forster resonance energy transfer (FRET) cascades through the films.[140]

The following chapter details the transfer of the previously made solution phase CPE–surfactant self assembled structures to the solid phase via high speed spin coating. Layer-by-layer techniques are also used to analyze the optical characteristics of dual layer thin films of PTEBS and FPQ-Br in order to create a FRET based energy transfer between the FPQ-Br and PTEBS.

5.2 Transfer of Solution Phase Characteristics to Solid Phase

The transition of solution to solid phase was completed via spin coating concentrated (3 mg mL^{-1}) PTEBS solutions with varying concentration of DOD surfactant. 120 μL solutions were depositied onto 1 cm diameter fused quartz substrates and spun at 8000 rpm for 30 seconds to allow for thin film deposition. DOD was the surfactant of choice due to the large optical and physical characteristic changes seen with this surfactant in the solution phase (see chapter 3). For consistency and direct comparison between solution and solid phase characteristics, the concentration range of DOD additions remained constant. The effect of DOD additions on the optical and physical characteristics of PTEBS in the solid state was examined through UV/Vis and fluorescence spectroscopy. All emission spectra were excited at the absorption peak maximum and all data normalized for variation in the absorption intensity. All excitation measurements were excited at the same point to allow for direct comparison between measurements. Little change is seen in the peak shape for absorbance measurements whilst shouldering was observed in fluorescence spectroscopy. For these reasons, only the absorbance wavelength, fluorescence emission (intensity and shape) and excitation measurements are shown in the following plots.

The fluorescence emission intensity and absorbance wavelengths of all solutions analyzed are shown in Figure 5.2. From this figure it can be seen that there was a small increase in fluorescence intensity to approximately 1.1 times that of PTEBS alone over the low concentration DOD addition regime (0–1×10^{-3} M). This was then followed by a decrease in fluorescence intensity over the remaining concentration range (1×10^{-3}–1.2×10^{-4} M) with the final fluorescence quenching resulting in an intensity of approximately 0.3 times that of PTEBS alone.

The absorbance wavelength of the films has been shown to be correlated with the changes in emission intensity. PTEBS in the solid state has been shown to have an absorbance shifted to longer wavelengths (red shifted) of 489 nm, from that of the solution phase (453 nm). The absorbance wavelength is shown to be blue shifted

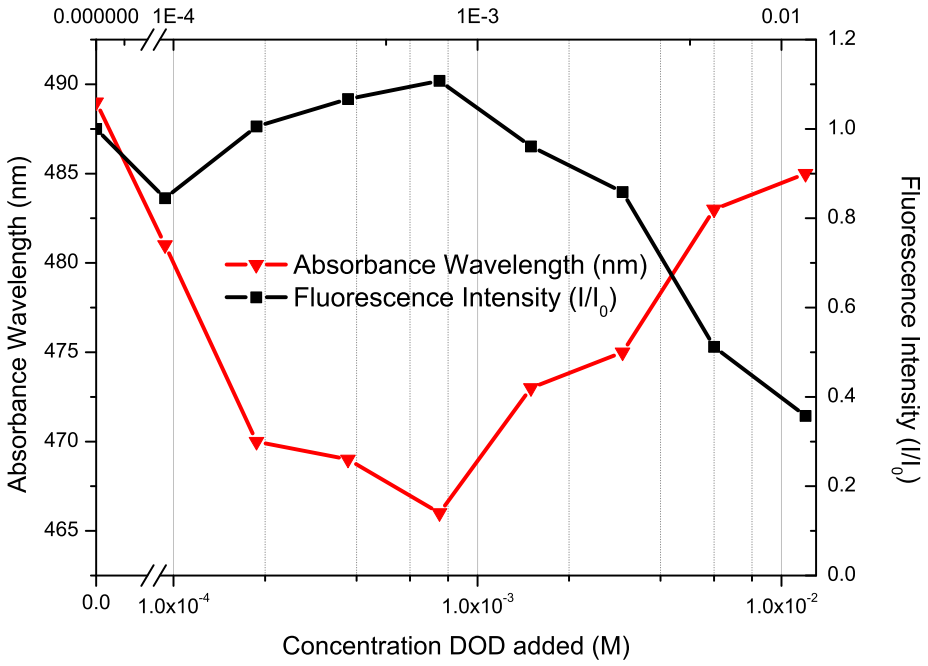

Figure 5.2 Plot of PTEBS absorbance wavelength and fluorescence intensity with a range of DOD concentrations.

with DOD additions to 466 nm over the 0–1×10^{-3} M concentration range. The wavelength was then observed to red shift back to higher wavelengths peaking at 485 nm over the remaining 1×10^{-3}–1.2×10^{-2} M DOD concentration range.

The fluorescence emission spectral line shape also shows large changes in shape as well as intensity when in the solid phase. The normalized fluorescence emission spectra of PTEBS with a range of DOD additions is shown as Figure 5.3. The plot shows PTEBS solutions with no DOD addition, 0.00019 M DOD addition, 0.0015 M DOD addition, and 0.006 M DOD addition relating to 0, $\frac{1}{64}$. $\frac{1}{8}$, and $\frac{1}{2}$ the CMC of DOD, respectively. As can be seen, the peak shape begins to change with increasing DOD concentration with an observable shoulder occurring at approximately 605 nm with the relative intensity of the shoulder increasing with more concentrated DOD additions.

In order to determine the source of the emission spectra shoulder, excitation spectra were taken of the solutions. All excitation measurements were scanned at 605 nm with a solution of PTEBS also taken as a control. The excitation spectra are shown in Figure 5.4. For consistency, the solutions shown in the excitation spectra are those shown in Figure 5.3. The spectra are all normalized to the known PTEBS excitation peak showing the change in shape relating to the shoulder.

The points of interest of the excitation spectra of the analyzed PTEBS solutions are

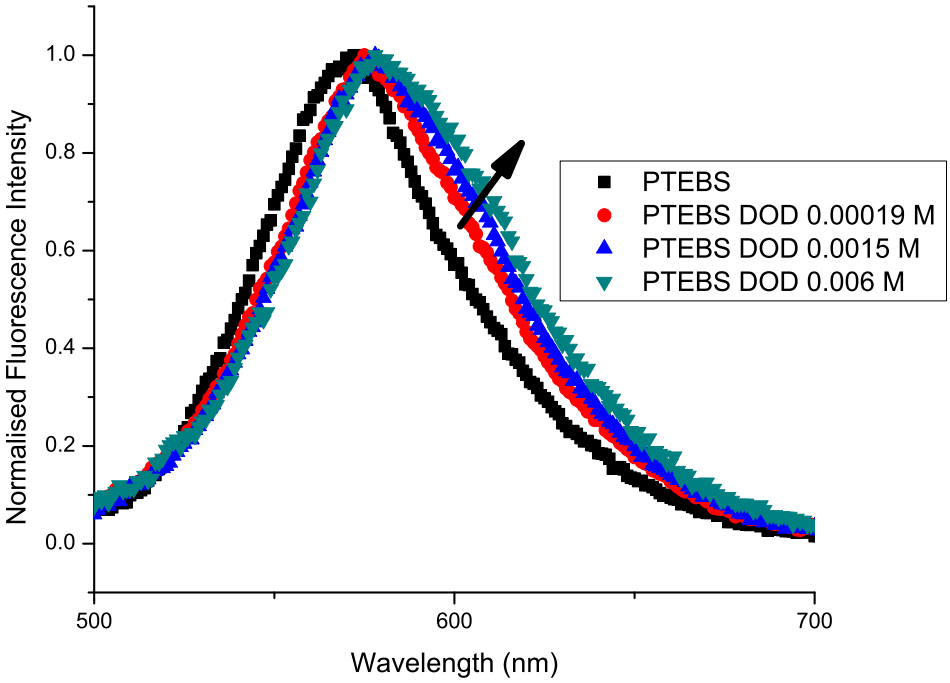

Figure 5.3 Plot of PTEBS fluorescence intensity with a range of DOD concentrations. Shown are the normalized spectra of PTEBS films with no DOD addition, 0.00019 M DOD addition, 0.0015 M DOD addition, and 0.006 M DOD addition. Marked with an arrow is the shouldering effect seen with increased DOD concentration.

labeled as 1–3 on Figure 5.4. Point one shown are the small peaks at approximately 390–400 nm. These peaks can be ignored as they are attributed to scattering of the excitation light. The excitation peak labeled (2) was the excitation relating to PTEBS in the solid state with all four spectra being normalized to this point and all showing the same peak shape at this point. The peak labeled (3) was the peak of greatest interest in this set of spectra. This peak is shown to only be present with DOD additions and is shown to increase in intensity relative to the PTEBS (2) peak with increased DOD concentration. This peak is therefore considered to be due to specific interactions of PTEBS with DOD in the solid state.

The fluorescence intensity plot shows similar effects to that of the early concentration effects seen in the solution phase PTEBS with DOD additions. The observed initial rise in fluorescence intensity is speculative as the increase is small and potentially within the uncertainty range of measurements, however the mid–high concentration DOD addition quenching effect is well outside this range showing that the decrease in fluorescence intensity is a real effect, and dependant on the concentration of surfactant in the film.

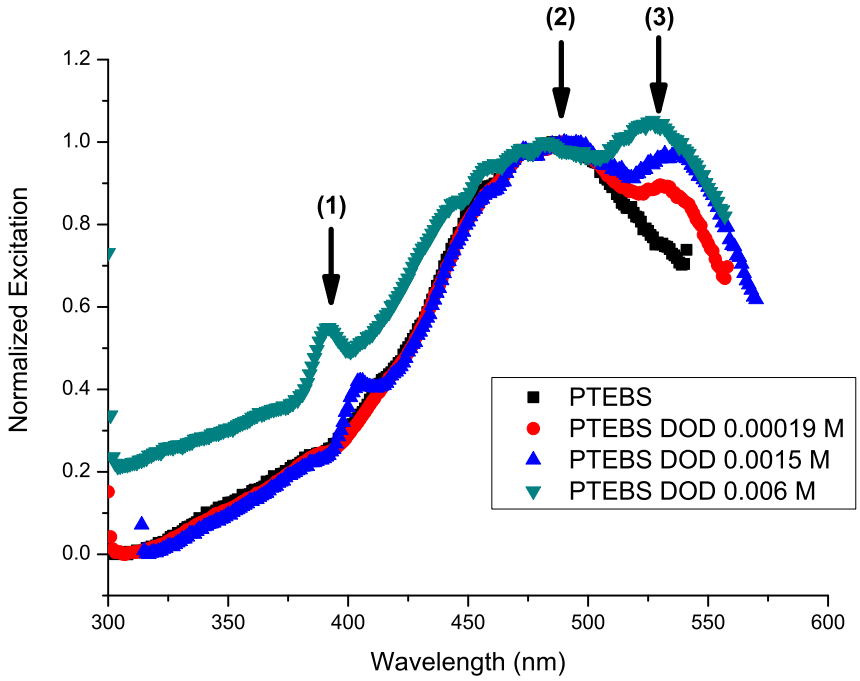

Figure 5.4 Plot of PTEBS excitation spectra with a range of DOD concentrations. Shown are the normalized spectra of PTEBS films with no DOD addition, 0.00019 M DOD addition, 0.0015 M DOD addition, and 0.006 M DOD addition. Marked with arrows are the features of the excitation spectra.

When comparing the observed quenching effect with that of the solution phase(Figure 4.1), there are two distinct differences. The first is that the solution phase shows an increase in the fluorescence intensity with the aggregation induced quenching while the solid phase shows a dramatic quenching. The second is that within the solid phase regime there is no recovery and large increase in fluorescence intensity with additional surfactant addition showing that the high concentration effects of the solution phase and solid phase are not the same.

When casting a film of CP or CPE onto the solid phase via spin coating, the purpose was to remove any solvent from the system causing the CP or CPE to fall out of solution and disperse onto the substrate, thus any solution phase driving forces are lost during casting. This results in the CP or CPE being deposited onto the substrate in a highly disordered manner resulting in an initial disordered film of CP or CPE. This aggregation effect is seen spectroscopically through the large red shift in the absorbance wavelength of the PTEBS control film in comparison to that of the solution phase.

As previously stated, the disordered structure of the casting process is an effect commonly seen throughout literature with the CP P3HT showing the most pronounced effects. With P3HT films, initial films are shown to be highly disordered

with the UV/Vis and fluorescence spectra of these films showing little to or vibronic structure. When the films are annealed allowing for melting and diffusion controlled reorganization, the films are then shown to have a greatly increased vibronic structure in their optical spectra. Thus the applied thermal energy allows for a change in the ordering of the CP via diffusion to a much more favorable state. The diffusion controlled effect is also seen with CPEs and surfactants where SANS studies have shown that when cast into films, regions of high polymer density and high surfactant density are seen.[57] In these cases, no thermal energy is required as the driving force for diffusion becomes self-assembly of the surfactant and polymer within the film. This shows that there is likely regions of self assembly (ordered) and loose aggregates (disordered) throughout the film.

The concentration of the PTEBS in each film is roughly the same with variations in the absorbance intensity taken into account for the fluorescence intensity measurements. As there is no change in concentration of the CPE, the observed decrease in fluorescence intensity must be due to DOD addition effects with the quenching appearing at approximately 10^{-3} M. In the solution phase, this concentration is related to the proposed cross-linking effects of CPE aggregates in solution via surfactant self assembly. As the films are cast from solutions with this effect, it is likely these ordered cross-linked structures have been transferred to the solid phase with the resulting solution phase ordered aggregation characteristics being accentuated by the solid phase disordered aggregation casting effects.

The driving force for the surfactant tail embedding into the CPE aggregate core and subsequent cross-linking effect is hydrophobically driven by the aqueous solvent environment (from chapter 3). When cast into a solid state film, the solvent is removed resulting in the driving force for the surfactants to be embedded into the CPE aggregate core being lost whilst the surfactant still remains bound to the CPE aggregate. As the solid films are originally cast from solutions of PTEBS with surfactant addition, it can be assumed that the solution phase concentration effects (surfactant tails embedding into CPE aggregate cores, aggregation, and micelle templating) are present in the solutions being cast. It has been shown that some solution phase characteristics do indeed get carried through to the solid phase. With these effects and the loss of the self assembly driving force in mind, the surfactants within the films cast from the aggregated PTEBS–DOD solutions have the potential to diffuse out of the CPE aggregate core due to the loss of the hydrophobic effect.

The conversion and self assembly of the of the CPE backbone and surfactant systems is possible due to the loss of the hydrophobic driving force. When casting a film, this effect is reduced as the solvent is evaporated resulting in the self assem-

bly forces changing during the evaporation process. This coupled with the natural orientation/polaristation of CPEs in the solid phase, would result in the CPE backbone twisting in order to allow for greater π–π interactions. This would cause the ionic side chains (and electrostatically associated surfactant molecules) being preferentially in one direction while the CPE backbone aligns in another. The combined with the above mentioned self-assembly of the surfactant molecules results is a diffusion/self-assembly controlled cross-linking effect and the introduction of the new CPE–surfactant–surfactant–CPE phase.

The proposed surfactant cross-linking effects being transferred to the solid state giving rise to the new phase within the film is further exemplified by the excitation spectra shown in Figure 5.4. The peak labeled (3) is potentially due to electronic transitions of CPE chains in a different state to that of the bulk aggregates. The dynamic red shift in absorbance wavelength once at the point where the second phase is noticable in the excitation spectra indicating the reformation of π–π interactions within the film also reinforces the proposal of rearrangement within the film. This transition is proposed to be due to the diffusion controlled self assembly of surfactant molecules in the solid state giving rise to a lamellar type system within the CPE aggregate.

As mentioned above, this effect has been shown in CPE literature by Pace *et al.* using zwitterionic surfactants complexed to CPEs. In this publication, with increased concentration of surfactant the authors noted a secondary peak to the red of the natural CPE absorbance which is also seen in our data. The authors then completed small angle X-ray scattering (SAXS) experiments of films exhibiting this peak and found scattering peaks showing the lamellar structure within CPE aggregates.[135] As stated in the introduction, the lamellar structure is also common in the CPE-surfactant and PE-surfactant literature with a wide range of surfactants showing these effects.[136–138,141]

With these publications and our observed results, it is proposed that the aggregation and ordered cross-linking effects in the solution phase are transferred in the casting process. The resulting thin film would then be composed of a disordered array of ordered surfactant cross-linked CPE aggregates resulting in a quenched fluorescence intensity. Provided that the concentration is large enough to allow for the short range self assembly effects to become favorable, diffusion controlled surfactant self assembly then occurs. This results in the formation of lamellar type structures within the CPE aggregate film giving rise to a second emissive phase and subsequent shoulder in the excitation spectra. This proposed model of interactions is shown pictorially in Scheme 5.1.

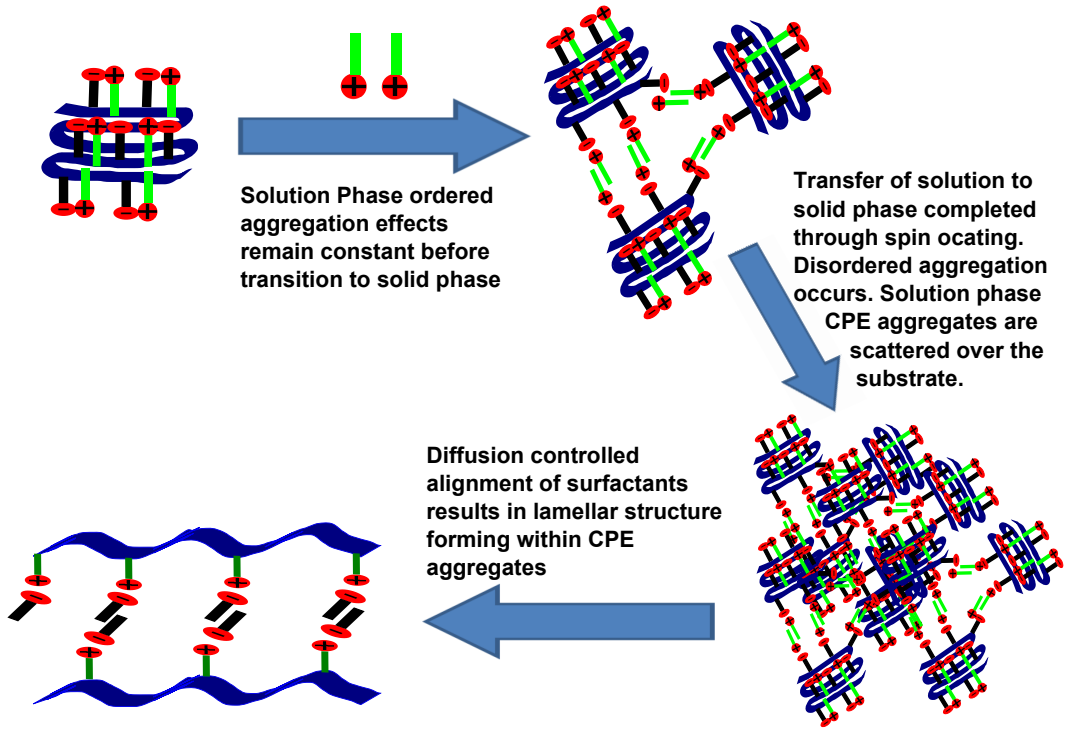

Scheme 5.1 Depiction of CPE with surfactant addition in the solid state. Solution phase ordered aggregates are cast onto the substrate causing a combination of ordered and disordered aggregation throughout the film. With increased surfactant concentration, diffusion controlled self assembly of surfactant molecules results in the formation of lamellar type structures throughout the CPE film.

In summary, this shows that solution phase CPE–surfactant characteristics can be transferred to the solid phase via spin coating concentrated solutions of CPE with surfactant additions. The surfactant self assembly via van der Waals and electrostatic interactions reinforces the requirement for complementary electrostatics within CPE–surfactant systems. Similar work was completed using FPQ-PB and FPQ-IB and SDS, however little effects were seen (data not shown).

5.3 FRET Study of FPQ-Br and PTEBS Layer-by-Layer Assemblies

FPQ-Br and PTEBS have a large optical overlap in their absorbance and emission spectra (see Figure 5.5). This allows for favorable Förster resonance energy transfer (FRET) between the two CPEs in the solution and solid phase. PTEBS is directly soluble in distilled water whilst FPQ-Br is not directly soluble in the same solvent giving rise to the layer-by-layer (LBL) thin film fabrication method. This technique is not likely to produce unique layers with the CPEs in this case however. This is due to FPQ-Br being soluble in (and thin films cast from) methanol. When the

thin film cast from methanol is dipped into the PTEBS–distilled water mixtures, the second layer is added resulting in a reordering of the FPQ-Br backbone to allow for charge neutralization of the underlying layer allowing for the two layers to effectively combine at the interface resulting in roughness of the films. Further PTEBS is then attracted to result in the inversion of charge on the new top layer.[142] The miscibility of methanol in water would further enhance this effect by allowing any trapped methanol in the film dispersing into the distilled water in the dipping process with further changes in the FPQ-Br structure.

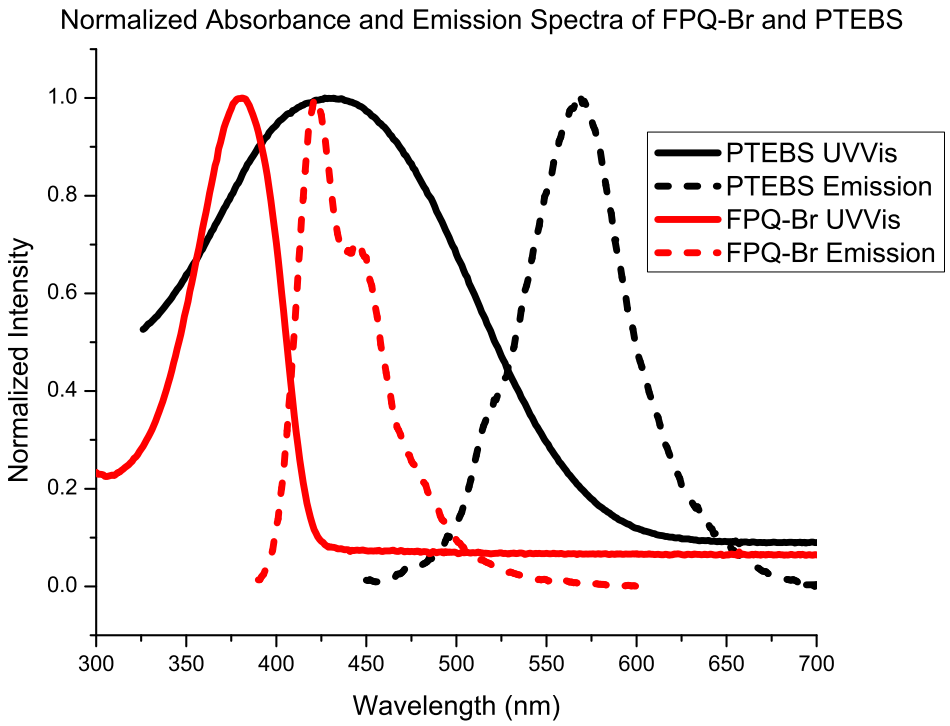

Figure 5.5 Normalized absorbance and emission spectra of FPQ-Br and PTEBS showing strong emission and absorption overlap of the two CPEs.

Layer-by-layer (LBL) assembly is a technique well established throughout literature. This technique involves layering of two complementary charged systems such as anionic and cationic CPEs (CPE1 and CPE2) on top of each other via favorable electrostatic interactions.[71] The technique begins with the casting of a single layer of CPE1 onto a substrate and washing with an orthogonal solvent. This leaves a layer of charged CPE1 at the surface of the substrate. This solution is then dipped into a solution of complementary charged CPE2 solution allowing the favorable electrostatic interactions of the ionic interactions to couple the two CPEs together resulting in the formation of a second layer of CPE2 to be adsorbed on top of the first (CPE1) with the surface layer now being composed of the opposite charge to the first. The film can then be washed again in an orthogonal solvent system and dipped into a solution of CPE1 resulting in formation of a third layer being cast on top of the first being composed of CPE1. A pictorial representation of this technique

is shown below in Scheme 5.2.

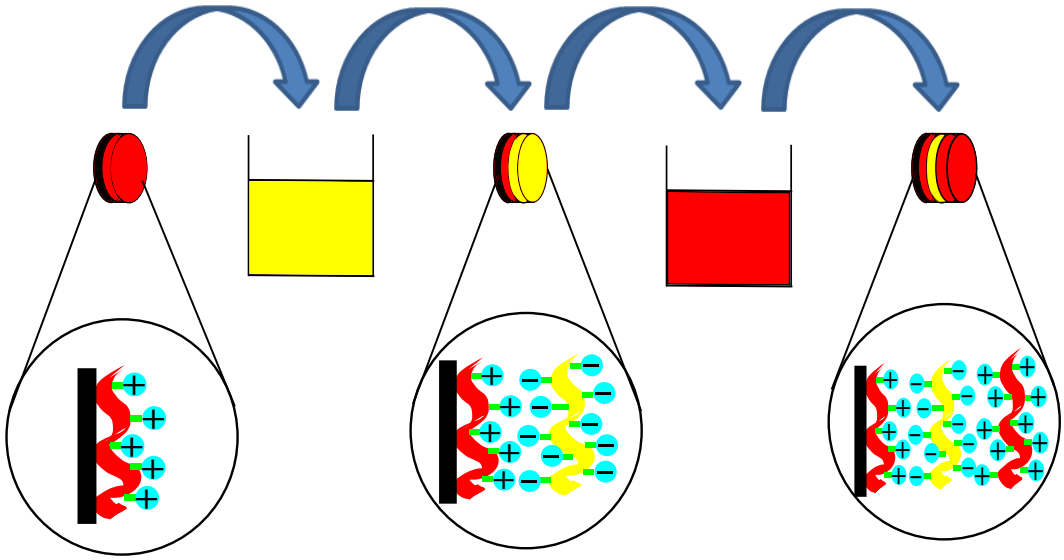

Scheme 5.2 Depiction of the layer-by-layer technique showing electrostatic formation between CPE1 (red) and CPE2 (yellow). The electrostatic attraction allows for build up of multiple alternating layers of CPE.

The solid phase FRET based characteristics of LBL thin films composed of FPQ-Br and PTEBS were created by initial deposition of FPQ-Br directly onto a fused quartz substrate via spin coating from methanol. 70 μL solutions of FPQ-Br (7.5 mg mL^{-1}) were titrated onto 1 cm diameter fused quartz substrates and spun at 5000 rpm for 30 seconds to allow for thin film deposition. A concentrated PTEBS solution (3.6×10^{-4} M) was used for the dipping solution. All emission spectra were excited at the absorption peak maximum and all data normalized for variation in the absorption intensity. The FRET based emission is also normalized for direct emission of PTEBS with the excitation of FPQ-Br. All excitation measurements were excited at the peak wavelength of FPQ-Br after each dip to allow for direct comparison between measurements.

In order to prove that the emission of PTEBS is coming from FRET based energy transfer process rather than direct excitation of the PTEBS chromophore, an excitation spectrum was run to show the absorbing chromophores of the PTEBS emission. The resulting excitation spectrum is shown below as Figure 5.6. From this spectrum it can be seen that there is a large peak near 390 nm (1, FPQ-Br) and a much smaller peak near 480 nm (2, PTEBS). These peaks are associated to the with the absorbing species with the intensities sohwing their relative contribution to the emission. As can be seen peak 1 (FPQ-Br) has a much larger contribution to the emission than peak 2 (PTEBS) thus the bulk of the PTEBS emission comes from the excited FPQ-Br chromophore (peak 1) rather than excitation from PTEBS (peak 2).

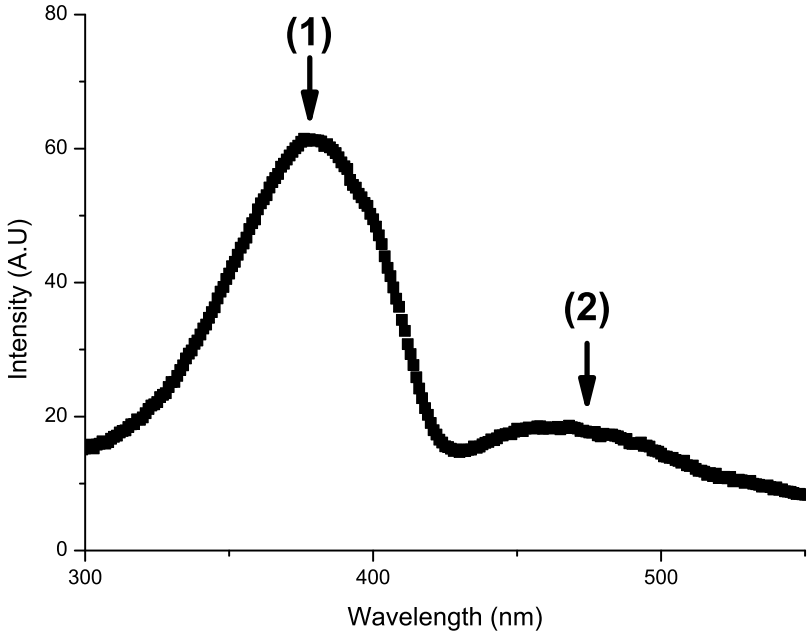

Figure 5.6 Excitation spectra of the measured PTEBS emission. Labelled are the excitations relating to FPQ-Br (1) and PTEBS (2).

The emission and subsequent FRET based emission of PTEBS with increased dip number is shown as Figure 5.7. The FPQ-Br fluorescence intensity was shown to have been dramatically quenched to approximately 10% of the FPQ-Br film alone when the film is first dipped into the PTEBS solution. This was followed by a slight increase in intensity to approxiamtely 20% of the original fluorescence intensity over the remaining (2–7) dips. The PTEBS emission shown is solely due to FRET based emission from FPQ-Br excitations with any emission from PTEBS being directly excited, normalized out. As can be seen, the emission is shown to increase with the initial dip showing that the layer-by-layer technique has allowed PTEBS adherence to the FPQ-Br film. The PTEBS intensity was then shown to gradually decrease over the remaining dip numbers (2–7) to approximately 0.5 times that of the initial FRET based emission.

The emission wavelength of FPQ-Br and FRET based emission wavelength of PTEBS is shown as Figure 5.8 as a function of dip number. The FPQ-Br film emission wavelength was shown to gradually blue shift in position from the original 427 nm through to 411 nm over the dipping process. The FRET based PTEBS emission wavelength is shown to also have a general blue shift from 567 nm through to 547 nm with increased dip numbers. There are large fluctuations in the observed FRET emission wavelengths, with wavelengths fluctuating approximately 5 nm either side of the general observed blue shift.

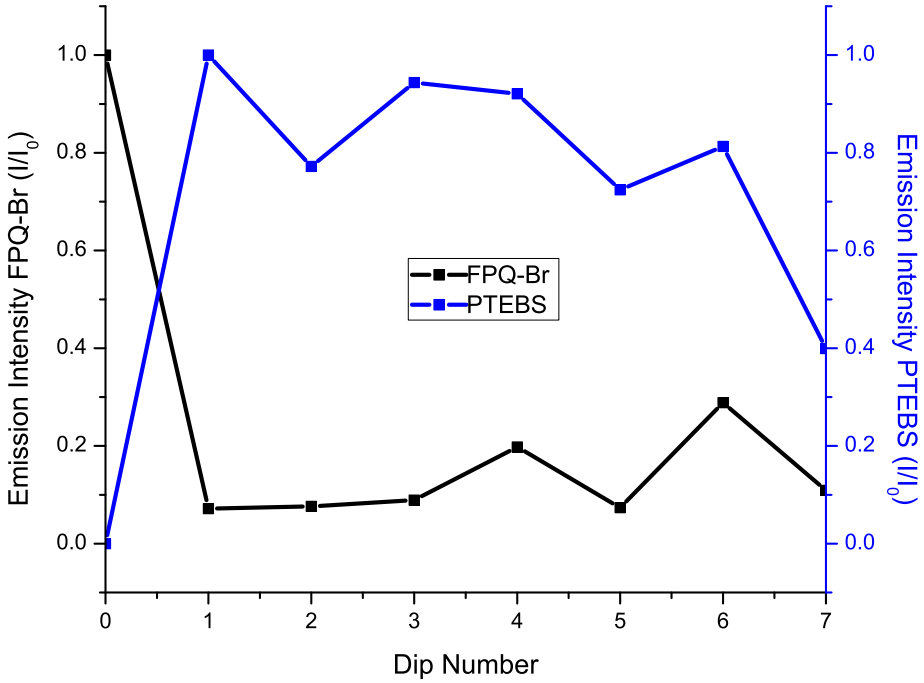

Figure 5.7 Plot of emission intensities of FPQ-Br and PTEBS over multiple FPQ-Br film dipping steps into PTEBS solution.

The initial quenching of FPQ-Br with dipping and subsequent layering of PTEBS onto the film is primarily a result of FRET based energy transfer to the PTEBS molecule. This transfer results in the emission observed from PTEBS whilst not being directly excited. The following slight increase in emission intensity over the remaining dip numbers can be attributed to two different effects: The first is a change in ordering of the FPQ-Br CPE backbone due to the swelling of the FPQ-Br film to release trapped methanol solvent. The second is a change in the FRET energy transfer distances resulting in a reduced FRET based transfer to the PTEBS CPE.

The emission of PTEBS was shown to increase from no emission through to maximum measured with the first dip layer. The decrease in emission intensity with further layering attempts is consistent with both of the above mentioned effects causing the changes in FPQ-Br fluorescence intensity. With increased FPQ-Br emission due to the FRET distance increasing, the amount of energy being transferred to the PTEBS is reduced as a function of the sixth root of the distance between chromophores.[79,80] This results in the emission of PTEBS being reduced with the increased separation distance.

The change in backbone ordering is also consistent when considering the solubility

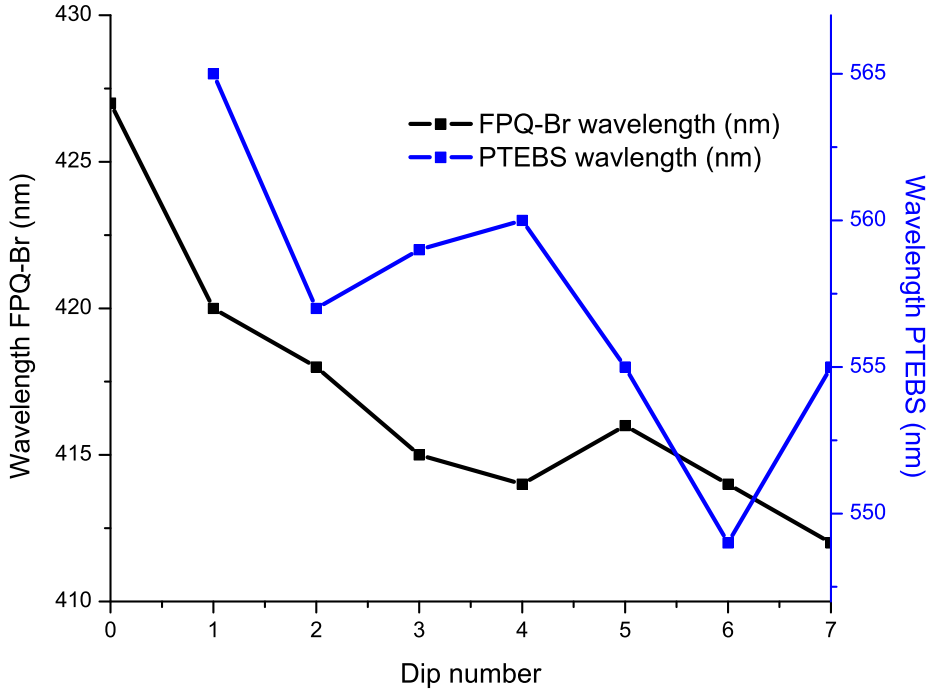

Figure 5.8 Plot of emission wavelength of FPQ-Br and PTEBS over multiple FPQ-Br film soaking steps in PTEBS solution.

of PTEBS in distilled water. With each dip into the PTEBS solution, it is unlikely that any further PTEBS molecules are being electrostatically bound due a finite thickness of film being able to be deposited with each layering step. However, the dip into solution does still allows for swelling and reordering of both the FPQ-Br and PTEBS molecules on the film to release trapped solvent and rearrange into more favorable structures. This results in any PTEBS polymer chains that were within the film due to any non-electrostatic means being dispersed back into solution. Any successive dip further reduces the number of non-electrostatically bound PTEBS chains thus reducing the fluorescence intensity from the PTEBS layer due to reducing the number of emissive chromophores.

The fluorescence wavelength measurements show a large blue shift in emission peak position for both FPQ-Br and PTEBS. This indicates that each dip is resulting in a reordering of both CPEs to a more favorable state. This reinforces the proposal of CPE backbone reordering when immersed into the PTEBS solutions due to swelling. This allows for an increased emissive intensity of FPQ-Br due to extending into a more extended state, while decreased emission intensity PTEBS due to reducing the number of non-electrostatically bound emissive chromophores.

The reordering of the CPE backbones shows a further change however. Provided

that reordering is indeed occurring, this shows that the CPEs are mixing with each other in the film when immersed into the solution rather than forming distinct layers on top of each other. This shows the need for orthogonal solvent systems to be used with the CPE layer-by-layer technique in order to form the unique CPE layers. Scheme 5.3 shows a pictorial representation of the CPE washing effect.

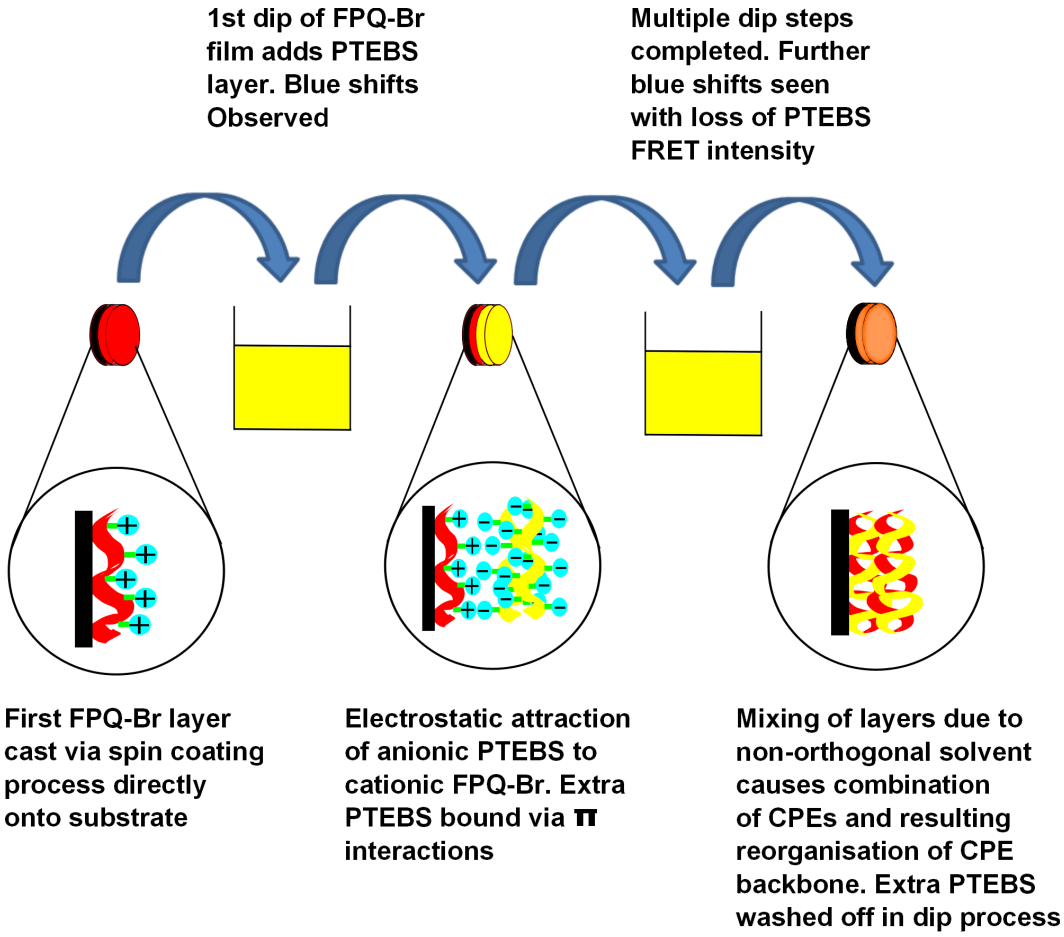

Scheme 5.3 Depiction of formation of the altered backbone structure of FPQ-Br and PTEBS via a multiple soak processes. Each soak is shown to alter the backbone structure of the CPEs resulting in a final mixed CPE layer system.

5.4 Summary

This chapter has outlined the characteristics of CPEs with complementary surfactant addition in the solid phase. FRET based studies of PTEBS and FPQ-Br layers in non-orthogonal solvent systems where the layers were created via the LBL technique are presented and discussed.

The transfer of PTEBs with complementary charged DOD additions has been shown to result in the natural disordered aggregation associated with the stacking of CPE in the solid phase and also concentration dependant ordered aggregation within

the CPE aggregates. The ordered phase has been attributed to diffusion controlled surfactant self-assembly within the CPE aggregates causing lamellar type assemblies within the CPE films. This ordering is known throughout the literature of both PE with complementary surfactant systems and CPE with zwitterionic surfactant systems.

The layering of the two studied CPEs via the layer-by-layer technique has been shown to result in FRET based emission of PTEBS via excitation of FPQ-Br. The optical data has also been shown to have variations in both the peak position (blue shifts) and fluorescence intensity of both CPEs. These changes have been attributed to the reorganization of the CPE backbones when immersed into the solvent system and a wash effect of the upper PTEBS layer due to both FPQ-Br and PTEBS being soluble in distilled water.

This chapter has shown that some CPE solution phase characteristics are able to be transfered to the solid phase via simple spin coating techniques. This allows for study of how ion addition affects the electronic properties of CPEs in the solid state via device fabrication. The following chapter details the field effect transistor (FET) characteristics of a CP with surfactant ion addition.

Chapter 6

OFET Devices from CPE–Surfactant Complexes

6.1 Introduction

Conjugated polymer light emitting diodes (PLEDs) and thin film field effect transistors (FETs) are an exciting new technology in the optical electronics field. Devices from these materials have the potential to to create low cost displays, memory storage, and solid state lighting.[143,144] In order to achieve these potential devices, a few problems need to be addressed. One of the outstanding problems is balanced electron and hole injection into the devices at unequal rates. In general, a large contribution of the device efficiency comes from the injection of electrons and holes from the electrodes to the emissive layers. Injection efficiency is determined by the energy difference between the Fermi level of the electrode and the highest occupied molecular orbital (HOMO) or lowest unoccupied molecular orbital (LUMO) for hole and electron injection respectively. Thus the electrodes and polymer species need have well matched HOMO and LUMO levels for efficient devices.[145]

Most conjugated polymer species whether they be CP or CPEs, the comparatively low HOMOs levels of the polymers result in the need for low work function metals such as calcium or barium to be used as electrodes for efficient injection.[146] These low work function metals have been show to be both air sensitive[90] and unstable in devices with metal ions being formed at the polymer–electrode interface and migrating into the polymer layer, affecting long term stability of devices.[147]

When placed into films, CPEs were found to have characteristics that are not seen in

CP systems due to their ionic characteristics. As discussed in the introduction, these characteristics include polarization of ionic side chains towards electrodes resulting in increased injection capabilities, and the introduction of mobile ions within the film resulting in changes to the internal electric field and work function of electrodes.[148]

The general mechanism for the change in work function of the electrodes with CPE use is one that is a combination of the two effects. Authors have suggested that the introduction of a permanent dipole between the cathode and the semiconducting layer allows for more favorable electron injection due to the reduced electrode work function.[149] This is evident by the favorable results seen with CPEs with ammonium based CPEs with high work function metals such as gold where the ammonium ions have favorable interactions with the gold resulting in a high level of polarization.[150]

The alternative mechanism is that of mobile ion migration throughout the CPE film. The introduction of a bias through the film allows for a driving force to allow mobile ions (counter ions of CPE or extrinsic ions) to migrate to electrodes resulting in an accumulation of mobile ions at the polymer-electrode interface.[94] This results in changes in the internal electric field on the device allowing for diffusion controlled electron and hole movements throughout the films.[151,152] This effect has been proven through devices being fabricated with CPEs with the same backbone but different counter-ions, resulting in different device characteristics.[153] This effect is also shown when the CPEs are used as single component light emitting electrochemical cells, devices that function through ion migration,[154] and ultra-fast spectroscopy techniques.[155]

This effect has allowed for the formation of efficient devices using CPE layers as both blocking layers and injection layers throughout organic devices. The effect of the ionic nature has allowed for the formation of devices using more stable work function electrodes (such as gold) allowing for increased device stability.[156] Reports have also shown that devices that use of CPE injection layers with high work function electrodes have increased efficiency in comparison to similar devices using calcium or barium electrodes.[152,157]

The introduction of mobile ions within FETs has also been shown to significantly alter overall FET device characteristic. Reports throughout literature have noted changes in FET character through both the overall device performance with lower turn-on voltages at varying concentrations of mobile ions in devices[158,159] and observed hysteresis of gate voltages with mobile ion additions.[160,161] The introduction of the hysteresis to the transistors provides an interesting new possibility for the creation of devices with potential applications sensing,[160] low turn on displays,[162]

memory storage applications,[144] and inject printed devices.[163]

The final goal of this research was to utilize the controlled assembly and counter-ions of CPE–extrinsic ion systems to create a range of devices. The devices were to be of organic field effect transistor (OFET) type with surfactants and/or metal ions making up mobile ions within the CPE film while also inducing the previously discussed self-assembled structures. CPEs mobile ions and inherent polarization is shown to result in significant changes in the work function of electrodes. With this in mind, the mobile ions placed into the CPE films were to be a melt/freeze type system where the film would be annealed, and then biased allowing for the mobile ions to migrate throughout the film. The film would then be allowed to cool resulting in the mobile ions being trapped in their biased location. This has the potential to result in the formation of devices with unequal work function due to ion accumulation. The result of which is the formation of assymetric work function OFET devices from symmetrical electrodes.

Due to material supply problems of PTEBS and the known thermal degradation problems of polyfluorene based polymers such as the FPQ-X series[154] only proof of concept OFET devices could be created using P3HT in chloroform with surfactants added as mobile ions. Due to the non-ionic and non-water soluble nature of P3HT, no control of the aggregation state or CPE counter-ion movement was possible with these devices. Time and instrumentation issues also hindered analysis of the devices, thus only preliminary data of the P3HT with DOD devices is presented in this chapter. Due to devices being tested in air and over several days, the performance cannot be directly related to the literature. Therefore a control device is used for comparative purposes.

6.2 P3HT OFETs with DOD Additions

P3HT with titrated DOD made into OFETS were created through spin coating concentrated P3HT solutions (10 mg mL^{-1}) in chloroform with 10 μL spiking of various concentrations of DOD also dissolved in chloroform. 80 μL aquilots of the P3HT–DOD mixtures were deposited onto pre-cleaned silicon dioxide on silicon (SiO_2/Si) substrates and spin coated immediately at 2500 rpm for 30 seconds to create the P3HT–DOD film. 50 nm gold electrodes were then deposited onto the film through metal evaporation with a channel spacing of 100 μm between the source and drain electrode. OFET character was examined through the use of an Agilent 4156C precision semiconductor parameter analyzer with a probe station and current

vs voltage (I/V) plots obtained for gate voltages varying between -10 and -40 V. Time dependant tests were attempted using the repeat scan function of the parameter analyzer to analyze changes in current vs time. A schematic of the OFET device configuration is shown below as Figure 6.1

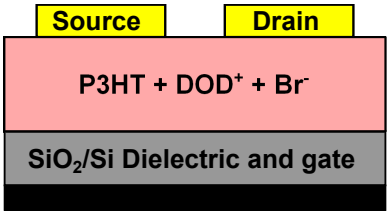

Figure 6.1 Depiction of the OFET device layers and structure fabricated and used for P3HT–DOD OFET devices

The voltage between source and drain (Vds) vs drain current (Id) for devices with P3HT as a control (no DOD addition), P3HT with 0.0002 weight% DOD, and 0.02 weight% are shown below as Figure 6.2, Figure 6.3, and Figure 6.4, respectively. With all devices, the line shape of the measurements remains that of a typical FET curve and all measurements are taken under the same conditions and voltage biases.

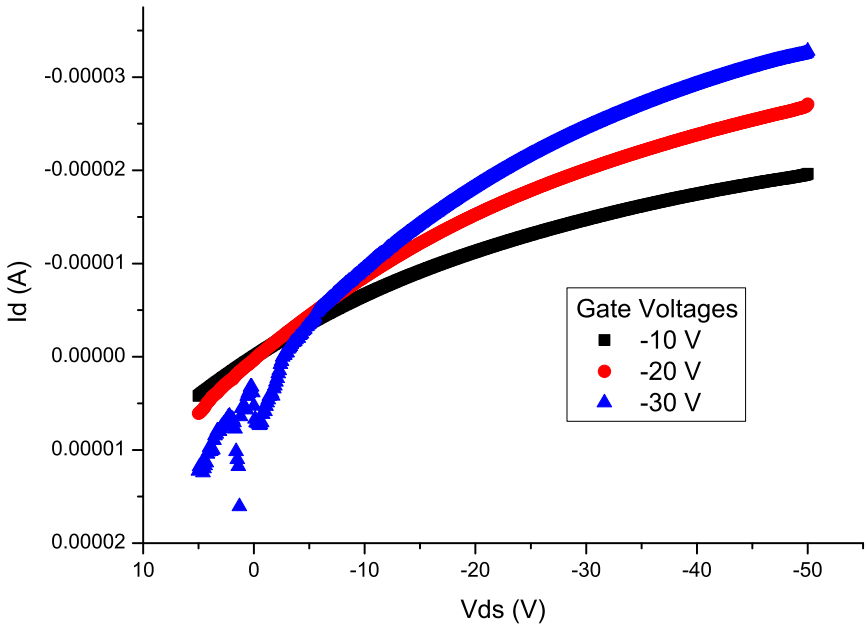

Figure 6.2 Plot I/V curves of P3HT control OFET at -10 – -30 V gate bias. The variation towards the 0–0 point of the -30 V gate sweep is due to degradation of the P3HT film.

The P3HT control device plot (Figure 6.2) shows the current at the drain electrode with an applied source–drain bias of 5 – -40V at applied gate voltages of -10, -20, and -30 V. Gate voltages of -40 V and -50 V were also attempted however the plots showed high levels of variation attributed to degradation of the P3HT film which likely occurred either in the spin coating process where a non-uniform film

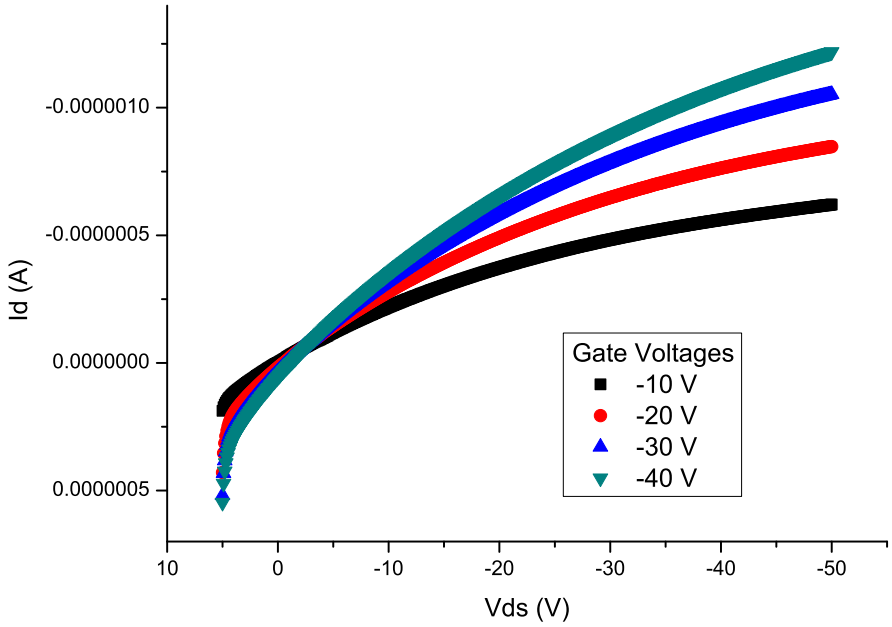

Figure 6.3 Plot I/V curves of P3HT with 0.0002 w% OFET at -10 – -40 V gate bias.

was created, or when the electrodes were evaporated on top of the film. Some degradation is also observed in the -30 V plot with the low current measurements (5 – -5 V) shown as interference within this region.

The plots of current vs. source–drain bias are all shown to have similar line shapes with each plot peaking at different current levels dependant on the applied gate voltage within the measured source–drain bais. In all cases, the maximum measured current was recorded at -50 V source–drain voltage. The current data at the -50 V source–drain bias with the three applied gate voltages is summarized below in Table 6.1

Table 6.1 Measured current at -50 V Vds at various gate voltages of the P3HT control device

Gate Voltage (V)	Current at -50 V Vds (A)
-10	-2.0×10^{-5}
-20	-2.7×10^{-5}
-30	-3.3×10^{-5}

The FET character plots of the devices with DOD addition were observed to be quite different to the control. Figure 6.3 shows the device performance of P3HT with 0.0002 weight% DOD additions. With this plot the first thing of note is the scale of the current in comparsion to that of the P3HT control. With the DOD

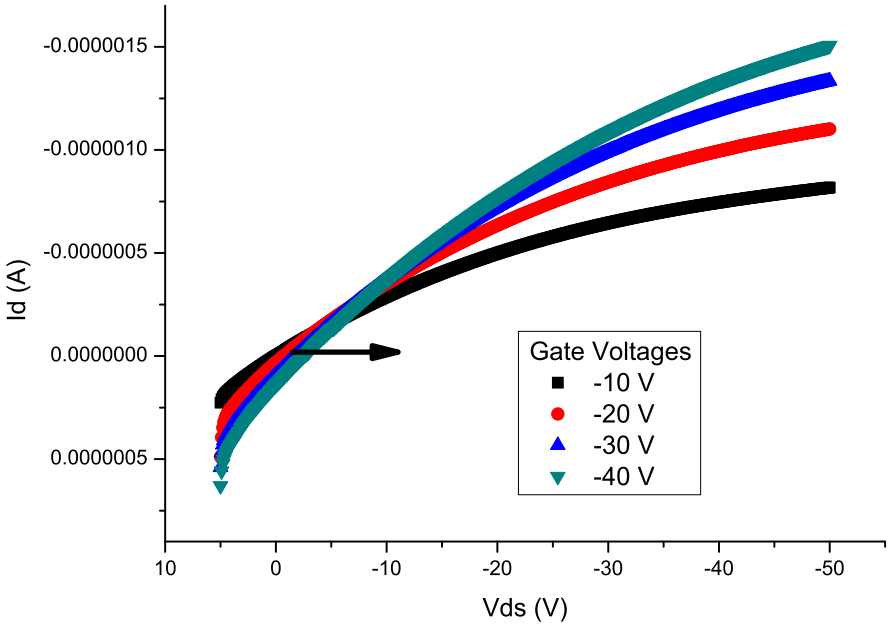

Figure 6.4 Plot I/V curves of P3HT with 0.02 w% OFET at -10 – -40 V gate bias. The arrow indicates the noticable movement away from the 0–0 origin with increased gate bias. The arrow emphasizes the movement of each successive run from the origin.

additions, the measured drain current was significantly reduced across all measured gate voltages and source–drain biases. P3HT with 0.0002 weight% DOD showed no degradation at higher gate voltages allowing for the -40 V gate sweep to be measured. As with the control sample, the maximum current at -50 V source–drain voltage for P3HT with 0.0002 weight% DOD additions is summarized below in Table 6.2.

Table 6.2 Measured current at -50 V Vds at various gate voltages of the P3HT with 0.0002 weight %DOD

Gate Voltage (V)	Current at -50 V Vds (A)
-10	-6.2×10^{-7}
-20	-8.4×10^{-7}
-30	-1.0×10^{-6}
-40	-1.2×10^{-6}

The P3HT with 0.02 weight% (Figure 6.4) DOD also showed significantly reduced drain current in comparison to the control device while maximum currents are larger than that of the P3HT with 0.0002 weight% DOD. As with P3HT with 0.0002 weight%, the device shows no signs of degradation at the higher gate voltages allowing for the -40 V gate voltage sweep. The maximum currents of the

P3HT with 0.02 weight% DOD device is summarized below in Table 6.3.

Table 6.3 Measured current at -50 V Vds at various gate voltages of the P3HT with 0.02 weight %DOD

Gate Voltage (V)	Current at -50 V Vds (A)
-10	-8.2×10^{-7}
-20	-1.1×10^{-6}
-30	-1.3×10^{-6}
-40	-1.5×10^{-6}

With all the mentioned devices, there is also an observable non-zero voltage measured at 0 current indicating either a residual charge is induced in the system, or the devices are leaking in some manner. This is shown to shift with increasing gate voltage with the devices with DOD addition showing a very pronounced movement. Due to the degradation of the control sample at the higher voltages, this effect is not explicitly seen in the -30 V gate bias, however the effects are seen clearly in the devices with DOD addition.

In order to analyze this effect, a plot of the current measured at the 0 source–drain voltage (Vds) with increasing gate voltage was created. In this plot, the -10 V gate sweep current for all 3 devices was set to 0 with all higher voltage sweeps normalized to this point. This was done to allow for comparison between the devices. Figure 6.5 shows the resultant plots of current vs applied gate voltage at 0 applied bias.

As can be seen, there was an obvious linear trend in the current measured at the different gate voltages. The linearity of the changes suggests that this effect was probably due to charges leaking through the SiO_2 dielectric layer into the P3HT layer as the gate voltage was increased. The smaller currents being measured with increased DOD addition can then be speculatively assigned to leak charges being trapped by the DOD^+ surfactant with both DOD devices providing similar levels of electron trap sites in comparison to the control (same order of magnitude) with differences potentially being due to self assembled surfactant states within the films. Electron trap sites would reduce the amount of leak electrons being measured at the drain electrode thus the control device has the largest observed 0 bias current.

Time resolved measurements at 0 Vds were attempted using the Agilent 4156C semiconductor analyzer and probe station and using a stop watch to take manual time measurements over a 10 minute time scale. Each scan was run between 5 and -40 Vds for each 0 Vds measurement. These results showed little current over the

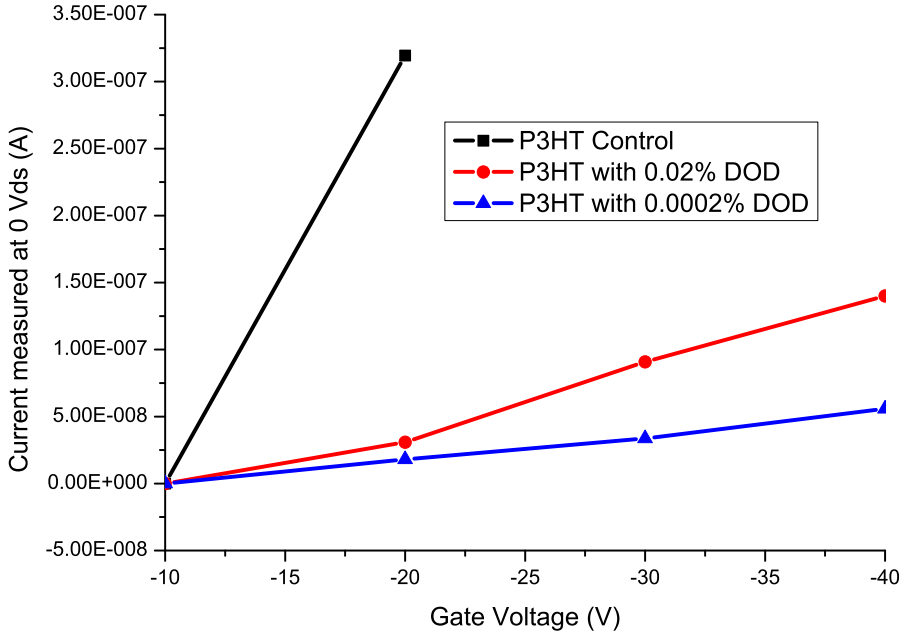

Figure 6.5 Plot of Current vs. applied voltage plot at 0 gate voltage for all three fabricated devices.

measured time scale ($\times 10^{-9}$ A). The repetition of the entire sweep range may have resulted in a repositioning of ions with each scan at the low (5 V) and high (-40 V) source–drain voltages and due to the measurements needing to be stopped for each scan to be recorded, the repetition level and reliably of the results is low. As a consequence these results are not believed to be reliable and are not further discussed. The plots of the measured current at '0' Vds vs time for the measured devices can be viewed as Figure 9.8, Figure 9.10, and Figure 9.9 in the appendix. Repetition of device fabrication with both the same P3HT batch and a higher regioregularity, high molecular weight P3HT, yielded non-operational control devices thus further comparison data could not be taken.

In order to be able to fully assign this trapping effect, new experiments would need to be completed. These experiments would involve monitoring the internal electric field of the devices with DOD addition and taking time resolved current measurements after biasing. Monitoring of the internal electric field within the device may allow for monitoring of changes in the mobile ion location within the film due to the applied gate voltage, while the time resolved current measurements will allow for monitoring the relaxation of any ion movement back to equilibrium. These experiments may also give insight to the amount of (if any) surfactant charge trap sites within the film. Due to time restrains and inadequate instrumentation, these experiments could not be undertaken within the time limits of this thesis. A rig for testing time resolved current is currently under construction where the the measurements will be able to

be undertaken once complete.

The large reduction in the amount of current measured with DOD addition to the P3HT films can be explained through the changes in morphologies of the film. While the surfactants do not directly interact with the P3HT through any formal electrostatic or van der Waals interactions (see chapter 4), when cast into a film the surfactants and P3HT are mixed into a blend creating a disordered mixture of polymer and surfactant throughout. This would result in some of the surfactant molecules interrupting the P3HT self-assembly resulting in increasing the level of disorder and loss of crystallinity of the P3HT matrix. Increased disorder of the P3HT film domains is known inhibit charge hopping processes, thus reducing the charge carrier mobilities.[164] Given the charge trapping hypothesis speculated above, this would also decrease the overall device performance due to the DOD trapping a portion of the charges.

6.3 Summary

This chapter showed the device characteristics of three devices made from P3HT with 0, 0.02, and 0.0002 weight% DOD addition. The aim of these devices was to show a proof of concept system where the mobile ions added to the P3HT matrix could alter the effective workfunction of electrodes resulting in an effective assymetric electrode device made from symmetric electrodes. However, this goal was not attained.

Working OFET devices were fabricated from P3HT containing the DOD surfactant with the device performance being shown to be reduced with DOD addition. The reduction in device performance has been attributed to the interruption of the P3HT self-assembly with subsequent loss of crystallinity resulting in a reduction in charge carrier mobility. DOD charge trapping sites may also play a role in the loss of device performance. However, without further experimentation, this effect cannot be accurately assigned. Further experiments have been outlined that may provide useful information in assigning the speculative data. Due to time and instrumentation limitations, these experiments could not be completed.

Chapter 7

Conclusions

In conclusion, a variety of means of controlling the optical and physical characteristics of the conjugated polyelectrolytes (CPEs) PTEBS and FPQ-X, (where X denotes the various counter-ions of the polymers) have been shown, each with varying effects and stengths. Change in CPE aggregation state and backbone conformation was investigated through solvent composition effects, metal ion addition, and surfactant addition in the solution phase. The surfactant addition effects were shown to have significant effects on both the optical and physical characteristics of the CPE solutions, with large particle size and fluorescence intensity changes being observed.

A variety of surfactant additions (complementary charged, non-complementary charged, non-micellular, and non-ionic) and concentrations were analyzed in order to extract specific interactions of the CPE–surfactant complex. Comparisons between the interactions seen with these surfactants allowed for a model of interactions between CPE–complementary charged surfactants to be formed. This model detailed the driving forces and resulting complexes formed between CPEs and the added surfactant with increased surfactant concentration in the pre-micellular concentration range.

The surfactant based control of CPE optical physical characteristics is also able to be transfered to the solid state. This was completed through spin coating concentrated solutions of CPE with surfactant additions onto optically transparent substrates. The films have been shown to result in two emissive phases within the film, attributed to the formation of a lamellar type structure within the CPE-surfactant film.

A solid state layer-by-layer based study of the two CPEs analyzed was shown to allow for FRET based energy transfer from the donor FPQ-Br chromophores through

to the PTEBS acceptor resulting in the enhancement of the PTEBS emission at the expense of the FPQ-Br. The films themselves were cast through a dip process allowing for favorable electrostatic attraction to create the mutli-layer film. This was found to result in an interdigitated film rather than discrete layers due to reorganization of the CPEs within the film.

Finally, solid state devices fabricated from the proof of concept CP P3HT with DOD additions. These devices were shown to have a greatly reduced efficiency in comparison to that of the control. The ability to alter the electrode work function, or changes in the internal electric field due to the addition of mobile ions, was not able to be analyzed due to the time and instrumentation issues. Further experimentation into this effect has potential to allow for the fabrication of asymmetric work function devices from symmetric stable work function electrodes (such as gold), through mobile ion accumulation altering the effective work function of the electrodes. This has potential to aid in reducing one of the large problems with organic devices of the current time.

Chapter 8

Future Work

The future for this work would be mainly focused on the solid state and device fabrication due to the drive of most scientific research with the conjugated polymer field being for device purposes. However, filling a few holes in the final experimental proofs for the solution phase would also be advantageous.

Future solution phase work could involve replication of experiments completed by Chapman *et al.* when using a range of non-polymeric fluorescent molecules. This work has shown that both the solvent and ionic strength effects can be combined to result in significant changes in the optical character of non-polymeric fluorescent chromophores. This was completed through addition of a range of (and a range of concentration) metal ions to the fluorescent chromophores in different polarity solvents.[165] Replication of this type of experiment with ionic polymers is likely to result in further changes in the optical and physical characteristics of the CPE through the combined electrostatic and solvophobic forces.

As stated in Chapter four, there is a large variation in publications of CPE–surfactant systems with a wide range both CPEs and surfactants studied and concentration ranges studied. Here we studied the effects of surfactants in the pre-micelle concentration range on two CPEs thus limiting the range of interactions studied. In order to address this, and increase the understanding of full range interactions, experiments should be repeated in the post-CMC concentration range and with a wider range of CPEs. This would allow for studies of post-CMC surfactant concentrations interactions and how the rigidity, molecular weight, and electron density of CPEs affects the results.

In chapter five, the solid state effects are discussed with the proposal of a diffusion

controlled reorganization of the CPE and surfactant systems resulting in a lamellar structure within the film. Two further experiments could be completed to aid in the structure design and formation. The first is a X-ray study of the second phase (SANS or SAXS) to attain structural detail about the layer so accurate identification can be completed. The second involves testing the diffusion control proposal via a layer-by-layer assembly experiment. This along with optical and SANS studies of the film, would allow for verification of the diffusion driving force proposal.

Fabrication of devices would benefit from further experimentation. Due to the supply issues of PTEBS, devices in this work were fabricated from P3HT thus the control of aggregate structure and the mobile ion content of the films was greatly reduced. Repeating the devices fabricated using a the PTEBS CPE would allow for the full study of CPE OFET devices and the role of the mobile ions within the film. This again may also benefit from studies of a wide range of CPEs also with the rigidity and ion density changes in CPEs potentially having a large effect on the characteristics of the devices fabricated.

The transfer of the solid state lamellar phase within devices would also be interesting to study. The lamellar phase is likely to interrupt the electron flow within the CPE layers, however, a recent study by Dutta *et al.* has shown that self assembled structures within CPE/PE systems can be dispersed and reformed with the applied voltage.[166] This coupled with publications showing that surfactants can induce similar effects as CPEs with changing the work function of electrodes,[146] may result in interesting device characteristics.

Chapter 9

Appendix

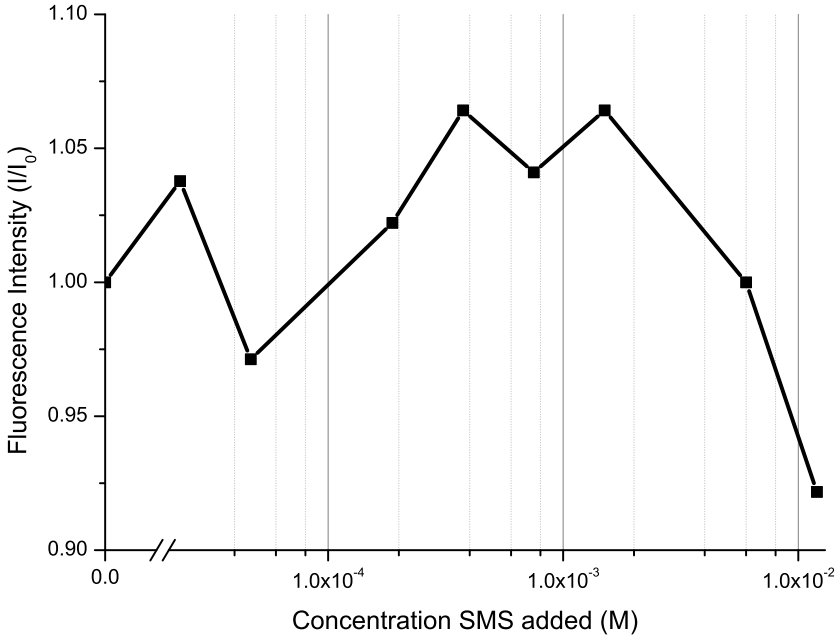

Figure 9.1 Plot of FPQ-Br maximum fluorescence intensities with SMS additions over a range of concentrations.

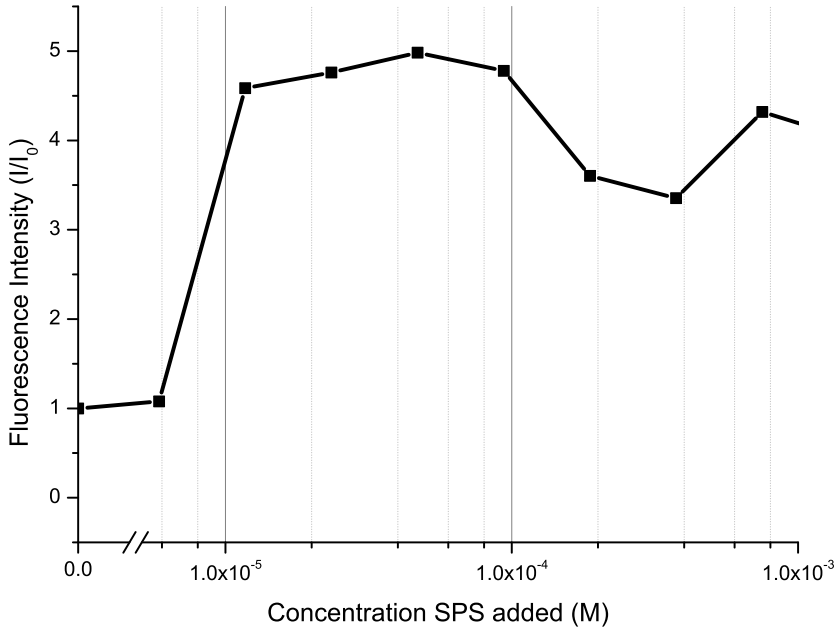

Figure 9.2 Plot of FPQ-Br maximum fluorescence intensities with SPS additions over a range of concentrations.

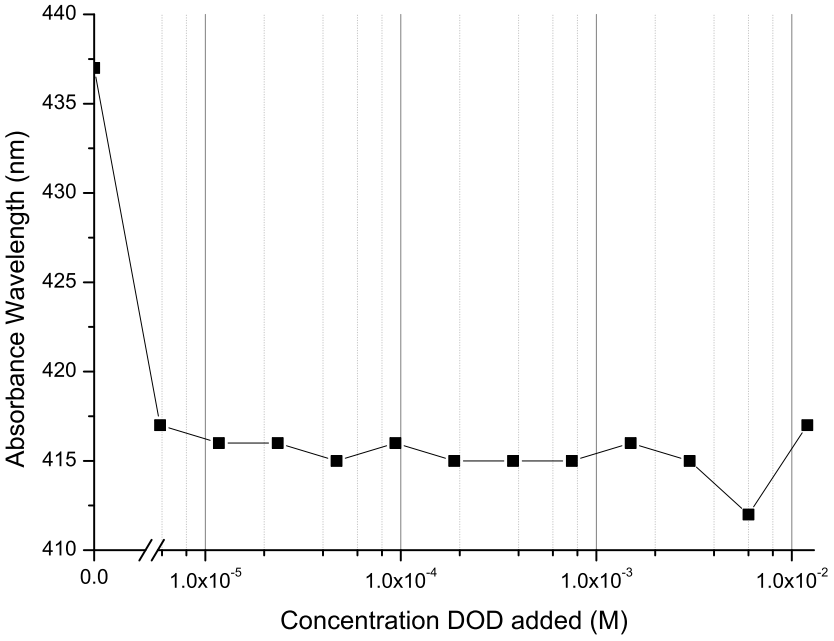

Figure 9.3 Plot of PTEBS maximum absorbance wavelengths with DOD additions over a range of concentrations.

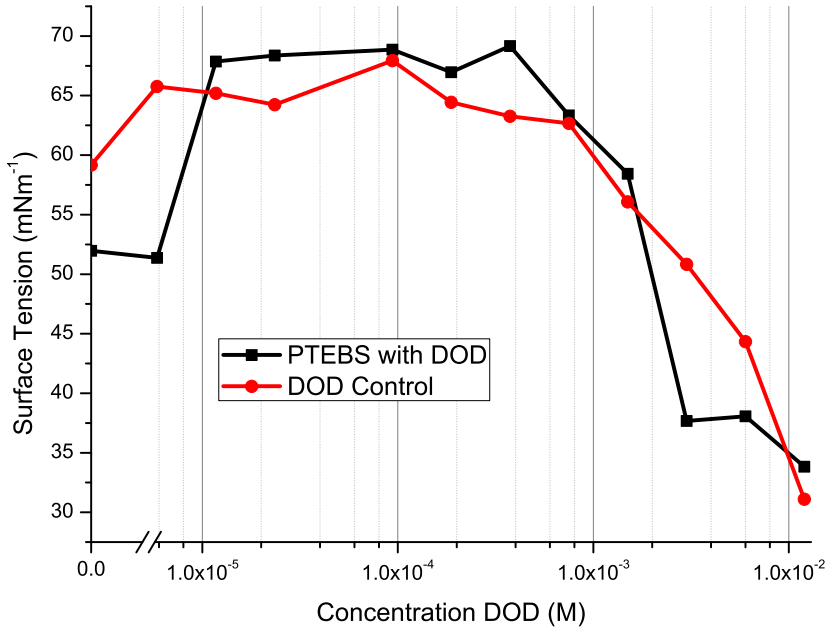

Figure 9.4 Plot of PTEBS surface tension with DOD additions over a range of concentrations with control plot.

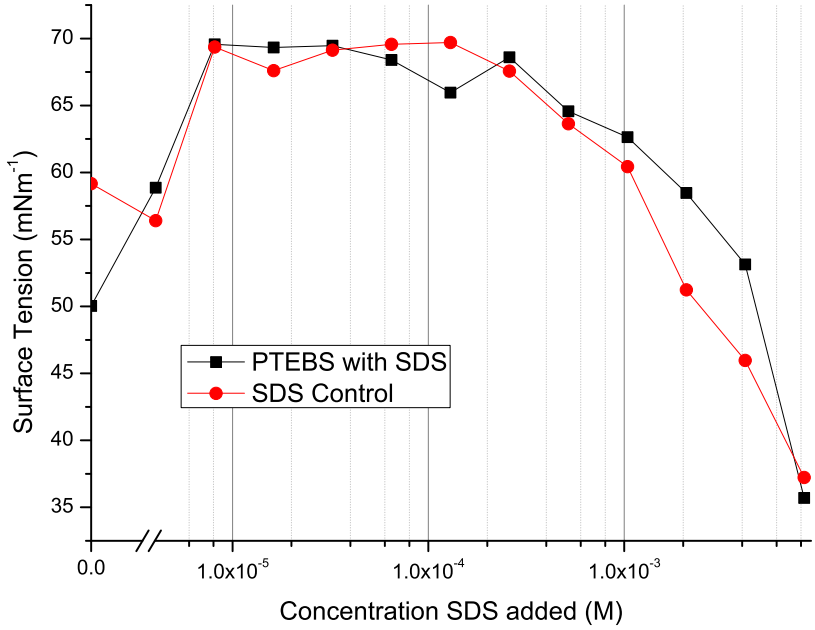

Figure 9.5 Plot of PTEBS surface tension with SDS additions over a range of concentrations with control plot.

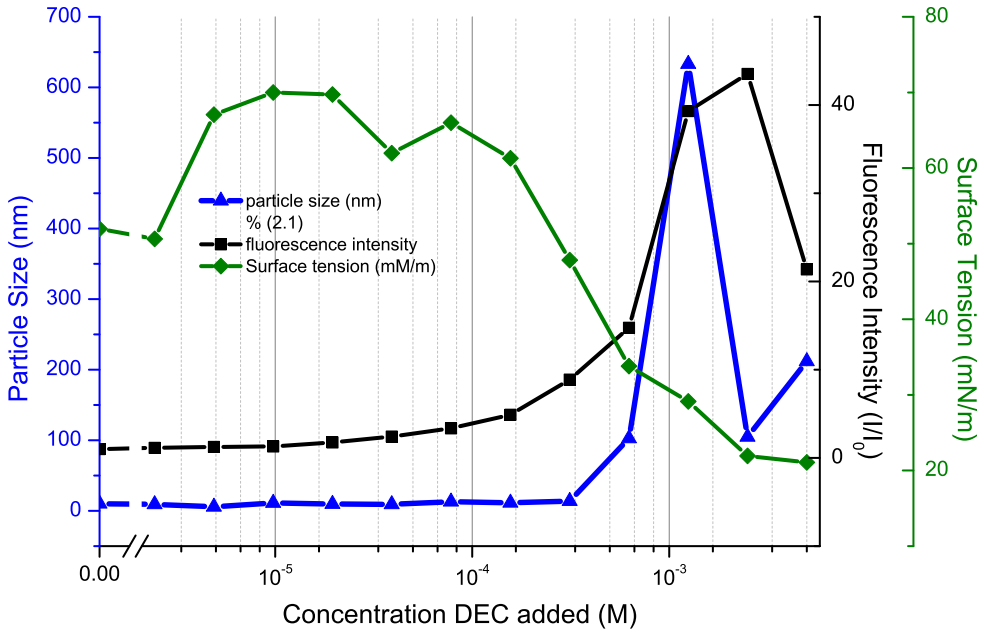

Figure 9.6 Plot of PTEBS with DEC additions over the full concentrations range including clouded solutions. Shown are the particle size, fluorescence intensity, and surface tension measurements taken.

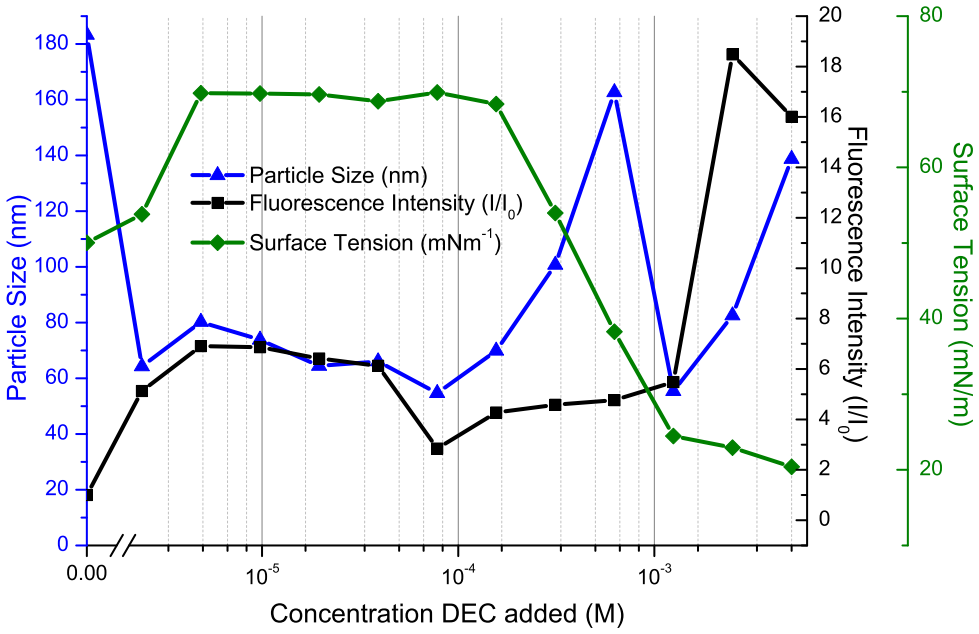

Figure 9.7 Plot of FPQ-Br with DEC additions over the full concentrations range including clouded solutions. Shown are the particle size, fluorescence intensity, and surface tension measurements taken.

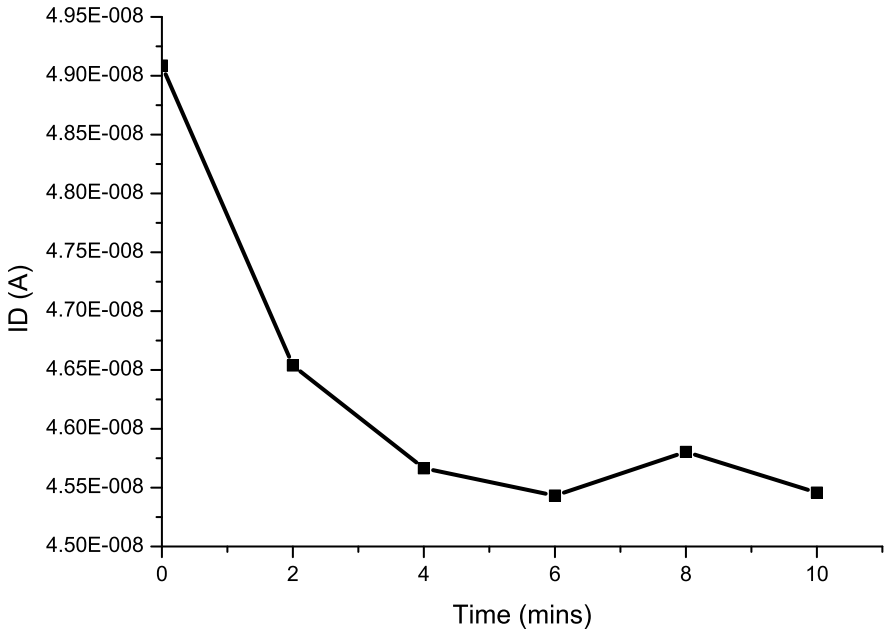

Figure 9.8 Plot of the current measured at 0 V VDS voltage at 0 V gate voltage of P3HT control device. Repeated VDS sweeps of 5– -50 V were completed over 10 mins with measurements taken at the shown time intervals

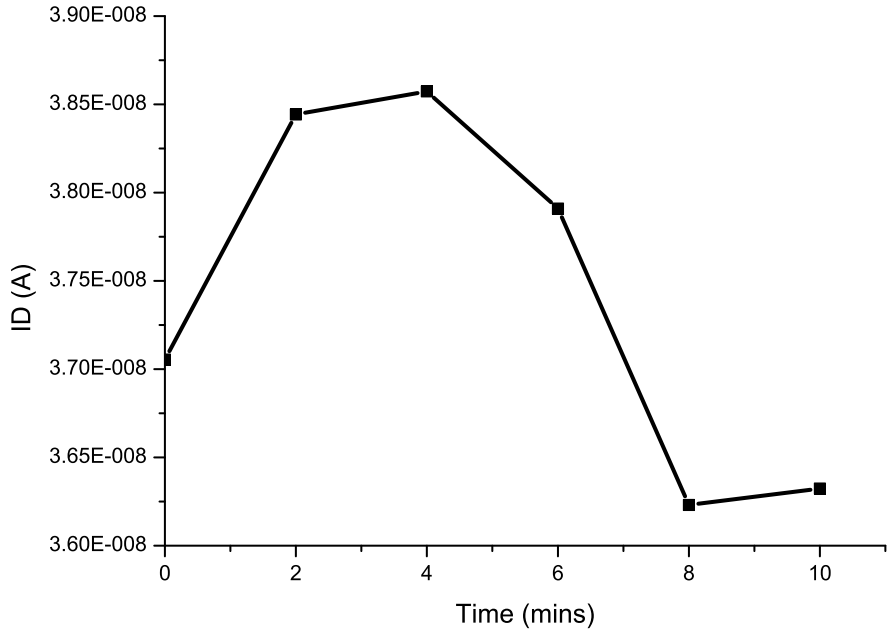

Figure 9.9 Plot of the current measured at 0 V VDS voltage at 0 V gate voltage of P3HT with 0.0002w%DOD device. Repeated VDS sweeps of 5– -50 V were completed over 10 mins with measurements taken at the shown time intervals

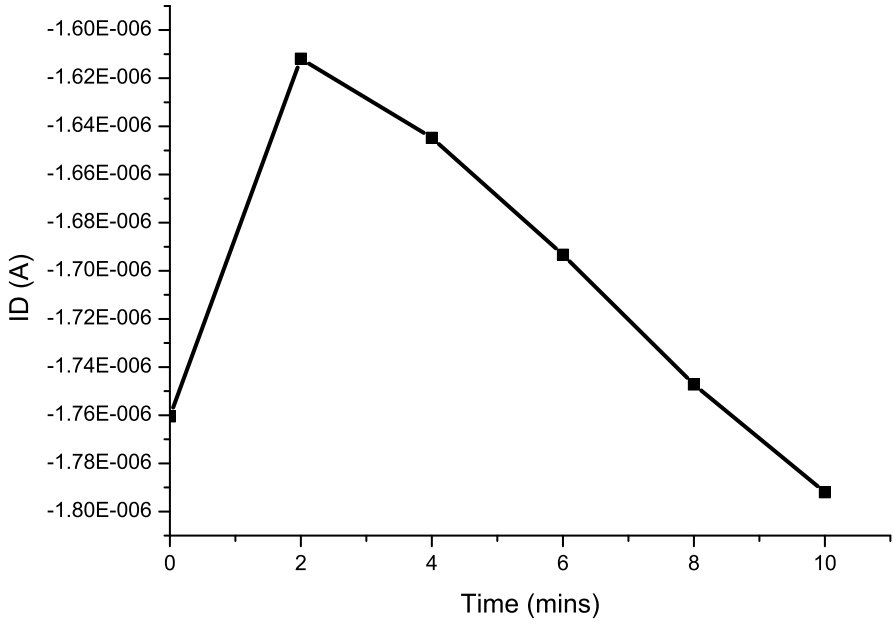

Figure 9.10 Plot of the current measured at 0 V VDS voltage at 0 V gate voltage of P3HT with 0.02w%DOD device. Repeated VDS sweeps of 5– -50 V were completed over 10 mins with measurements taken at the shown time intervals

References

1. McCullough, R. D. *Advanced Materials* **1998**, *10*, 93–116.

2. Jiang, H.; Taranekar, P.; Reynolds, J. R.; Schanze, K. S. *Angewandte Chemie International Edition* **2009**, *48*, 4300–4316.

3. Jeong, E.; Kim, S. H.; Jung, I. H.; Xia, Y.; Lee, K. et al. *Journal of Polymer Science Part A: Polymer Chemistry* **2009**, *47*, 3467–3479.

4. Coakley, K. M.; McGehee, M. D. *Chemistry of Materials* **2004**, *16*, 4533–4542.

5. Peet, J.; Heeger, A. J.; Bazan, G. C. *Accounts of Chemical Research* **2009**, *42*, 1700–1708, PMID: 19569710.

6. Duarte, A.; Pu, K.-Y.; Liu, B.; Bazan, G. C. *Chemistry of Materials* **2011**, *23*, 501–515.

7. Fei Huang, H. W.; Cao, Y. *Chemical Society Reviews* **2010**, *39*, 2500–2521.

8. Hoven, C. V.; Garcia, A.; Bazan, G. C.; Nguyen, T.-Q. *Advanced Materials* **2008**, *20*, 3793–3810.

9. Laschewsky, A. *Current Opinion in Colloid & Interface Science* **2012**, *17*, 56–63.

10. Xuli Feng, S. W., Libing Liu; Zhu, D. *Chemical Society Reviews* **2010**, *39*, 2411–2419.

11. Zhao, X.; Pinto, M. R.; Hardison, L. M.; Mwaura, J.; Mller, J. et al. *Macromolecules* **2006**, *39*, 6355–6366.

12. Hardy Sze On Chan, S. C. N. *Progress in Polymer Science* **1998**, *23*, 1167–1231.

13. Yang, R.; Tian, R.; Hou, Q.; Yang, W.; Cao, Y. *Macromolecules* **2003**, *36*, 7453–7460.

14. Chen, L.; Xu, S.; McBranch, D.; Whitten, D. *Journal of the American Chemical Society* **2000**, *122*, 9302–9303.

15. Liu, X.; Wang, Y.; Lu, Z.; Chen, Q.; Feng, Y. *Journal of Applied Polymer Science* **2012**, *125*, 4041–4048.

16. Timsit, Y.; Moras, D. *Embo Journal* **1994**, *13*, 2737–2746.

17. Hoeben, F. J. M.; Jonkheijm, P.; Meijer, E. W.; Schenning, A. P. H. J. *Chemical Reviews* **2005**, *105*, 1491–1546.

18. Rothemund, P. W. K. *Nature* **2006**, *440*, 297–302.

19. Wang, H.; Lu, P.; Wang, B.; Qiu, S.; Liu, M. et al. *Macromolecular Rapid Communications* **2007**, *28*, 1645–1650.

20. Traub, M. C.; Vogelsang, J.; Plunkett, K. N.; Nuckolls, C.; Barbara, P. F. et al. *ACS Nano* **2012**, *6*, 523–529.

21. Magid, L. J. *The Journal of Physical Chemistry B* **1998**, *102*, 4064–4074.

22. Yeh, L.-H.; Liu, K.-L.; Hsu, J.-P. *The Journal of Physical Chemistry C* **2012**, *116*, 367–373.

23. Yang, R.; Garcia, A.; Korystov, D.; Mikhailovsky, A.; Bazan, G. C. et al. *Journal of the American Chemical Society* **2006**, *128*, 16532–16539.

24. Pinto, M. R.; Kristal, B. M.; Schanze, K. S. *Langmuir* **2003**, *19*, 6523–6533.

25. Min Zheng, D. Z., Fenglian Bai *Journal of Photochemistry and Photobiology A: Chemistry* **1998**, *116*, 143–145.

26. Lemmer, U.; Heun, S.; Mahrt, R.; Scherf, U.; Hopmeier, M. et al. *Chemical Physics Letters* **1995**, *240*, 373–378.

27. Franco, I. E.; Lorchat, P.; Lamps, J.-P.; Schmutz, M.; Schrder, A. et al. *Langmuir* **2012**, *28*, 4815–4828.

28. Nguyen, T.-Q.; Doan, V.; Schwartz, B. J. *The Journal of Chemical Physics* **1999**, *110*, 4068–4078.

29. Andrey V. Dobrynina, M. R. *Progress in Polymer Science* **2005**, *30*, 1049–1118.

30. Szilagyi, I.; Sadeghpour, A.; Borkovec, M. *Langmuir* **2012**, *28*, 6211–6215.

31. Shen, D.; Wang, L.; Pan, Z.; Cheng, S.; Zhu, X. et al. *Macromolecules* **2011**, *44*, 1009–1015.

32. Xu, Z.; Tsai, H.; Wang, H.-L.; Cotlet, M. *The Journal of Physical Chemistry B* **2010**, *114*, 11746–11752.

33. Chunyan Tan, M. R. P.; Schanze, K. S. *Chemical Communications* **2002**, *5*, 446–447.

34. Kaur, P.; Yue, H.; Wu, M.; Liu, M.; Treece, J. et al. *The Journal of Physical Chemistry B* **2007**, *111*, 8589–8596.

35. Olvera de la Cruz, M.; Belloni, L.; Delsanti, M.; Dalbiez, J. P.; Spalla, O. et al. *Journal of Chemical Physics* **1995**, *103*, 5781–5792.

36. Forsman, J. *Langmuir* **2012**, *28*, 5138–5150.

37. Jiang, H.; Zhao, X.; Schanze, K. S. *Langmuir* **2006**, *22*, 5541–5543.

38. Trotsenko, O.; Roiter, Y.; Minko, S. *Langmuir* **2012**, *28*, 6037–6044.

39. Chen, Y.; Pu, K.-Y.; Fan, Q.-L.; Qi, X.-Y.; Huang, Y.-Q. et al. *Journal of Polymer Science Part A: Polymer Chemistry* **2009**, *47*, 5057–5067.

40. Kim, I.-B.; Bunz, U. H. F. *Journal of the American Chemical Society* **2006**, *128*, 2818–2819.

41. Shaw, D. J. *Introduction to colloid and surface chemistry*; Butterworths, 1970.

42. Tanford, C. *Journal of Physical Chemistry* **1972**, *76*, 3020–3024.

43. Leibner, J. *Journal of Physical Chemistry* **1977**, *81*, 130–136.

44. Pileni, M. P. *The Journal of Physical Chemistry* **1993**, *97*, 6961–6973.

45. Isemura, T.; Kimura, Y. *Journal of Polymer Science* **1955**, *16*, 92–93.

46. Faul, C.; Antonietti, M. *Advanced Materials* **2003**, *15*, 673–683.

47. Badoga, S.; Pattanayek, S. K.; Kumar, A.; Pandey, L. M. *Asia-Pacific Journal of Chemical Engineering* **2011**, *6*, 78–84.

48. Bronich, T. K.; Popov, A. M.; Eisenberg, A.; Kabanov, V. A.; Kabanov, A. V. *Langmuir* **2000**, *16*, 481–489.

49. Wallin, T.; Linse, P. *Langmuir* **1996**, *12*, 305–314.

50. Wallin, T.; Linse, P. *The Journal of Physical Chemistry B* **1997**, *101*, 5506–5513.

51. Nakamura, K.; Fukao, K. *Macromolecules* **2011**, *44*, 3053–3061.

52. Burrows, H.; Loboa, V.; Pina, J.; Ramos, M.; Seixas de Melo, J. et al. *Colloids and Surfaces A: Physicochemical and Engineering Aspects* **2005**, *270-271*, 61–66.

53. Winnik, M. A.; Bystryak, S. M.; Chassenieux, C.; Strashko, V.; Macdonald, P. M. et al. *Langmuir* **2000**, *16*, 4495–4510.

54. Messzaros, R.; Thompson, L.; Bos, M.; Varga, I.; Gilnyi, T. *Langmuir* **2003**, *19*, 609–615.

55. Hansson, P. *Langmuir* **2001**, *17*, 4167–4180.

56. Jiang, L. X.; Huang, J. B.; Bahramian, A.; Li, P. X.; Thomas, R. K. et al. *Langmuir* **2012**, *28*, 327–338.

57. Matsuoka, H.; Schwahn, D.; Ise, N. *Macromolecules* **1991**, *24*, 4227–4228.

58. Claesson, P. M.; Bergstrm, M.; Dedinaite, A.; Kjellin, M.; Legrand, J.-F. et al. *The Journal of Physical Chemistry B* **2000**, *104*, 11689–11694.

59. Zhou, S.; Hu, H.; Burger, C.; Chu, B. *Macromolecules* **2001**, *34*, 1772–1778.

60. Magny, B.; Iliopoulos, I.; Zana, R.; Audebert, R. *Langmuir* **1994**, *10*, 3180–3187.

61. Chen, Z.; Li, X.-W.; Zhao, K.-S.; Xiao, J.-X.; Yang, L.-K. *The Journal of Physical Chemistry B* **2011**, *115*, 5766–5774.

62. Hoffmann, I.; Heunemann, P.; Preivost, S.; Schweins, R.; Wagner, N. J. et al. *Langmuir* **2011**, *27*, 4386–4396.

63. Wallin, T.; Linse, P. *The Journal of Physical Chemistry* **1996**, *100*, 17873–17880.

64. Liu, Z.; Shang, Y.; Feng, J.; Peng, C.; Liu, H. et al. *The Journal of Physical Chemistry B* **2012**, *116*, 5516–5526.

65. Peng, R.; Zhu, J.; Pang, W.; Cui, Q.; Wu, F. et al. *Journal of Macromolecular Science, Part B* **2011**, *50*, 624–636.

66. Lomas, C. R.; Hodgkiss, J. M. *Supramolecular Chemistry* **2012**, *24*, 526–531.

67. Chirvase, D.; Parisi, J.; Hummelen, J. C.; Dyakonov, V. *Nanotechnology* **2004**, *15*, 1317.

68. Y. Shi, Y. Y., J. Liu *Journal of Applied Physics* **2000**, *87*, 4254–4264.

69. Li, H.; Xu, Y.; Hoven, C. V.; Li, C.; Seo, J. H. et al. *Journal of the American Chemical Society* **2009**, *131*, 8903–8912.

70. Seo, J. H.; Namdas, E. B.; Gutacker, A.; Heeger, A. J.; Bazan, G. C. *Advanced Functional Materials* **2011**, *21*, 3667–3672.

71. Decher, G. *Science* **1997**, *277*, 1232–1237.

72. Kotov, N. *Nanostructured Materials* **1999**, *12*, 789 – 796.

73. Losche, M.; Schmitt, J.; Decher, G.; Bouwman, W. G.; Kjaer, K. *Macromolecules* **1998**, *31*, 8893–8906.

74. Jin, H.; Choi, S.; Velu, R.; Kim, S.; Lee, H. J. *Langmuir* **2012**, *28*, 5417–5426.

75. McClure, S. A.; Worfolk, B. J.; Rider, D. A.; Tucker, R. T.; Fordyce, J. A. M. et al. *ACS Applied Materials & Interfaces* **2010**, *2*, 219–229.

76. Kang, J.; Dahne, L. *Langmuir* **2011**, *27*, 4627–4634.

77. Johal, M. S.; Chiarelli, P. A. *soft matter* **2007**, *3*, 34–46.

78. Chassepot, A.; Gao, L.; Nguyen, I.; Dochter, A.; Fioretti, F. et al. *Chemistry of Materials* **2012**, *24*, 930–937.

79. Lakowicz, J. R. *Principles of Fluorescence Spectroscopy*; Springer science and buisness media, 1999.

80. Jack G. Calvert, J. N. P. J. *Photochemistry*; John Wiley & Sons, Ltd., 1967.

81. Nayak, R. R.; Nag, O. K.; Kang, M.; Jin, Y.; Suh, H. et al. *Macromolecular Rapid Communications* **2009**, *30*, 633–638.

82. Woo, H.; Vak, D.; Korystov, D.; Mikhailovsky, A.; Bazan, G. et al. *Advanced Functional Materials* **2007**, *17*, 290–295.

83. Samuel, I.; Rumbles, G.; Collison, C.; Moratti, S.; Holmes, A. *Chemical Physics* **1996**, *227*, 75–82.

84. Liu, B.; Bazan, G. C. *Journal of the American Chemical Society* **2004**, *126*, 1942–1943.

85. Wang, F.; Bazan, G. C. *Journal of the American Chemical Society* **2006**, *128*, 15786–15792.

86. McLeskey, J. T. J.; Qiao, Q. *International journal of photoenergy* **2006**, 1–6.

87. Yang, J.; Garcia, A.; Nguyen, T. *Applied Phyiscs letters* **2007**, *90*, 103514,1–3.

88. Qiao, Q.; Xie, Y.; McLeskey, J. T. J. *Journal of Physical Chemistry C* **2008**, *112*, 9912–9916.

89. deMello, J. C.; Halls, J. J. M.; Graham, S. C.; Tessler, N.; Friend, R. H. *Physical Review Letters* **2000**, *85*, 421–424.

90. Wu, H.; Huang, F.; Mo, Y.; Yang, W.; Wang, D. et al. *Advanced Materials* **2004**, *16*, 1826–1830.

91. Ma, W.; Iyer, P.; Gong, X.; Liu, B.; Moses, D. et al. *Advanced Materials* **2005**, *17*, 274–277.

92. Garcia, A.; Yang, R.; Jin, Y.; Walker, B.; Nguyen, T.-Q. *Applied Physics Letters* **2007**, *91*, 153502.

93. Hou, L.; Huang, F.; Peng, J.; Wu, H.; Wen, S. et al. *Thin Solid Films* **2006**, *515*, 2632 – 2634.

94. deMello, J. C.; Tessler, N.; Graham, S. C.; Friend, R. H. *Phys. Rev. B* **1998**, *57*, 12951–12963.

95. Jou, J.-H.; Hwang, P.-Y.; Wang, W.-B.; Lin, C.-W.; Jou, Y.-C. et al. *Organic Electronics* **2012**, *13*, 899 – 904.

96. Lin, C.-E.; Wang, T.-Z.; Chiu, T.-C.; Hsueh, C.-C. *Journal of High Resolution Chromatography* **1999**, *22*, 265–270.

97. Mandal, A. B.; Nair, B. U.; Ramaswamy, D. *Langmuir* **1988**, *4*, 736–739.

98. Oakenfull, D. G. *Chemical Communications* **1970**, *1447*, 1655.

99. Xie, D.; Parthasarathy, A.; Schanze, K. S. *Langmuir* **2011**, *27*, 11732–11736.

100. Tan, C.; Atas, E.; Müller, J. G.; Pinto, M. R.; Kleiman, V. D. et al. *Journal of the American Chemical Society* **2004**, *126*, 13685–13694.

101. Tan, C.; Pinto, M.; Kose, M.; Ghiviriga, I.; Schanze, K. *Advanced Materials* **2004**, *16*, 1208–1212.

102. Tapia, M. J.; Montsern, M.; Valentb, A. J.; Burrows, H. D.; Mallavia, R. *Advances in Colloid and Interface Science* **2010**, *158*, 94–107.

103. Fang, Z.; Pu, K.-Y.; Liu, B. *Macromolecules* **2008**, *41*, 8380–8387.

104. Kim, I.-B.; Dunkhorst, A.; Gilbert, J.; Bunz, U. H. F. *Macromolecules* **2005**, *38*, 4560–4562.

105. Gallaher, J. K.; Aitken, E. J.; Keyzers, R. K.; Hodgkiss, J. M. *Chemical Communications* **2012**, *48*, 7961–7963.

106. Andrey V. Dobrynin, M. R. *Progress in Polymer Science* **2005**, *30*, 1049–1118.

107. Ray, J.; Manning, G. S. *Macromolecules* **2000**, *33*, 2901–2908.

108. Yan Liu, K. S. S., Katsu Ogawa *Journal of Photochemistry and Photobiology C: Photochemistry Reviews* **2009**, *10*, 173–190.

109. Montesern, M.; Burrows, H. D.; Valente, A. J. M.; Lobo, V. M. M.; Mallavia, R. et al. *The Journal of Physical Chemistry B* **2007**, *111*, 13560–13569, PMID: 17994719.

110. Laurenti, M.; Rubio-Retama, J.; Garcia-Blanco, F.; López-Cabarcos, E. *Langmuir* **2008**, *24*, 13321–13327.

111. López-Cabarcos, E.; Retama, J. R.; Sholin, V.; Carter, S. A. *Polymer International* **2007**, *56*, 588–592.

112. Hameed, A.; Attar, A.; Norden, J.; OBrien, S.; Monkman, A. P. *Biosensors and Bioelectronics* **2008**, *23*, 1466–1472.

113. Lavigne, J. J.; Broughton, D. L.; Wilson, J. N.; Erdogan, B.; Bunz, U. H. F. *Macromolecules* **2003**, *36*, 7409–7412.

114. Burrows, H. D.; Tapia, M. J.; Fonseca, S. M.; Pradhan, S.; Scherf, U. et al. *Langmuir* **2009**, *25*, 5545–5556.

115. Nagesh Kolishetti, S. R. *Journal of chemical sciences* **2007**, *119*, 185–193.

116. Stork, M.; Gaylord, B.; Heeger, A.; Bazan, G. *Advanced Materials* **2002**, *14*, 361–366.

117. Burrows, H.; Lobo, V.; Pina, J.; Ramos, M.; de Melo, J. S. et al. *Colloids and Surfaces A: Physicochemical and Engineering Aspects* **2005**, *270*, 61 – 66.

118. Tapia, M. J.; Burrows, H. D.; Valente, A. J. M.; Pradhan, S.; Scherf, U. et al. *The Journal of Physical Chemistry B* **2005**, *109*, 19108–19115.

119. Knaapila, M.; Almsy, L.; Garamus, V. M.; Pearson, C.; Pradhan, S. et al. *The Journal of Physical Chemistry B* **2006**, *110*, 10248–10257.

120. Al Attar, H. A.; Monkman, A. P. *The Journal of Physical Chemistry B* **2007**, *111*, 12418–12426.

121. Bergstrm, L. M.; Kjellin, U. R. M.; Claesson, P. M.; Grillo, I. *The Journal of Physical Chemistry B* **2004**, *108*, 1874–1881.

122. Kim, T. M., J. Swager *Nature* **2001**, *411*, 1030–1034.

123. Burrows, H. D.; Tapia, M. J.; Silva, C. L.; Pais, A. A. C. C.; Fonseca, S. M. et al. *The Journal of Physical Chemistry B* **2007**, *111*, 4401–4410.

124. Anthony, O.; Zana, R. *Langmuir* **1996**, *12*, 1967–1975.

125. Wilson, J.; Frampton, M.; Michels, J.; Sardone, L.; Marletta, G. et al. *Advanced Materials* **2005**, *17*, 2659–2663.

126. Zhou, S.; Yeh, F.; Burger, C.; Chu, B. *The Journal of Physical Chemistry B* **1999**, *103*, 2107–2112.

127. Thnemann, A. F.; Ruppelt, D. *Langmuir* **2001**, *17*, 5098–5102.

128. Dutta, K.; Mahale, R. Y.; Arulkashmir, A.; Krishnamoorthy, K. *Langmuir* **2012**, *28*, 10097–10104.

129. Lam, V. D.; Walker, L. M. *Langmuir* **2010**, *26*, 10489–10496.

130. Waigh, T. A.; Ober, R.; Williams, C. E.; Galin, J.-C. *Macromolecules* **2001**, *34*, 1973–1980.

131. Vilgis, T.; Johner, A.; Joanny, J. *The European Physical Journal E: Soft Matter and Biological Physics* **2000**, *2*, 289–300.

132. Woo, H. Y.; Nag, O. K.; Kim, J.; Kang, M.; Bazan, G. C. *Molecular Crystals and Liquid Crystals* **2008**, *486*, 244–249.

133. Clark, J.; Silva, C.; Friend, R. H.; Spano, F. C. *Physical review letters* **2007**, *98*, 206406,1–2.

134. Nguyen, T.-Q.; Martini, I. B.; Liu, J.; Schwartz, B. J. *The Journal of Physical Chemistry B* **2000**, *104*, 237–255.

135. Pace, G.; Tu, G.; Fratini, E.; Massip, S.; Huck, W. T. S. et al. *Advanced Materials* **2010**, *22*, 2073–2077.

136. Ober, C. K.; Wegner, G. *Advanced Materials* **1997**, *9*, 17–31.

137. Sergeeva, I.; Sobolev, V.; Dibrov, G.; Churaev, N. *Colloid Journal* **2011**, *73*, 378–383.

138. MacKnight, W. J.; Ponomarenko, E. A.; Tirrell, D. A. *Accounts of Chemical Research* **1998**, *31*, 781–788.

139. Paul, P. K.; Hussain, S. A.; Bhattacharjee, D.; Pal, M. *Chinese Journal of Chemical Physics* **2011**, *24*, 348.

140. Bricaud, Q.; Fabre, R. M.; Brookins, R. N.; Schanze, K. S.; Reynolds, J. R. *Langmuir* **2011**, *27*, 5021–5028.

141. Antonietti, M.; Conrad, J.; Thuenemann, A. *Macromolecules* **1994**, *27*, 6007–6011.

142. van der Gucht, J.; Spruijt, E.; Lemmers, M.; Stuart, M. A. C. *Journal of Colloid and Interface Science* **2011**, *361*, 406–422.

143. D'Andrade, B.; Forrest, S. *Advanced Materials* **2004**, *16*, 1585–1595.

144. Katz, H. E.; Hong, X. M.; Dodabalapur, A.; Sarpeshkar, R. *Journal of Applied Physics* **2002**, *91*, 1572–1576.

145. Hoven, C. V.; Yang, R.; Garcia, A.; Crockett, V.; Heeger, A. J. et al. *Proceedings of the National Academy of Sciences of the United States of America* **2008**, *105*, 12730–12735.

146. Niu, Y.-H.; Jen, A. K.-Y.; Shu, C. *The Journal of Physical Chemistry B* **2006**, *110*, 6010–6014.

147. Huang, F.; Niu, Y.-H.; Zhang, Y.; Ka, J.-W.; Liu, M. et al. *Advanced Materials* **2007**, *19*, 2010–2014.

148. Hoven, C.; Yang, R.; Garcia, A.; Heeger, A. J.; Nguyen, T.-Q. et al. *Journal of the American Chemical Society* **2007**, *129*, 10976–10977.

149. Park, J. S.; Lee, B. R.; Jeong, E.; Lee, H.-J.; Lee, J. M. et al. *Applied Phyiscs letters* **2011**, *99*, 163305,1–3.

150. Hongbin Wu, J. P. Y. C., Fei Huang *Organic Electronics* **2005**, *6*, 118–128.

151. Brewer, P.; Lane, P.; deMello, A.; Bradley, D.; deMello, J. *Advanced Functional Materials* **2004**, *14*, 562–570.

152. Yang, R.; Xu, Y.; Dang, X.-D.; Nguyen, T.-Q.; Cao, Y. et al. *Journal of the American Chemical Society* **2008**, *130*, 3282–3283.

153. Yang, R.; Wu, H.; Cao, Y.; Bazan, G. C. *Journal of the American Chemical Society* **2006**, *128*, 14422–14423.

154. Edman, L.; Liu, B.; Vehse, M.; Swensen, J.; Bazan, G. C. et al. *Applied Phyiscs letters* **2005**, *98*, 044502,1–8.

155. Hodgkiss, J. M.; Tu, G.; Albert-Seifried, S.; Huck, W. T. S.; Friend, R. H. *Journal of the American Chemical Society* **2009**, *131*, 8913–8921.

156. Huang, F.; Wu, H.; Wang, D.; Yang, W.; Cao, Y. *Chemistry of Materials* **2004**, *16*, 708–716.

157. Huang, F.; Hou, L.; Shen, H.; Jiang, J.; Wang, F. et al. *Journal of Materials Chemistry* **2005**, *25*, 2499–2507.

158. Rep, D.; Morpurgo, A. F. *Journal of Applied Physic* **2003**, *93*, 2082–2090.

159. Lan, L.; Xu, R.; Peng, J. *Japanese Journal of Applied Physics* **2009**, *48*, 080206,1–3.

160. kieth Bradley,; Cummings, J.; Stae, A.; Gabriel, J.-C. P.; Gruner, G. *Nano* **2003**, *3*, 639–641.

161. Egginger, M.; Irimia-Vladu, M.; Schwodiaur, R.; Tanda, A.; Frischauf, I. et al. *Advance Materials* **2008**, *20*, 1018–1022.

162. Laiho, A.; Herlogsson, L.; Forchheimer, R.; Crispin, X.; Berggren, M. *Proceedings of the National Academy of Sciences of the United States of America* **2011**, *108*, 15069 – 15073.

163. Zeng, W.; Wu, H.; Zhang, C.; Huang, F.; Peng, J. et al. *Advanced Materials* **2007**, *19*, 810–814.

164. Sirringhaus, H.; Brown, P. J.; Friend, R. H.; Nielsen, M. M.; Bechgaard, K. et al. *Nature* **1999**, *401*, 685–688.

165. Chapman, C. F.; Maroncelli, M. *The Journal of Physical Chemistry* **1991**, *95*, 9095–9114.

166. Dutta, K.; Mahale, R. Y.; Arulkashmir, A.; Krishnamoorthy, K. *Langmuir* **2012**, *28*, 10097–10104.